**Bayerische Julius-Maximilians-Universität Würzburg**
Institut für Informatik
Lehrstuhl für Verteilte Systeme
Prof. Dr. P. Tran-Gia

# Analytical Modeling of Power Control and its Impact on Wideband CDMA Capacity and Planning

**Kenji Leibnitz**

Würzburger Beiträge zur
Leistungsbewertung Verteilter Systeme
Bericht 01/03

**Würzburger Beiträge zur**
**Leistungsbewertung Verteilter Systeme**

**Herausgeber**

Prof. Dr. P. Tran-Gia
Universität Würzburg
Institut für Informatik
Lehrstuhl für Verteilte Systeme
Am Hubland
D-97074 Würzburg

Tel.: +49-931-888-6630
Fax.: +49-931-888-6632
email: trangia@informatik.uni-wuerzburg.de

**Satz**

Reproduktionsfähige Vorlage vom Autor.
Gesetzt in LaTeX Computer Modern 9pt.

**ISSN 1432-8801**

# Analytical Modeling of Power Control and its Impact on Wideband CDMA Capacity and Planning

Dissertation zur Erlangung des
naturwissenschaftlichen Doktorgrades
der Bayerischen Julius–Maximilians–Universität Würzburg

vorgelegt von

**Kenji Leibnitz**

aus

Djidda

Würzburg 2003

Eingereicht am: 14.11.2002
bei der Fakultät für Mathematik und Informatik
1. Gutachter: Prof. Dr.-Ing. P. Tran-Gia
2. Gutachter: Prof. Dr. D. Everitt
Tag der mündlichen Prüfung: 14.02.2003

# Danksagung

An dieser Stelle möchte ich allen Personen danken, die einen wesentlichen Beitrag dazu geleistet haben, die vorliegende Arbeit erfolgreich abzuschließen. Allen voran gilt mein besonderer Dank meinem Doktorvater und Betreuer dieser Arbeit, Herrn Prof. Dr. Phuoc Tran-Gia, der mich durch unermüdliche Anregung und sachkundigen Rat bei der Bearbeitung des Themas unterstützte. Durch sein Engagement, das einen maßgeblichen Einfluss auf das fachlich kompetente und kollegiale Klima am Lehrstuhl ausübt, entstand ein äußerst produktives Umfeld, von dem diese Arbeit sehr profitierte. Seine Förderung der Kontakte zur Industrie und zu anderen nationalen wie internationalen Forschern eröffnete mir die Möglichkeit an aktuellen und relevanten Problemstellungen auf diesem Arbeitsgebiet mitzuwirken und so wertvolle Erfahrungen in meinem Forschungsbereich zu sammeln. Für sein Verständnis und Vertrauen, das er mir als Vorgesetzter während meiner Zeit als wissenschaftlicher Mitarbeiter am Lehrstuhl entgegengebracht hat, bin ich zu tiefstem Dank verpflichtet.

My deepest appreciation and gratitude goes to Prof. Dr. David Everitt, who acted as a reviewer of this thesis and provided me with valuable comments on my research.

A large number of ideas in this work originated from discussions with the members of the Wireless Systems Engineering group of Nortel Net-

works in Richardson, TX. I am very much indebted to Dr. Nikhil Jain, Prof. Dr. Kalyan Basu, and Dr. John E. Miller for their support.

Furthermore, I would like to thank Prof. Dr. Konosuke Kawashima and Prof. Dr. Richard Harris for providing me with the ability to visit their research labs, and Prof. Dr. Marie-Ange Remiche for the fruitful collaboration.

Weiterhin möchte ich mich bei Dr. Bernd Schröder, Dr. Albert Weller, Konstantin Tsipotis und Bart Sanders für die gute Zusammenarbeit in den gemeinsamen Forschungsprojekten bedanken.

Wichtig für das Gelingen der Arbeit war jedoch auch der Kontakt zu den Menschen, mit denen ich am Lehrstuhl täglichen Umgang hatte. Neben den fachspezifischen Fragen und Diskussionen mit den Kollegen, blieb auch oft noch Zeit für gemeinsame Aktivitäten außerhalb der Arbeitszeit. Allen meinen Kollegen, die mich im Laufe der Jahre begleitet haben, möchte ich an dieser Stelle meinen aufrichtigen Dank aussprechen: Mathias Dümmler, Dr. Notker Gerlich, Klaus Heck, Stefan Köhler, Michael Menth, Jens Milbrandt, Dirk Staehle, Dr. Michael Ritter, Dr. Oliver Rose, Dr. Kurt Tutschku, Norbert Vicari und Patricia Wilcox.

Ein besonderes Dankeschön für ihre Unterstützung bei der Verwaltungsarbeit geht an unsere Sekretärin Frau Gisela Alt.

Einen großen Anteil an dem Gelingen dieser Arbeit haben selbstverständlich auch die studentischen Hilfskräfte des Lehrstuhls, sowie die Studenten Wolfgang Jodl, Ulrich Ehrenberger und Armin Krauß, die mir mit ihren Diplomarbeiten zuarbeiteten.

Zum Schluss gilt mein besonderer Dank meinen Eltern Kazuko und Klaus Leibnitz, die mich unermüdlich unterstützen und mir die Kraft gaben, die Studien- und Promotionszeit erfolgreich zu absolvieren.

Würzburg, im Februar 2003 *Kenji Leibnitz*

# Contents

# 1 Introduction

Currently, the development of wireless communication systems is undergoing an important paradigm shift. The transition from purely voice-oriented wireless telephony to the so-called third generation (3G) is imminent or has already begun in a few countries. This leads to the possibility of introducing new services to the wireless community that were so far only available in wireline networks. The growing importance of internet applications such as browsing the World Wide Web or sending and receiving electronic mail has made it a necessity for many users to have access to these applications from anywhere the user wants just like using a wireless phone.

However, most of these new applications also demand a higher bandwidth than voice traffic and require the introduction of new technologies that permit the transmission of circuit-switched and packet-switched traffic. The tendencies that can be seen here lead to the gradual convergence of the internet and the wireless world. So far, this wireless world consisted mainly of heterogeneous systems where mobile service providers from different countries or territories operate their networks with different access technologies. For example in Europe predominantly GSM services can be found, whereas in the USA only limited GSM coverage is provided and other systems, e.g. AMPS or cdmaOne, are mainly in use. The aims of the standardization organizations towards the third genera-

tion are to achieve a truly ubiquitous wireless system that permits global roaming.

The aforementioned aims are attempted with the introduction of Wideband CDMA as access technology for the air interface. This is mainly due to its superior capacity compared to narrowband systems. However, the significant differences between Wideband CDMA and conventional second generation systems requires also new paradigms in the dimensioning and planning of networks. Unlike GSM the capacity of CDMA-based networks is not a fixed term, but its soft capacity leads to a description of the term coverage that differs from its conventional use. Instead of being dominated solely by the RF transmission aspects, there is an interaction in CDMA networks between coverage, capacity, and the quality of service. It is therefore especially important to investigate the stability of the system and all influences on the capacity and coverage before rolling out new networks.

The intention of this monograph is to provide analytical models to facilitate the performance evaluation of third generation wireless networks. Detailed knowledge of the system behavior is therefore a crucial issue for a proper dimensioning and planning of communication networks. Therefore, Chapter 2 presents a brief introduction to the basic principles of CDMA technology and discusses the essential features that influence the evaluation of the system capacity. At the end of this chapter, simple capacity equations are discussed which serve as the foundation for the extensions in the following chapters. As the focus of this work lies on the modeling of the behavior of the power control mechanism, Chapter 3 provides some theoretical aspects that can be found in the literature. This includes a mathematical formulation as an optimization problem and several approaches to solving this problem will be outlined. This is followed in Chapter 4 by the derivation of analytical models for the power control loops, which allow for a stochastic description of the transmission power of the mobile stations. The modeling technique is based

on a Markov chain that is discrete in time and state. After investigating the performance of a single user, Chapter 5 provides an examination of the performance on the system level. A stochastic spatial model is used for randomly characterizing the user locations within the cells. The analysis of the system performance is at first considered for a cell with a single class of users and extended to include also multiple service classes and the influence of soft handover between multiple cells. The obtained results can be used to provide some hints to the network planner and Chapter 6 discusses two examples utilizing the spatial stochastic traffic model. Finally, Chapter 7 summarizes this monograph and provides an outlook on further research.

# 2 Principles of Code Division Multiple Access

This chapter serves as an overview of the *Code Division Multiple Access* (CDMA) technology. We begin with the fundamentals of spread spectrum modulation and derive simple equations describing the capacity of CDMA systems. The essential features of CDMA will be presented and the most important differences between the second generation system *cdmaOne* and third generation *Universal Mobile Telecommunication System* (UMTS) will be pointed out.

## 2.1 Multiple Access Schemes

In any communication system where many users simultaneously share a common resource there is a need for a multiple access scheme. All users compete for an often only limited pool of resources, e.g. a limited number of traffic channels. This is especially true in wireless communications, where the communication is performed by modulating the information signal onto an RF (radio frequency) carrier in a very limited frequency spectrum. The multiple access scheme is required in order to utilize the bandwidth efficiently and to achieve a high system capacity.

Additionally to the access scheme, *duplexing* is required for wireless systems. Duplexing is the feature of transmitting and receiving at the same time and can be performed either in the frequency or time domain. In *Frequency Division Duplexing* (FDD) two separate frequency bands are used for the uplink direction, i.e. the connection from the mobile station (MS) to the base station (BS), and the downlink, i.e. the BS-to-MS path. Alternatively, *Time Division Duplexing* (TDD) utilizes the same frequency band for both link directions and separates the user signals by time slots.

Among the multiple access schemes, *Frequency Division Multiple Access* (FDMA), *Time Division Multiple Access* (TDMA), and *Code Division Multiple Access* (CDMA) are the most popular, see Rappaport (1996). In FDMA, a frequency band or channel is assigned to each user and is maintained for the complete duration of the connection. Examples of FDMA systems are the US analog cellular system Advanced Mobile Phone System (AMPS), which is based on FDMA/FDD, or the Digital Enhanced Cordless Telephone (DECT), operating with FDMA/TDD. In TDMA, the spectrum is divided into cyclically repeating time slots in which only a single user can transmit or receive. A prominent example for a system operating with TDMA/FDD is the Global System for Mobile Communication (GSM), see Mouly and Pautet (1992).

In contrast to the aforementioned access schemes, CDMA uses orthogonal codes to distinguish the individual traffic channels. As the focus of this monograph lies on systems based on CDMA, we will elaborate on this access scheme in greater detail in the following section.

### 2.1.1 Spread Spectrum Multiple Access

CDMA is a multiple access system based on *Spread Spectrum* that has enormously gained in importance since its introduction to wireless communications. Spread spectrum systems were originally developed for

military applications in the mid 1950's due to their robustness against jamming and interference and the low probability of intercept. A definition of spread spectrum is given by Pickholtz et al. (1982):

**Definition 2.1**
***Spread spectrum*** *is a means of transmission in which the signal occupies a bandwidth in excess of the minimum necessary to send the information; the band spread is accomplished by means of a code which is independent of the data, and a synchronized reception with the code at the receiver is used for despreading and subsequent data recovery.*

In this work, we focus on the most common form of spread spectrum, which is known as *Direct Sequence Spread Spectrum* (DS-SS). Here, the spreading codes are pseudo-noise sequences with a transmission rate measured in chips per second (cps) that is many times greater than the information bandwidth in terms of the user data rate in bits per second (bps). The energy in each mobile station's signal is, therefore, spread over the entire transmission bandwidth and appears like noise over the radio channel. Another spread spectrum variant is *Frequency Hopping Spread Spectrum* (FH-SS) where the carrier frequency is hopped pseudo-randomly within the transmission band. This method is used for example in Bluetooth technology, cf. Haartsen (2000).

In DS-SS systems, each user transmits with a certain information bit rate $R$ and shares the same radio frequency (RF) bandwidth $W$ with the other users. The ratio between $W$ and $R$ is commonly referred to as the *spreading gain* or *processing gain*.

The spreading itself is performed by modulating the user's data signal on a noise-like carrier with higher frequency, see Fig. 2.1. The major benefit of using noise-like carriers is that the system becomes more robust to interference. However, since each user's signal appears as noise over the air interface, he contributes to the total interference. Since the connection quality requires a minimum quality in terms of *bit-energy-to-noise*

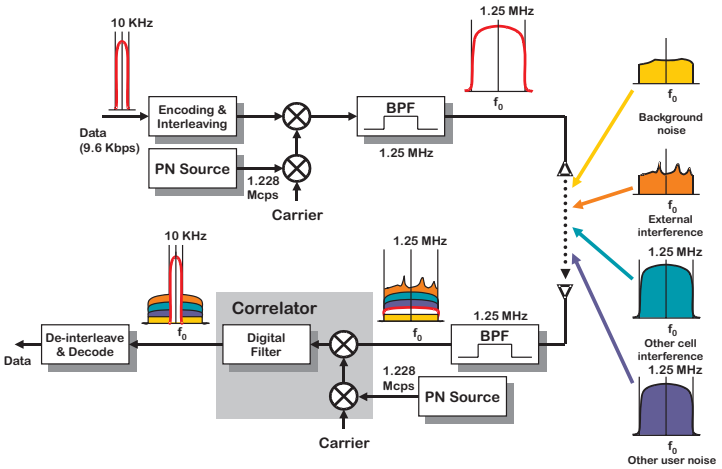


Figure 2.1: *Simplified voice transmission in cdmaOne*

*ratio* ($E_b/N_0$), the total level of interference ultimately limits the capacity of CDMA systems.

The reduction of interference is, therefore, essential in order to maximize the system capacity in CDMA. This is enforced by a number of means, e.g. the use of transmission power control, variable bit rate voice coding, and antenna sectorization. The influence of these mentioned items on the system capacity will be sketched in the Section 2.4.

## 2.1.2 Examples of CDMA-based Systems

### cdmaOne/IS-95

In 1993 the Telecommunications Industry Association (TIA) interim standard IS-95A (TIA / EIA / IS-95 1993) was completed. It was proposed by Qualcomm Inc., San Diego, and defined the three lowest layers of the protocol stack for a CDMA wireless system. Later, in June 1997, an extended standard was proposed by the name IS-95B, which included data transmission with 64 kbps. From then on, the family of IS-95 standards was renamed to *cdmaOne*. Today, cdmaOne is operated worldwide with major markets in North and South America, as well as in Asia. The number of subscribers surpassed the 100 million boundary in September 2001, see CDMA Developers Group (2001).

| | | |
|---|---|---|
| multiple access | CDMA / FDD | |
| chip rate | 1.2288 Mcps | |
| carrier bandwidth | 1.25 MHz | |
| spreading factor | 128 (Rate Set 1) | |
| frame length | 20 ms / 16 slots | |
| modulation | QPSK / OQPSK | |
| synchronization | BS: via GPS, MS: via Pilot- / Sync-channels | |
| handover | mobile assisted | |
| power control | uplink: | open loop / closed loop, 800 Hz |
| | downlink: | slow p.c. for Paging-Ch. |
| frequency band | uplink: | 869-894, 1930-1980 MHz |
| | downlink: | 824-849, 1850-1910 MHz |

Table 2.1: *Air interface parameters of IS-95*

The parameters of the air interface specification in IS-95 are given in Tab. 2.1. The user data rate for traffic channels in cdmaOne is commonly 9.6 kbps (Rate Set 1) or 14.4 kbps (Rate Set 2).

As specified in Tab. 2.1, fast power control is performed only on the uplink. We will discuss the involved mechanisms in greater detail in Section 2.2. On the downlink, the IS-95 standard does not specify any exact algorithm for power control, but leaves it to the manufacturer. The MS measures the downlink quality in terms of frame error rate and reports this in a *power measurement report message* (PMRM) to the base station. This report is sent either periodically or when a certain threshold is exceeded and the base station may then update its power according to these reports. The step size of power control is about 0.5 dB and the dynamic range is $\pm$ 6 dB. Power updates are performed every 20 ms.

### Universal Mobile Telecommunication System (UMTS)

The *Universal Mobile Telecommunication System* (UMTS) is the European proposal for third generation wireless communication (3G). It is part of the ITU's approach to provide a global family of 3G wireless systems known as IMT-2000 (International Mobile Telephony). The main goal is to replace second generation systems that are limited to voice or short message services and to provide high speed, packet-oriented access to wireless terminals. Especially with the enormous increase in importance of Internet applications, e.g. the World Wide Web (WWW) or E-Mail, the introduction of 3G will provide a convergence of wireless and wireline communications.

Several IMT-2000 approaches exist worldwide. The coordination of the standardization is performed in international organizations, like the 3rd Generation Partnership Project (3GPP) which combines the Japanese and the European standardization efforts. Especially the Japanese market has shown that a demand for wireless data services exists. The introduction of *i-mode*, which is a mobile packet-oriented Internet access, has seen a tremendous increase in the number of subscribers which has reached 30 million in December 2001. Capacity limitations of the existing

systems have also led to the first commercial introduction of 3G in the greater Tokyo area in October 2001 under the name of FOMA (Freedom of Multimedia Access).

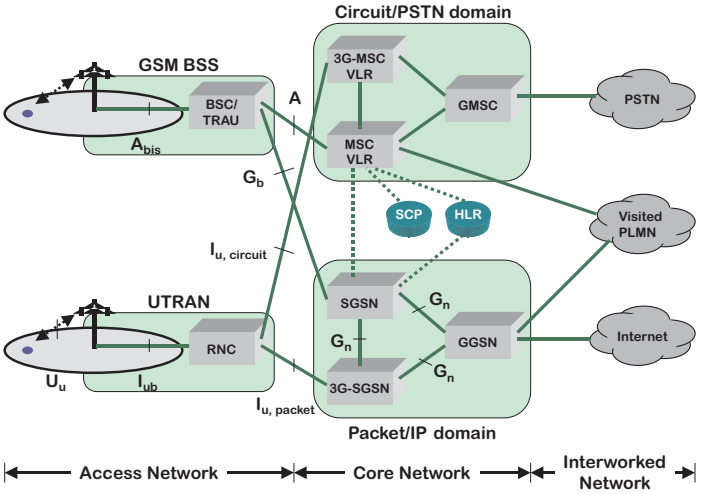


Figure 2.2: *Architecture of UMTS Release 99*

Although a truly global wireless standard is attempted, difficulties due to political and economical decisions remain. For example, the North American proposal for 3G is CDMA2000, which provides a backward compatibility to cdmaOne, but uses a slightly different chip rate compared to UMTS. The first phase of CDMA2000 is known as CDMA2000 1x, which refers to the existing spectrum allocations for cdmaOne with 1.25 MHz carriers. The future evolution of CDMA2000 is denoted as CDMA2000 1xEV which consists of CDMA2000 1xEV-DO (Evolution - Data Only) with data rates up to 2.4 Mbps and CDMA2000 1xEV-DV

(Evolution Data/Voice), which integrates voice and data on the same 1.25 MHz carrier and offers data speeds of up to 4.8 Mbps.

In Europe the existing GSM system is supported in the standardization of UMTS in order to provide a seamless migration from 2G to 3G. Fig. 2.2 shows that the GSM base station subsystem (BSS) is not only connected to the GSM core network, but also to the UMTS/GPRS packet-oriented core network. Handovers between both systems will also be possible. Note that in the following we will mainly use the conventional terminology for a base station and base station controller, but wherever appropriate we will use the new terms NodeB and Radio Network Controller (RNC) when we specifically refer to UMTS.

The air interface of UMTS is denoted as UTRA (UMTS Terrestrial Radio Access), which operates in two modes, FDD and TDD. Since FDD will be the most common duplex method, we will focus on the FDD mode, which is also known as WCDMA (Wideband CDMA) in order to distinguish it from the narrowband second generation cdmaOne technology. WCDMA operates with a chip rate of 3.84 Mcps and data rates between 12.2 kbps for voice up to 2 Mbps for high speed multimedia services. The higher chip rate increases multipath diversity especially in small urban cells and leads to a higher coverage than cdmaOne. Table 2.2 summarizes the most important air interface parameters for WCDMA in UMTS.

Although both systems, cdmaOne and UMTS, operate with DS-CDMA, there are several major differences between them, the most striking one being the support of for multimedia services. In the following two sections we will elaborate on two main features of CDMA networks: *power control* and *soft handover*. The implementation of soft handover varies slightly for both systems. Whereas, cdmaOne uses fixed thresholds for maintaining the set of connected BS (active set), UMTS uses relative thresholds based on the strongest (or weakest) pilot powers.

| | |
|---|---|
| multiple access | CDMA / FDD |
| chip rate | 3.84 Mcps |
| carrier spacing | 5 MHz |
| spreading factor | uplink: 4-256, downlink: 4-512 |
| frame length | 10 ms / 15 slots |
| modulation | uplink: (dual channel) BPSK, downlink: QPSK |
| synchronization | not required |
| handover | soft, softer, and hard (for interfrequency HO) |
| power control | open loop / closed loop, 1500 Hz |
| frequency band | uplink: 1920-1980 MHz |
| | downlink: 2110 - 2170 MHz |

Table 2.2: *UMTS (WCDMA) air interface parameters*

## 2.2 Power Control

In the previous sections we have already seen that all users on the uplink of a CDMA system share the same transmission band and therefore interfere with each other. Furthermore, mobile stations will be located in the cell at varying distances from the BS. If all users were transmitting at equal strengths, users near the base station would dominate over the users located farther away. This is known as the *near-far effect*. In order to operate efficiently, CDMA requires that all users are received with nearly equal power at the base station. To achieve this goal, transmission power control is implemented, where the receiver controls the power of the transmitter in order to achieve a certain target link quality in terms of received bit-energy-to-noise ratio ($E_b/N_0$). In addition to compensating the interference by other users, power control also improves the performance against fading and the power reduction also prolongs battery lifetime.

Power control is by no means only limited to CDMA systems. In fact it is also used in GSM to reduce the inter-cell interference and increase the frequency reuse factor and capacity, see Pichna and Wang (1999). Other systems like the cordless telephony standards CT2/CT2PLUS or Bluetooth also employ power control.

In CDMA systems two types of power control are used on the uplink:

- *open loop*, and
- *closed loop*.

In open loop power control the MS uses the received signal strength on the downlink Pilot-channel as an estimation of the path loss and sets its transmit power accordingly. If the quality of the channel changes rapidly, open loop can react very fast (in the range of microseconds). In spite of the fast reaction to variations in the channel, open loop power control is not able to compensate for Rayleigh-Fading. Uplink and downlink connections are performed in separate frequency bands, which makes the occurrence of Rayleigh fading effects independent for both channel directions, see Walke (1998).

Contrary to that, closed loop power control works in a tight cooperation between mobile and base station to overcome fluctuations on the traffic channel. The closed loop itself consists of an inner and outer loop. Within the *inner loop*[1], the BS continually monitors the link quality of the uplink in terms of received $E_b/N_0$ and compares it with a certain threshold. If the received value is too high, then the MS is told to decrease its power. On the other hand, if it is too low, the link quality is not good enough and a *power-up* command is sent. The time cycles of the power updates is referred to as power control groups (PCG) and is 16 or 15 times per frame for cdmaOne or UMTS, respectively.

[1] In 3GPP terminology the inner loop is also simply denoted as closed loop.

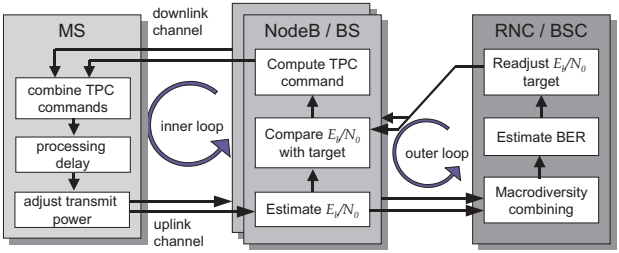


Figure 2.3: *Basic closed loop power control in cdmaOne and UMTS*

After a complete frame has been transmitted, the power control algorithm enters the *outer loop*. Its main goal is to maintain an acceptable *frame error rate* (FER) by readjusting the $E_b/N_0$ threshold of the inner loop after every frame, cf. Sampath et al. (1997), Holma and Toskala (2000). The interaction between inner and outer loop is illustrated in Fig. 2.3. It should also be noted that an MS in soft handover communicates with the BSC or RNC via all base stations in its active set. In this case it also receives several power control commands on the downlink. The MS combines the received power control commands and only increases its power if all base stations participating in soft handover demand an increase in transmit power. Details on the soft handover mechanism will be given in the following section.

An example of a simulation of closed loop power control in cdmaOne is depicted in Fig. 2.4. The top figure illustrates the channel loss in dB of a 3-ray multipath fading channel. It shows the typical behavior of fast fading where the signal strength fluctuates rapidly over several dB. In the center figure, the transmitted power is shown in dBm. It can be seen that the shape is roughly the inverse of the channel loss. Whenever there are fading drops, the transmitted power is increased in order to overcome

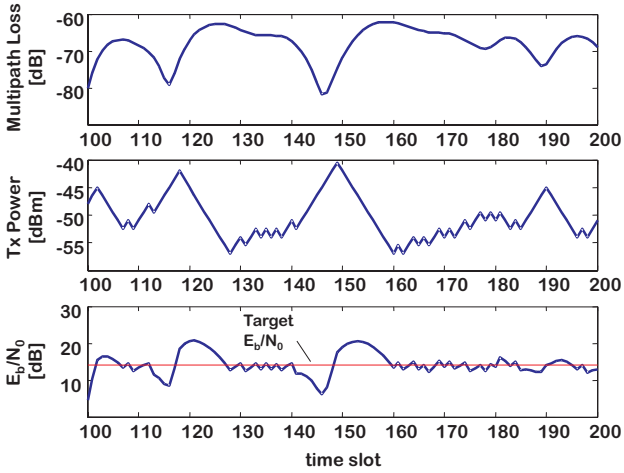


Figure 2.4: *Example of power control updates*

the signal attenuation. The dynamic behavior of the transmitted power is therefore influenced by the update rate and the power control step size. The zigzag shape of the transmission power is caused by the discrete power steps of 0.5 dB. In cdmaOne only a single bit is used for power control that is multiplexed on the traffic channel after the convolutional encoding and is therefore not error-protected. The transmission of a single bit also results in the fact that there are only commands for increasing or decreasing, but none for maintaining a certain power level. The bottom figure shows the effective $E_b/N_0$ that is achieved. The target $E_b/N_0$ is kept approximately constant at 14 dB. It can be seen that the fluctuations of the channel have an effect on the received link quality and that the power control loops operate imperfectly.

## 2.3 Soft Handover

Another appealing feature of CDMA systems is during handover, i.e. how an active connection is handled when the mobile leaves the coverage area of one base station and enters that of another. Beside the possibility of hard handover, where the connection to the new cell is established after terminating the one to the old cell ("break before make"), CDMA offers also the possibility to perform *soft handover*. In soft handover an MS is connected to several base stations simultaneously via independent channels, see Fig. 2.5.

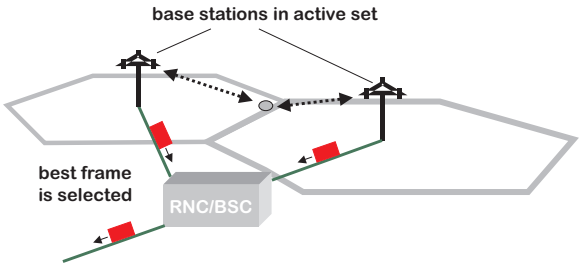


Figure 2.5: *Principle of soft handover with two base stations*

On the uplink, the signals of the MSs are received by the involved base stations and transferred to the BSC (or RNC). There, the received data is combined by selecting the frame with the least errors (selection combining). This effect is known as *macro-diversity* and greatly improves the error performance of the system. On the downlink, the Rake receiver at the mobile station can coherently combine the signals from all base stations by treating them as additional multipath components. Since in soft handover a new (additional) connection is always established before the old one is terminated, it is considered a "make before break" scheme.

There is another reason for employing soft handover in CDMA. In combination with power control, soft handover helps to reduce the interference from one cell to another. Since each connection to a base station in soft handover includes a separate inner loop power control, the mobile station's transmission power is effectively controlled by the base station with the least power requirements in order to maintain the desired target $E_b/N_0$, cf. Hashem and Secord (1999). Therefore, it is together with power control an important interference-mitigation tool.

Furthermore, *softer handover* is also performed, in which neighboring sectors of the same cell support the MS's connection. Both, soft and softer handovers, can enhance the quality of the connection and increase capacity and coverage area sizes, see Viterbi et al. (1994). Additionally, third generation UMTS will also support *inter-frequency hard handovers* to distribute the load among the frequencies of a cell and *inter-system hard handovers* between UMTS and other systems, e.g. GSM. The following sections provide more details on the soft handover implementations in cdmaOne and UMTS.

### 2.3.1 Soft Handover in cdmaOne

The soft handover mechanism as described in the IS-95 standard for cdmaOne is initiated from the measurements on the downlink channel at the MS. The mobile station registers the pilot signal strength in terms of the chip-energy-to-interference ratio ($E_c/I_0$) of each BS it receives and stores it in one of four exclusive sets: the *active*, *candidate*, *neighbor*, and *remaining* sets. Pilots are added and removed from the sets by comparing them to the following absolute thresholds, see Fig. 2.6(a):

T_ADD A pilot in the neighbor or remaining set is moved to the candidate set, if its $E_c/I_0$ is greater than T_ADD.

T_DROP A pilot in the active or candidate set is moved to the neighbor

set, if its $E_c/I_0$ falls below T_DROP for a period of T_TDROP seconds.

The reason for using two different threshold values is to induce a hysteresis to avoid an oscillation effect of a pilot continuously being added and removed from soft handover.

When an MS is in soft handover, i.e. two or more pilot signals are in its active set, the mobile simultaneously maintains traffic channel connections with these cells. On the downlink the mobile uses the Rake receiver to demodulate and combine the separate signals. On the uplink, the signal from the MS is received by both BSs and the frames are sent back independently to the selector at the BSC and combined there.

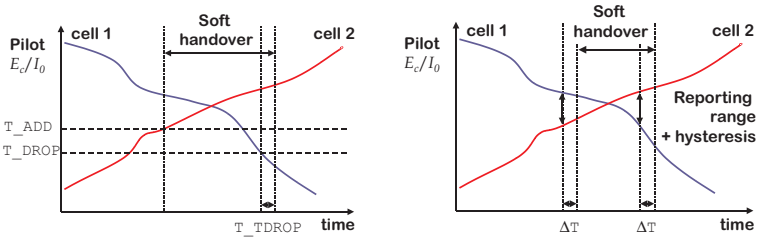


(a) Soft handover in cdmaOne

(b) Soft handover in UMTS

Figure 2.6: *Comparison of different soft handover implementations*

### 2.3.2 Soft Handover in UMTS

The soft handover algorithm that is used in UMTS (3GPP 1999b) differs slightly from the one in cdmaOne, cf. Fig. 2.6(b). While cdmaOne only

has absolute thresholds for set maintenance, UMTS uses a more flexible scheme with relative threshold levels. The following parameters are considered:

- *Reporting range* is the threshold for soft handover.
- *Hysteresis* is an additional margin to avoid the oscillation effect. There are several different hysteresis values for adding, removing, or replacing pilots in the active set.
- $\Delta T$ is the time delay until the update is triggered.

The operations are always performed on the strongest and weakest pilot signals in the active set, as well as the strongest measured cell in the candidate set. When the pilot signal lies in a margin less than the reporting range plus the addition hysteresis to the strongest pilot in the active set for a period of $\Delta T$ the new cell is added provided that the active set is not full. A pilot is removed from the active set, if it falls below the reporting range plus the removal hysteresis from the strongest pilot. Another case is that the active set is full and a pilot in the active cell falls below the strongest pilot in the candidate set. Then the weaker cell is removed from the active set and the one from the candidate set takes its place.

## 2.4 Simple Capacity Equations

In digital communication systems, the link quality is expressed by the bit-energy-to-noise-density ratio $E_b/N_0$. In the following we will describe the received $E_b/N_0$ by the variable $\varepsilon$. This term can be related to the conventional *signal-to-interference ratio* (SIR) $\Gamma$ by

$$\varepsilon = \frac{W}{R}\,\Gamma = \frac{W}{R}\,\frac{S}{I_{\text{total}}}, \tag{2.1}$$

where $S$ is the received signal power, $W$ is the frequency bandwidth, $R$ is the bit rate, and $I_{\text{total}}$ is the total received interference.

In the following, we examine the capacity for a simplified case of the uplink as this is the main focus of our investigation and generally also considered as the limiting link. Simple analytical expressions for the downlink can be found in Gilhousen et al. (1991), Rappaport (1996), Garg (2000), or Holma and Toskala (2000).

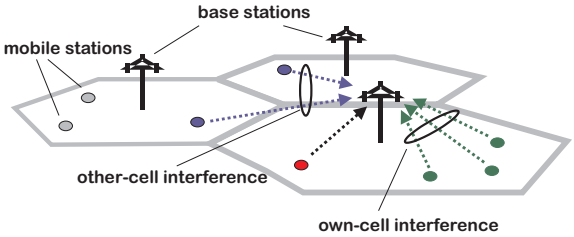


Figure 2.7: *Uplink own-cell and other-cell interference in CDMA*

An example of the uplink scenario is depicted in Fig. 2.7, where the $E_b/N_0$ for a specific user is measured at the BS. In order to evaluate the $E_b/N_0$ value we need to specify $I_{\text{total}}$ in Eqn. (2.1). It can be seen in Fig. 2.1 that the total interference power on the uplink consists of the following contributions:

- background (thermal) noise density $N_0$,
- external interference,
- own-cell (= intra-cell) interference $I_{\text{own}}$, i.e. the interference by other users in the same cell,
- other-cell (= inter-cell) interference $I_{\text{other}}$, i.e. the interference by other users in neighboring cells.

Whereas the first two sources of interference can be found in other wireless systems as well, the latter two are unique to CDMA. This is due to the fact that all users operate in the same RF transmission band. The fundamental capacity equations for the uplink were first given by Gilhousen et al. (1991) and are summarized in Viterbi (1995). In order to simplify the calculation, no other-cell interference is at first taken into account. Further studies by Viterbi, Viterbi, and Zehavi (1994) or Evans and Everitt (1999) extend these models to include the computation of the other-cell interference.

In the following, we will follow the derivation by Garg (2000). Let us consider a single cell loaded with $K$ users that are in power control with the base station. The total interference power for user $i$ is composed of the received signal powers $S_j$ from all other users in the cell

$$I_{\text{total}} = \sum_{j=1, j\neq i}^{K} \frac{\nu S_j}{W} + N_0, \tag{2.2}$$

where $\nu$ is the (voice) activity factor. Voice activity detection of the speech encoder causes that data is only transmitted at full rate when the user actively speaks. In silence periods the data rate is reduced to a much lower level and thus less interference is created.

If we assume perfect power control, all users are received with exactly the same signal power $S$. We can now simplify Eqn. (2.2) as

$$I_{\text{total}} = \frac{(K-1)\,\nu S}{W} + N_0. \tag{2.3}$$

Inserting Eqn. (2.3) in Eqn. (2.1), the $E_b/N_0$ on the uplink can be given for an arbitrary user as

$$\varepsilon = \frac{W}{R}\,\frac{S}{N_0 W + (K-1)\,\nu S} \tag{2.4}$$

Solving Eqn. (2.4) for $K$ yields the capacity in terms of the number of

users in the system

$$K = 1 + \frac{W}{R}\left(\frac{1}{\nu\varepsilon}\right) - \frac{N_0 W}{\nu S}. \tag{2.5}$$

Note that this is only a rough approximation that considers a single cell without any interference from neighboring cells. To roughly include the effects from the surrounding cells we at first need to introduce the *loading factor* $\eta$. This term indicates the increase in interference above the own-cell interference due to the neighboring cells. A related value to $\eta$ is the *frequency reuse factor* $F$,

$$F = \frac{1}{1+\eta}.$$

For a single cell, the reuse factor is then 1 and the loading is 0. When multiple cells are considered, the cell loading $\eta$ increases and $F$ decreases. A typical value of $\eta = 0.6$ is often found in the literature, see Ojanperä and Prasad (2001).

If we include the loading factor $\eta$ from the other cells, Eqn. (2.4) becomes

$$\hat{\varepsilon} = \frac{W}{R}\,\frac{S}{N_0 W + (K-1)\,\nu S\,(1+\eta)}. \tag{2.6}$$

Again, we can solve for $K$ and then get

$$K = 1 + \frac{W}{R}\left(\frac{1}{\nu\varepsilon\,(1+\eta)}\right) - \frac{N_0 W}{\nu S\,(1+\eta)}. \tag{2.7}$$

For a limit of $S \to \infty$, i.e. if we assume unlimited received powers, the last term in Eqn. (2.7) approaches zero and a maximum of $K$ is reached at

$$k_{\text{pole}} = 1 + \frac{W}{R}\left(\frac{1}{\nu\varepsilon\,(1+\eta)}\right), \tag{2.8}$$

which is called the *pole capacity* of the system.

We can also solve Eqn. (2.6) for $S$ to obtain the required received power of the MS and get

$$S = \frac{\varepsilon N_0 W}{\frac{W}{R} - (K-1)\,\nu\,(1+\eta)\,\varepsilon}. \tag{2.9}$$

We should keep in mind that Eqn. (2.6) only considers a single cell with a single class of service and is therefore only of limited use in UMTS capacity evaluation. For instance, in a 3G network the pole capacity would not be expressed by the number of users, but rather by the total data rate per cell. In Chapter 5 we will give a more detailed analysis of the uplink capacity in the presence of spatially distributed users.

# 3 Theoretical Aspects of Power Control

The simple capacity equations of Section 2.4 have shown that CDMA systems require a control of the transmission powers in order to reduce the overall interference in the system. In general, the problem is related to both link directions, uplink and downlink. However, as our focus in this monograph lies in the investigation of the uplink, we will always assume an uplink scenario, where the transmitters are the MS and the receiver is the BS. In this chapter we discuss theoretical aspects of power control that can be found in the literature. Since a large amount of this work was presented by Jens Zander of the KTH Stockholm, we will follow Zander and Kim (2001) as our main reference in notation and definitions.

## 3.1 Problem Formulation

Let us consider a receiver $i$ and a transmitter $j$ with a link gain $G_{ij}$ between $i$ and $j$. Further, assume there are $K$ transmitters, where transmitter $j$ uses a power $P_j$. We can arrange all transmission powers of the

transmitters as a transposed vector

$$P = (P_1, \ldots, P_K)^T .$$

In Section 2.4 we already encountered the formulation of the SIR which is now considered at the receiver $i$,

$$\Gamma_i = \frac{G_{ii}\, P_i}{\sum\limits_{j=1, j\neq i}^{K} G_{ij}\, P_j + n_i}, \tag{3.1}$$

where $n_i$ denotes the noise power at receiver $i$.

The transmitter $i$ is said to be *supported* if it has a SIR satisfying

$$\Gamma_i \geq \gamma_i , \tag{3.2}$$

where $\gamma_i$ is a target threshold indicating the lowest acceptable link quality for user $i$. Combining Eqns. (3.1) and (3.2) and solving for $P_i$ yields the minimal transmission power that transmitter $i$ should use to achieve the target SIR,

$$P_i \geq \gamma_i \left( \sum_{j=1, j\neq i}^{K} \frac{G_{ij}}{G_{ii}}\, P_j + \frac{n_i}{G_{ii}} \right). \tag{3.3}$$

In order to formulate the power control inequalities for all users, we introduce a $K \times K$ non-negative normalized link gain matrix $\mathbf{H}$ with entries

$$H_{ij} = \begin{cases} \gamma_i \, \frac{G_{ij}}{G_{ii}}, & i \neq j \\ 0, & i = j \end{cases} \tag{3.4}$$

and the normalized noise vector $N$ with entries $N_i = \gamma_i \frac{n_i}{G_{ii}}$. The Eqn. (3.3) can now be expressed with the new variables as

$$P_i \geq \sum_{j=1}^{K} (H_{ij}\, P_j + N_i) \tag{3.5}$$

and thus leads to a matrix notation for all $K$ inequalities

$$(\mathbf{I} - \mathbf{H})\ P \geq N, \tag{3.6}$$

where **I** is the identity matrix and the inequality comparison between two vectors represents a componentwise comparison between the entries of both vectors.

It can be observed that in some cases if the target SIR or the link gain increases, not all users can be accommodated by the system. One of the main goals of power control is therefore to find a power vector such that the number of supported users is maximized. This feature is reflected in the following definition.

**Definition 3.1**
*The target SIR $\gamma_i$ is said to be **achievable** if there exists a non-negative power vector $P$ such that $\Gamma_i \geq \gamma_i$ for all $i$.*

Zander and Kim (2001) show that $\gamma_i$ is achievable if the dominant eigenvalue of the matrix **H** is less than or equal to one. In case it is one, the target SIR is only achievable when the receiver noise is zero.

So far only the transmitter power was considered as adjustable factor for the radio resource management. This is true for 2nd generation wireless systems. 3G systems, however, offer multimedia services and, thus, the transmission data rate and the quality of service also become adjustable radio resources. This leads to the possibility of a joint power-rate-QoS control, see Yanikömeroglu (2000). We will discuss this type of power control in Section 3.5.

In summary, the goal of power control can be perceived as finding the power vector $P$ and the rate vector $R = (R_1, \ldots, R_K)^T$ that will satisfy the QoS, power, and rate constraints

$$\Gamma_i \geq \gamma_i \qquad 0 < P_i \leq P_i^{\max} \qquad R_i \geq R_i^{\min} \qquad \forall i, \tag{3.7}$$

where $P_i^{\max}$ is the maximum allowable transmission power for user $i$ and $R_i^{\min}$ is the minimum required bit rate for MS $i$.

If there is more than one solution of Eqn. (3.7), an optimization is necessary to find the vectors $P$ and $R$.

$$\min_{P,R} \sum P_i \qquad \text{or} \qquad \max_{P,R} \sum R_i \tag{3.8}$$

$$\text{subject to} \quad \Gamma \geq \gamma, \qquad 0 < P \leq P^{\max}, \qquad R \geq R^{\min},$$

Here $\gamma = (\gamma_1, \ldots, \gamma_K)^T$ is a vector containing the minimum required SIR for all users and $R^{\min}$ and $P^{\max}$ are vectors with the rate and power bounds.

There are in general three different categories of approaches to solving the power control problem. These methods depend on the link information that is available at the computation time. The methods are shown in Figure 3.1 and consist of the *centralized*, *cooperative*, and *distributed* methods.

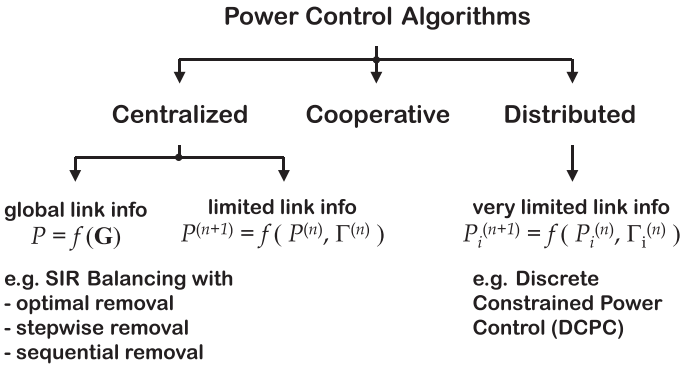


Figure 3.1: *Overview of power control algorithms*

The centralized power control methods assume a global knowledge of the link gain matrix **G** and permit an instantaneous computation of the entire power vector $P$. Although an optimum solution is possible with this method, it has several drawbacks which make it less practical for implementation.

Due to these drawbacks, other algorithms are considered that require less link information and therefore also a more limited data flow, such as the cooperative or the distributed algorithms. However, this limited link information leads to a decrease in performance as well. The following sections provide a detailed introduction to all three methods.

## 3.2 Centralized Power Control

In order to find a solution to the power control problem, the first approach we discuss is the class of centralized algorithms. In this category, the entire power vector $P$ is controlled by a central controlling unit. This unit requires that each base station reports the current link information in order to perform the power assignments for the whole (or parts) of the network. The information of each link is stored in a global link gain matrix **G** which permits the computation of an optimal assignment. However, the drawbacks are a significant amount of control information, introduced delays, and the high complexity due to finding a solution for the entire network.

The centralized approach is based on Aein (1973) dealing with satellite communication. Here, the term SIR balancing is introduced which leads to the formulation as an eigenvalue problem. Nettleton and Alavi (1983) extended this approach to spread spectrum communication systems and showed that SIR balancing substantially improves the capacity of the system. Zander (1992b) discussed that centralized algorithms can be considered as the optimal solutions to power control in the sense that the interference is minimized.

### 3.2.1 Centralized SIR-Balanced Power Control

We consider now Eqn. (3.6) and our goal is to maximize the minimum SIR in all links. It can be proved that such a power control is achieved by making every transmitter's received SIR balanced while keeping the SIR level as high as possible, see Zander and Kim (2001). For the sake of simplicity we consider a noise-less case in the following, i.e. $N = 0$, and the same target SIR value for all users, i.e. $\gamma_i = \gamma_0$ for all $i$ .

Let us define a matrix $\mathbf{A}$, such that $\mathbf{H} = \gamma_0 \mathbf{A}$. Zander and Kim (2001) give a proof that the inequality

$$(\mathbf{I} - \gamma_0 \mathbf{A}) \geq 0 \tag{3.9}$$

has solutions in $P \geq 0$ if and only if

$$\gamma_0 \leq \frac{1}{\rho(\mathbf{A})} = \gamma^*, \tag{3.10}$$

where $\rho(\mathbf{A})$ is the dominant eigenvalue of matrix $\mathbf{A}$. The power vector satisfying Eqn. (3.9) with equality and achieving the largest SIR $\gamma^*$ for all links is $P^*$, i.e. the eigenvector corresponding to the eigenvalue $\rho(\mathbf{A})$.

If the maximum achievable SIR $\gamma^*$ lies for all links above the target SIR $\gamma_0$, all links reach acceptable performance. On the other hand, if $\gamma^* < \gamma_0$, all links would drop below $\gamma_0$ and SIR balancing would be catastrophic, see Fig. 3.2 taken from Zander and Kim (2001). The occurrence of such an event is an indication that the channel can not support the number of links. In such a case it is necessary to remove certain terminals in order to maximize the number of connections with sufficient SIR.

### 3.2.2 Transmitter Removal Methods

We now provide an overview over transmitter removal algorithms, where users are removed from the system in order to achieve a sufficient SIR balancing for all other users. In the following we add a subscript index to

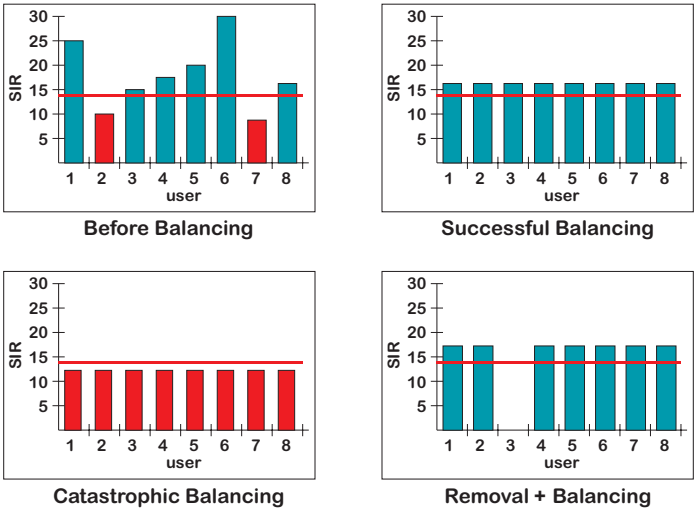


Figure 3.2: *Example of SIR Balancing for eight users*

the values which indicates the number of users that are SIR-balanced, i.e. $\mathbf{A}_{(K)}$ denotes the matrix $\mathbf{A}$ from Eqn. (3.9) for $K$ users and is thus $K \times K$ in dimension.

### Brute-Force Algorithm

The first method we consider is by Zander (1992b) and can be considered the most fundamental algorithm. The *Brute-Force Algorithm* (BFA) is considered to be an optimum removal algorithm as it tries to find a largest square submatrix of $\mathbf{A}$ by removing as few MSs as possible. However, this problem is NP-complete and therefore without heuristics not suitable for practical implementation.

**Brute-Force Algorithm (BFA)**

1. Determine $\gamma^*$ corresponding to matrix $\mathbf{A}_{(K)}$.
   If $\gamma^*_{(K)} \geq \gamma_0$ use the eigenvector $P^*_{(K)}$ and terminate.

2. Set $k = 1$.
   While $k < K$,
   Find the submatrix $\tilde{\mathbf{A}}_{(K-k)}$ that will yield the highest achievable SIR $\tilde{\gamma}_{(K-k)}$.
   If $\tilde{\gamma}_{(K-k)} \geq \gamma_0$, then use $\tilde{P}^*_{(K-k)}$ and terminate,
   otherwise set $k = k + 1$.

### 3.2.3 Stepwise Removal Algorithm (SRA)

In the *Stepwise Removal Algorithm (SRA)*, see (Zander and Kim 2001), the MS $k$ is removed for which the maximum of the row and column sums is maximized.

**Stepwise Removal Algorithm (SRA)**

1. Determine $\gamma^*$ corresponding to matrix $\mathbf{A}_{(K)}$.
   If $\gamma^*_{(K)} \geq \gamma_0$ use the eigenvector $P^*_{(K)}$ and terminate.

2. Set $k = 0$ and $\tilde{\mathbf{A}}_{(K)} = \mathbf{A}_{(K)}$.
   While $k < K$,
   form submatrix $\tilde{\mathbf{A}}_{(K-k-1)}$ from $\tilde{\mathbf{A}}_{(K-k)}$ by removing MS $\ell$ for which

$$\max\left\{\tilde{a}_\ell = \sum_{j=1}^{K-k} \tilde{\mathbf{A}}_{\ell j}, \tilde{a}_\ell^T = \sum_{j=1}^{K-k} \tilde{\mathbf{A}}_{j\ell}\right\} \geq \max\left\{\tilde{a}_i, \tilde{a}_i^T\right\}, \forall i$$

   If $\tilde{\gamma}_{(K-k-1)} \geq \gamma_0$, then use $\tilde{P}^*_{(K-k-1)}$ and terminate,
   otherwise set $k = k + 1$.

The SRA seeks to maximize the lower bound for $\gamma^*$ and shows linear complexity in the computation of the eigenvalues. However, full knowledge of the link gain matrix is necessary in order to calculate its eigenvalues.

### Stepwise Maximum-Interference Removal Algorithm (SMIRA)

Another variation of a transmitter removal algorithm is given in Lee, Lin, and Su (1995). This method is called the *Stepwise Maximum-Interference Removal Algorithm* (SMIRA) and considers also the transmitter power for the removal process. The idea behind this method is that MSs transmitting with a high power should be remove first as they cause the highest interference.

**Stepwise Maximum-Interference Removal Algorithm (SMIRA)**

1. Determine $\gamma^*$ corresponding to matrix $\mathbf{A}_{(K)}$.
   If $\gamma^*_{(K)} \geq \gamma_0$ use the eigenvector $P^*_{(K)}$ and terminate.

2. Set $k = 0$, $\tilde{\mathbf{A}}_{(K)} = \mathbf{A}_{(K)}$, and $\tilde{P}_{(K)} = P_{(K)}$.
   While $k < K$,
   form submatrix $\tilde{\mathbf{A}}_{(K-k-1)}$ from $\tilde{\mathbf{A}}_{(K-k)}$ by removing MS $\ell$ for which for all $i$

$$\max\left\{\tilde{a}_\ell = \sum_{j=1}^{K-k} \tilde{P}_j \, \tilde{\mathbf{A}}_{\ell j}, \tilde{a}_\ell^T = \sum_{j=1}^{K-k} \tilde{P}_\ell \, \tilde{\mathbf{A}}_{j\ell}\right\} \geq \max\left\{\tilde{a}_i, \tilde{a}_i^T\right\}$$

   If $\tilde{\gamma}_{(K-k-1)} \geq \gamma_0$, then use $\tilde{P}^*_{(K-k-1)}$ and terminate,
   otherwise set $k = k + 1$.

The transmitter removal methods are not limited to centralized methods, but can also be used in combination with the distributed methods which will be presented in the following section.

## 3.3 Distributed Power Control

So far it was assumed that the link gain matrix **G** is known and that the power assignments can be done with the knowledge of **G**. However, in reality this is not feasible. Foschini and Miljanic (1993) therefore suggested an iterative method which is based on the Jacobi relaxation method used in linear algebra.

Assume that we have an ideal situation in Eqn. (3.6) with minimum transmission powers of all users.

$$(\mathbf{I} - \mathbf{H})\ P = N \tag{3.11}$$

We further assume that the receiver noise is not negligible and a solution $P^* > 0$ exists. This implies that $\rho(\mathbf{H}) < 1$ and that the matrix $(\mathbf{I} - \mathbf{H})$ is non-singular. Then we can give the solution of the power vector as

$$P^* = (\mathbf{I} - \mathbf{H})^{-1}\ N \geq 0 \tag{3.12}$$

The Jacobi relaxation method provides an iterative solution by using two matrices **L** and **M** and iterating over $P^{(n)}$ for $n = 0, 1, \ldots$.

$$P^{(n+1)} = \mathbf{L}^{-1}\,\mathbf{M}\,P^{(n)} + \mathbf{L}^{-1}\,N, \tag{3.13}$$

where

$$P^* = \mathbf{L}^{-1}\,\mathbf{M}\,P^* + \mathbf{L}^{-1}\,N. \tag{3.14}$$

Replacing the matrices **L** and **M** by **I** and **H** yields the *Distributed Power Control* (DPC) method for $n = 0, 1, \ldots$.

$$P^{(n+1)} = \mathbf{H}\,P^{(n)} + N \tag{3.15}$$

$$\begin{aligned} P_i^{(n+1)} &= \frac{\gamma_0}{G_{ii}} \left( \sum_{j=1, j\neq i}^{K} G_{ij}\,P_j^{(n)} + N_i \right) \\ &= \frac{\gamma_0}{\gamma_i^{(n)}}\,P^{(n)} \end{aligned} \tag{3.16}$$

On the convergence of DPC, Zander and Kim (2001) state that for an achievable target SIR $\gamma_0$, the error vector $\epsilon^{(n)} = P^{(n)} - P^*$ tends to the zero vector starting with any $\epsilon^{(n)}$ if and only if $\rho\left(\mathbf{L}^{-1}\,\mathbf{M}\right) < 1$.

### 3.3.1 Interference Function

A generalized formulation of Eqn. (3.15) can be given with the *interference function*,

$$P^{(n+1)} = I\left(P^{(n)}\right), \tag{3.17}$$

where $I(P) = I(I_1(P), \ldots, I_K(P))$ is the interference function, where $I_j(P)$ denotes the effective interference of other users that must be overcome by the transmitter power of user $j$.

**Definition 3.2**
*Assuming positive receiver noise, an interference function $I(P)$ is called* ***standard*** *if it satisfies for all non-negative power vectors:*

| | |
|---|---|
| *Positivity* | $I(P) > 0$ |
| *Monotonicity* | $P \geq P' \Rightarrow I(P) \geq I\left(P'\right)$ |
| *Scalability* | $\forall \alpha > 1, \quad \alpha\, I(P) > I(\alpha\, P)$ |

The sequence of power vectors from the standard interference function will converge to the solution of Eqn. (3.11) starting with any non-negative power vector, when the system of Eqn. (3.11) has the unique non-negative solution $P^*$.

According to Definition 3.2 the DPC belongs to the class of standard interference functions. Further examples of standard interference functions are given in the literature, see Yates (1996).

### Fixed Assignment

The assignment of an MS $j$ to BS $i$ is fixed or specified by outside means, e.g. the received pilot signal strength.

$$P_j \geq I_j^{\mathrm{FA}}(P) = \frac{\gamma_j}{\Gamma_{ij}(P)}$$

The centralized methods by Aein (1973) and Nettleton and Alavi (1983) as well as the distributed approaches by Foschini and Miljanic (1993) use this interference function for the synchronous case. Mitra (1994) proves geometric convergence for an asynchronous power control approach.

### Minimum Power Assignment (MPA)

At each iteration step, MS $j$ is assigned to the BS at which its SIR is maximized and where the minimum power is required to reach the target SIR $\gamma_j$. MPA can be also considered a generalization of soft handover and was investigated among others by Yates and Huang (1995) and Hanly (1995).

$$P_j \geq I_j^{\mathrm{MPA}}(P) = \min_i \frac{\gamma_j}{\Gamma_{ij}(P)}$$

### Macro Diversity Reception

In Hanly (1993) the signals from user $j$ are received with maximum ratio combining at all BSs leading to the SIR constraint. This method is based on the assumption that the interfering signals at different BSs appear to user $j$ as independent noise.

$$P_j \geq I_j^{\mathrm{MD}}(P) = \frac{\gamma_j}{\sum_i \Gamma_{ij}(P)}$$

### 3.3.2 Constrained Power Control

So far the transmitter power was assumed to be adjustable without limitations. In reality, however, due to the limited transmitter power, an upper bound exists. This leads to the introduction of the following constraint:

$$0 \leq P \leq P^{\max}, \tag{3.18}$$

where $P^{\max} = (P_1^{\max}, \ldots, P_K^{\max})$ is the vector of each transmitter's maximum power boundary.

The *Distributed Constrained Power Control* (DCPC) belongs to the class of standard interference functions and is given as:

$$P_i^{(n+1)} = \min\left\{ \frac{\gamma_0}{\gamma_i^{(n)}} P_i^{(n)}, P_i^{\max} \right\} \qquad n = 0, 1, \ldots \tag{3.19}$$

With Eqn. (3.19) a transmitter is limited by the maximum power when trying to achieve the target SIR. Unfortunately, the observed user may not recover very fast from his bad link situation and transmits for a longer period with maximum power. This in turn could cause severe interference for the other users and therefore, Zander and Kim (2001) recommend a more general variant of the DCPC which sets the power to a predefined value $\tilde{P}_i$ rather than the maximum value $P_i^{\max}$.

$$P_i^{(n+1)} = \begin{cases} \frac{\gamma_i}{\gamma_i^{(n)}} P_i^{(n)} & \text{if } \frac{\gamma_i}{\gamma_i^{(n)}} P_i^{(n)} \leq P_i^{\max} \\ \tilde{P}_i & \text{if } \frac{\gamma_i}{\gamma_i^{(n)}} P_i^{(n)} > P_i^{\max} \end{cases}, \tag{3.20}$$

where $0 \leq \tilde{P}_i \leq P_i^{\max}$. Note that Eqn. (3.20) does not satisfy the second condition of the standard interference function.

The constrained power control algorithm Eqn. (3.20) will converge to the solution of Eqn. (3.6) starting with any non-negative power vector, when the system Eqn. (3.6) has the unique solution $P^*$ within the power range in Eqn. (3.18).

### 3.3.3 Distributed SIR-Balancing and Transmitter Removal

Similar like in Section 3.2.1 for the centralized method, a SIR balancing can be performed for the distributed approach as well.

Zander and Kim (2001) present the *Distributed Balancing Algorithm* (DB) with the following iteration step.

$$P_i^{(n+1)} = \beta \cdot P_i^{(n)} \left(1 + \frac{1}{\gamma_i^{(n)}}\right) \qquad n = 0, 1, \ldots, \tag{3.21}$$

where $\beta > 0$ is a constant for tuning the convergence. It is shown in Zander (1992a) that

$$\lim_{n\to\infty} P^{(n)} = P^* \qquad \text{and} \qquad \lim_{n\to\infty} \gamma^{(n)} = \gamma^*$$

starting with any arbitrary power vector.

One problem that arises is that in DB all transmitter powers increase if not correctly balanced by the parameter $\beta$. The selection of

$$\beta = \beta^{(n)} = \frac{1}{\sum_{i=1}^{K} P_i^{(n)}} \qquad n = 1, 2, \ldots$$

ensures a constant sum of all terminal powers.

The question how to react when the target SIR is not achievable within the power range arises here as well. In congested situations when the interference level is high, users should also be removed like in the centralized case. As previously mentioned the algorithms from Section 3.2.2 can be used to perform transmitter removal in distributed power control.

## 3.4 Cooperative Power Control

The methods by Zander (1992a) and Grandhi, Vijayan, and Goodman (1994) described in the previous section require a normalization factor to

scale the user's power to a desired range without which no convergence can be achieved. Although both methods belong to the category of distributed power control algorithms, the computation of this normalization factor requires in both cases global link information.

To avoid this shortcoming of a global information exchange, Wong and Lam (1994) propose the *Cooperative Power Control* algorithm, where only limited control data flows are passed among the BSs which are interconnected by a wired backbone network. The underlying network structure, which the authors refer to as *control data flow structure* is represented as a directed graph. The aim is to keep the information exchange due to control data traffic to a minimum.

### 3.4.1 Basic Cooperative Power Control

The basic algorithm starts with each MS transmitting at the maximum power level $P_i^{\max}$, which is then reduced until convergence is reached. At each iteration step, every BS computes its current power level based on the level from the previous iteration, its current SIR, and the SIR information it receives from its neighbors within the control data flow structure. Each MS $i$ adjusts its power then according to the following rules:

$$
\begin{aligned}
P_i^{(0)} &= P_i^{\max} \\
P_i^{(n+1)} &= \alpha_i^{(n)} \, P_i^{(n)} \\
\text{where} \quad \alpha_i^{(n)} &= \sqrt[m]{\frac{\min\left(\Gamma_i^{(n)}, \max\left(\min_{j \in \mathcal{N}_i} \Gamma_j^{(n)}, \gamma_0\right)\right)}{\Gamma_i^{(n)}}},
\end{aligned}
$$

with $\mathcal{N}_i$ being the set of indices of BS that send control data information to BS $i$ according to the control data flow structure. The purpose of the parameter $m \geq 1$ is to control the rate of convergence.

### 3.4.2 Modified Cooperative Power Control Algorithm

This basic approach is later extended by Sung and Wong (1999) with the difference that the algorithm does not start with the maximum power and iteratively decreases the power until convergence, but instead it starts with the minimum power and monotonically adjusts the level upward until the SIRs are balanced. The advantages of this variation is that less battery power is used and that the disturbance to the balanced system by the admission of a new user is minimized.

$$
\begin{aligned}
P_i^{(0)} &= P^{\min} \\
P_i^{(n+1)} &= \alpha_i^{(n)} \, P_i^{(n)} \\
\text{where} \quad \alpha_i^{(n)} &= \sqrt[m]{\frac{\min\left(\Gamma_i^{(n)}, c \, \max\limits_{j \in \mathcal{N}_i} \Gamma_j^{(n)}, \gamma_0\right)}{\Gamma_i^{(n)}}},
\end{aligned}
$$

Here, a constant $c$ is additionally introduced for the convergence of the algorithm. The condition $c < 1$ ensures that the limit $\lim_{n\to\infty} P_i^{(n)}$ exists and therefore converges to a fixed point. The condition $c < 1 - \epsilon$ for an arbitrary small value $\epsilon$ ensures that the fixed point achieves SIR balancing.

### 3.4.3 Asynchronous Cooperative Power Control

The cooperative algorithms presented so far require a synchronous operation of the power updates. An extension to asynchronous operation is presented in Sung and Wong (1999) as well. This permits that power levels can be changed in different time and rate among each link and the control data for the SIRs can be sent at a different rate than the power updating. The modified algorithm of the cooperative power control just needs to replace the synchronous SIR measurements $\Gamma_i^{(n)}$ by delayed SIR

measurements $\tilde{\Gamma}_j^{(i,n)} = \Gamma_j^{(n-d_{ij})}$ for some delay $d_{ij} \leq d_{\max}$ bounded by the maximum delay $d_{\max}$.

Convergence of the asynchronous approach to finite values is proved by Sung and Wong (1999), however, it is required that the rate of convergence must be faster than the rate changes in the link gain matrix, e.g. due to shadow fading. Additionally, studies were performed that investigated the convergence behavior. When users depart from the system and all other users have high SIR values above a certain requirement $\tilde{\gamma}$ (protection ratio), the SIR balancing will result in unnecessary high SIR values for the users. Since all users already had satisfying SIR levels, a further increase is not necessary. Therefore, the cooperative algorithm can be further modified to also avoid this effect:

$$P_i^{(0)} = \bar{P}^{\min}$$

$$P_i^{(n+1)} = \alpha_i^{(n)} \, P_i^{(n)}$$

$$\text{where} \quad \alpha_i^{(n)} = \begin{cases} \sqrt[m']{\dfrac{\max\left(\Gamma_i^{(n)}, c \max\limits_{j \in \mathcal{N}_i} \Gamma_j^{(n)}, \gamma_0\right)}{\Gamma_i^{(n)}}}, & \text{if } \Gamma_i^{(n)} \leq \gamma_0 \\ \sqrt[m']{\dfrac{\gamma_0}{\Gamma_i^{(n)}}}, & \text{otherwise.} \end{cases}$$

Here, we again use $\gamma_0 \geq \tilde{\gamma}$ as the target SIR. With this modification the transmit power of an MS will decrease if its received SIR at the BS is higher than $\gamma_0$. Therefore, in a dynamic situation with a fluctuation of users entering and leaving the system, the power levels of the users in the system will not go to infinity.

## 3.5 Joint Power and Rate Control

So far the same target SIR was assumed for all users. This is a valid assumption when considering second generation systems with only a single

class of users. However, in 3G systems each user will access different services with different transmission rates and error requirements. Therefore, the radio resource management needs to assign each user his own target SIR level.

Rate adaptation sets the data rate $R_i$ of user $i$ with a monotonically increasing modem-dependent function $f(\gamma_i)$ of the SIR $\gamma_i$

$$R_i \leq f\left(\gamma_i\right).$$

The following two definitions are given by Zander and Kim (2001) to describe if a rate vector $R(P^{\max})$ is achievable for a maximum power vector $P^{\max}$.

**Definition 3.3**
*A rate vector $R(P^{\max}) = (R_1, \ldots, R_K)$ is **instantaneously achievable** if there exists a positive power vector*

$$P = (P_1, \ldots, P_K) \leq P^{\max}$$

*such that*

$$R_i \leq f\left(\gamma_i\right) \qquad \forall i$$

**Definition 3.4**
*A rate vector $R^*\left(P^{\max}\right) = (R_1^*, \ldots, R_K^*)$ is **achievable in the average sense** if it may be expressed as*

$$R^* = \sum_k \alpha_k \, \tilde{R}_k$$

*where*

$$\alpha_k \in [0, 1] \qquad\qquad \sum_k \alpha_k = 1.$$

*and where all $\tilde{R}_k$ are instantly achievable rate vectors.*

This definition implies using the set of instantly achievable rate vectors $\tilde{R}_k$ and switching between them during a fraction of time $\alpha_k$ in order to get the average rate $R^*(P^{\max})$.

There is also a constraint on the data rate. Unlike the transmission power which is bounded by the performance of the amplifier, each link requires a minimum data rate $R_i^{\min}$. Additionally, the service provider aims at offering as much excess data as possible to his customer. This leads to another optimization problem in the context of joint power and rate control.

$$\begin{aligned} & \max \sum_{i=1}^{K} R_i^*(P^{\max}) \\ \text{subject to} \quad & R_i^*(P^{\max}) \geq R_i^{\min} \qquad \forall i \end{aligned}$$

Work on joint power and rate control in the form of a constraint optimization problem can be found by Sampath, Kumar, and Holtzman (1995). The authors define the optimization problem as

$$\min \sum_{i=1}^{K} P_i \qquad \text{or} \qquad \max \sum_{i=1}^{K} R_i$$

subject to

$$\begin{aligned} \text{QoS constraint:} \quad & \frac{W}{R_i} \frac{P_i G_{ji}}{\sum_{k=1,k\neq i}^{K} P_k G_{jk}} \geq \gamma_i, \qquad \forall i \\ \text{rate constraint:} \quad & R_i \geq R_i^{\min}, \qquad \forall i \\ \text{power constraint:} \quad & 0 < P_i < P_i^{\max}, \qquad \forall i \end{aligned}$$

Note that in this case the SIR in the QoS constraint is understood as $E_b/N_0$[1]. The proposed method is a centralized scheme, where knowledge

[1] The relationship between SIR and $E_b/N_0$ is given in Eqn. (2.1) in Section 2.4.

of the link gain matrix is assumed. The authors consider the following criteria for optimization:

- minimization of the total transmitted power,
- maximization of the sum of the transmission rates.

The given problem can be solved by linear and non-linear programming methods and in the case that the system is not feasible, some users must be rejected or the constraints need to be relaxed.

# 4 Analytical Modeling of Power Control

In Chapter 3 we discussed theoretical models of transmission power control under the assumption that the control loops are operating perfectly. In reality, however, several influencing factors, e.g. fading effects on the transmission channel or processing delays, make it virtually impossible to assign the transmission powers in a perfect way. Therefore, transmission power control in existing systems is realized by a combination of open and closed control loops. In this chapter we derive an analytical model of the closed loop power control in the uplink direction. We begin with a simple model of a single cell and enhance it by including the delays due to the processing of the power control commands. The final model in Section 4.3 considers two inter-operating closed loops, as realized in WCDMA systems.

## 4.1 Inner Loop Model

In Section 2.2 we already briefly introduced the implementation of power control in CDMA-based systems. In this section we derive an analytical model of closed loop power control for a single cell based on a Markov

chain. Since closed loop power control is performed at a fixed update rate, the Markov chain is discrete in time and due to the fixed update steps it is also discrete in state space. The requirements for mobile terminals in the standards (3GPP 2000) specify a maximum transmission power of 21 dBm and a power control range of 65 dB. Furthermore, we assume a fixed update step size of 1 dB (3GPP 1999a).

The first model we consider is similar to the one by Ariyavisitakul and Chang (1993), where simulation studies of single and multi-cell systems were conducted and the dependence of the SIR on step size and processing delays was investigated, see Fig. 4.1.

The transmission power of the MS under observation is in the following denoted by an abstract index $j$, with $0 \leq j \leq J$ where $J$ is the maximum number of possible steps within the given range. Let $P^{(n)}$ be the random variable representing the MS transmit power at power control group $n$.

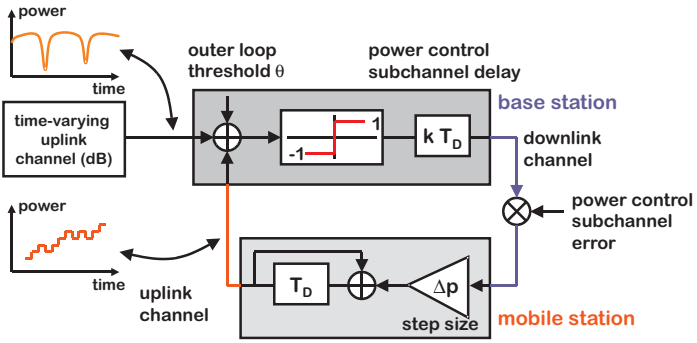


Figure 4.1: *Model of the inner loop*

As depicted in Fig. 4.1, the original MS signal is attenuated on the uplink channel by the channel gain. In our model we describe the channel

gain stochastically by the random variable $G^{(n)}$. At this point we only investigate the inner loop behavior of the closed loop and use a fixed outer loop threshold $\theta$ to determine the power control command for the next PCG. The probability for a power-up command at time cycle $n$ can be computed by comparing the effectively received $E_b/N_0$ with the threshold value $\theta$

$$\Pr[\text{“power-up”}] = \Pr\left[\varepsilon^{(n)} \leq \theta\right]. \tag{4.1}$$

We describe the probabilities for power-up and power-down commands under the condition that the observed MS transmits at level $j$ during PCG $n$ by

$$p_u^{(n)}(j) = \Pr\left[\varepsilon^{(n)} \leq \theta \mid P^{(n)} = j\right] \tag{4.2}$$

$$\begin{aligned} p_d^{(n)}(j) &= \Pr\left[\varepsilon^{(n)} > \theta \mid P^{(n)} = j\right] \\ &= 1 - p_u^{(n)}(j) \end{aligned} \tag{4.3}$$

In the next sections we provide the model of the uplink channel and the multi-access interference term which permit a computation of the Eqns. (4.2) and (4.3).

### 4.1.1 Channel Model and Multi-Access Interference (MAI)

Let us consider the scenario depicted in Fig. 4.2. The observed MS $i$ is located at a distance $x$ from the serving base station and transmits with power $P_i$. On the path to the base station, the signal power is being attenuated by the propagation loss $L(x)$, shadow fading, and multi-path fading and is finally received after a power control subchannel delay $\delta$ with power $S_i$ at the BS. Many models which statistically describe the propagation loss can be found in the literature. Most approaches for macrocell

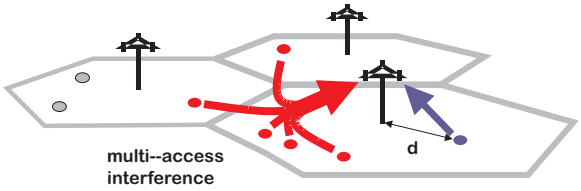


Figure 4.2: *Uplink multi-access interference*

propagation are based on Hata (1980) and consider urban or suburban areas with nearly equal building heights. In the following we will use a similar model given in (ETSI 1998):

$$L(x, f_c, \Delta h_b) = 40\,(1 - 4 \cdot 10^{-3} \Delta h_b)\,\log_{10}(x) - 18\log_{10}(\Delta h_b) + 21\log_{10}(f_c) + 80,$$

where $x$ is the base station to mobile station separation in kilometers, $f_c$ is the carrier frequency, and $\Delta h_b$ is the BS antenna height in meters above the average rooftop level. With a carrier frequency of 2 GHz and a base station antenna height of 15 meters, this equation can be simplified to:

$$L(x) = 128.1 + 37.6\log_{10}(x). \tag{4.4}$$

The result of Eqn. (4.4) is the propagation loss in *decibels* (dB).

Shadow fading is generally modeled using a zero-mean Gaussian random variable with standard deviation of 7–8 dB, see Yang (1998). Therefore, we can characterize the total gain on the uplink channel as a Gaussian random variable $G^{(n)}$ with mean $L(x)$ depending on the distance between transmitter and receiver and the standard deviation $\sigma_G$.

Recalling Eqns. (2.1) and (2.2), we can formulate the received $E_b/N_0$ $\hat{\varepsilon}_i$ of user $i$ as

$$\hat{\varepsilon}_i = \frac{W}{R} \frac{\hat{S}_i}{\sum\limits_{j=1, j\neq i}^{K} \hat{S}_j \nu_j + N}, \tag{4.5}$$

where $N$ is the thermal noise power, i.e. $N = N_0 W$. For the sake of simplicity we will consider at the moment that all users operate with the same data rate $R$. Since we will be considering variables in the following in dB, we will distinguish any power or signal-to-interference ratio $X$ in decibels from its transformation into linear space by using a hat to denote the latter, i.e. $X = 10 \log_{10}(\hat{X})$.

Many publications, e.g. Gilhousen et al. (1991), Veeravalli et al. (1997), or Schröder et al. (2001), have shown that the computation of Eqn. (4.5) is not a very straightforward task especially in the case of many base stations. Obviously, due to the imperfections of power control, all $\hat{S}_j$ values are not equal. Furthermore, as each user's power is controlled to balance the sum of the other users' powers, the variables $\hat{S}_j$ are not independent. In order to compute Eqn. (4.5) we need an approximation that corresponds to $\hat{\varepsilon}$, yet can be computed easily.

Let us define the multi-access interference (MAI) factor $\varphi$ as

$$\varphi = \frac{k_{\text{pole}} - K}{k_{\text{pole}} - 1}. \tag{4.6}$$

Inserting the term for $k_{\text{pole}}$ from Eqn. (2.8) into Eqn. (4.6) and after some simple transformations we obtain

$$\varphi = \frac{N}{N + (K-1)\,\nu \hat{S}\,(1+\eta)}.$$

We can therefore use $\varphi$ to express $\hat{\varepsilon}$ in a very simplified form as

$$\hat{\varepsilon}_i = \hat{S}_i\, \hat{\chi}, \qquad \text{with} \qquad \hat{\chi} = \frac{W\,\varphi}{R\,N}. \tag{4.7}$$

It is clear that $\varphi$ has values between 1 for a single user in the cell and 0, which it reaches when $K$ approaches $k_{\text{pole}}$. In this case the value of $\hat{\varepsilon}$ also approaches 0. Due to the aggregation of the multi-access interference into a single term $\varphi$, we no longer need to distinguish the individual users by their index and we therefore drop the user index $i$ focusing on our observed user. The relative cell loading factor can be given as the inverse of the MAI term, i.e. $\tilde{\rho} = 1/\varphi$.

Since we are especially interested in the behavior of the transmitted power of the observed user we need to describe the relationship between $S$ and $P$. The MS transmits the signal with a power level $P$. While traversing the uplink channel, the signal is being attenuated by the channel gain, see Section 4.1.1. The received signal $S$ can then be given as $S = P\,G$. We can then transform Eqn. (4.7) into decibels and write

$$\varepsilon^{(n)} = P^{(n)} + G^{(n)} + \underbrace{W - R - N + \varphi}_{\chi=\text{constant}}, \tag{4.8}$$

where we keep the term $\chi$ constant over time in our experiments. Since $\chi$ is constant we can simply add this value to the mean of the random variable $G^{(n)}$ to obtain $\mu_G = L(x) + \chi$. Only $\varepsilon^{(n)}$, $P^{(n)}$, and $G^{(n)}$ have a time index $n$.

The probability that a power-up command is sent at time slot $n$ can then be computed by comparing $\varepsilon^{(n)}$ with $\theta$, which we can rearrange to have $G^{(n)}$ on the left side of the inequality:

$$p_u^{(n)}(j) = \Pr\left[G^{(n)} \leq \theta - j\right] \tag{4.9}$$

In the following we assume an *Additive White Gaussian Noise* (AWGN) channel and the loop driving variable $G$ is as mentioned above Gaussian distributed with mean $\mu_G$ and standard deviation $\sigma_G$. This corresponds to a scenario with high MS speed when there is no correlation in the channel fading. Using the properties of the Gaussian distribution,

this probability can be written in a closed form

$$p_u^{(n)}(j) = \frac{1}{2} + \frac{1}{2} \operatorname{erf}\left(\frac{\theta - j - \mu_G}{\sqrt{2}\sigma_G}\right), \tag{4.10}$$

where the Gaussian error function is given as

$$\operatorname{erf}(x) = \frac{2}{\sqrt{\pi}} \int_0^x \exp(-t^2)\, dt. \tag{4.11}$$

If we consider the fading envelope to be distributed according to another distribution, e.g. Rayleigh, we can simply replace Eqn. (4.10) by using the Rayleigh CDF. However, the inclusion of correlated fading requires more complicated methods, e.g. the Memory Markov Chain (MMC) by Rose (1999), and can not be analyzed using standard Markov chain techniques.

Fig. 4.1 shows that the power control command can be affected by errors on the downlink transmission. This can happen especially in cdmaOne, where the command is transmitted without any error protection. In this case we can model the downlink channel as binary symmetrical channel with a bit error probability $p_b$. It is well known that the probability of bit errors in a QPSK modulated channel can be approximated by $p_b = \frac{1}{2}\, Q(\sqrt{\hat{\varepsilon}})$, where $Q(x)$ is the Gaussian Q-Function

$$Q(x) = \frac{1}{\sqrt{2\pi}} \int_x^\infty \exp\left(-\frac{t^2}{2}\right)\, dt. \tag{4.12}$$

In Fig. 4.3(a) the probability of “power-up” commands for given transmission powers levels is depicted. All users operate with a data rate of 12.2 kbps, corresponding to the voice services in UMTS and the cell is lightly loaded ($\tilde{\rho} = 0.2$). Three different cases of the MS-BS distance are considered: 0.5 km, 1 km, and 1.5 km. As expected, it can be seen from

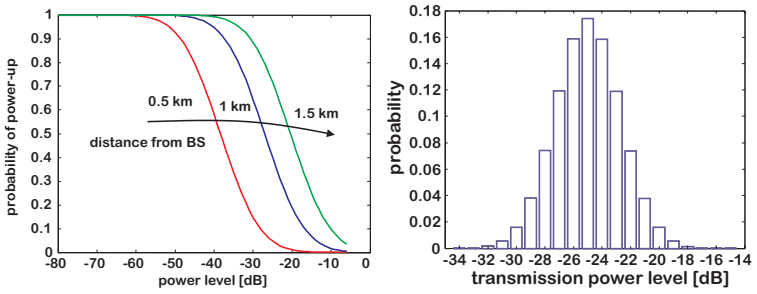


(a) Probabilities of "power-up" commands

(b) Stationary transmission power distribution

Figure 4.3: *Markov chain power control model*

Fig. 4.3(a) that with increasing distance, the user has a greater probability for "power-up" commands in order to overcome the signal attenuation and reach his desired $E_b/N_0$-target level.

With the knowledge of the transition probabilities it is now possible to give a state space diagram of the Markov chain in Fig. 4.4. For this Markov chain the stationary state probabilities

$$z(j) = \Pr[P = j] \qquad j = 0, \ldots, J,$$

can be computed analytically by solving the following matrix equation

$$(z(0), \ldots, z(J)) \cdot (\mathbf{Q} - \mathbf{I}) = 0. \tag{4.13}$$

Here, $\mathbf{I}$ is the identity matrix, $0$ is a row vector with zero entries, and $\mathbf{Q}$ the transition probability matrix with entries $p_u(j)$ and $p_d(j)$.

$$\mathbf{Q} = \begin{pmatrix} p_d(0) & p_u(0) & & & \\ p_d(1) & 0 & p_u(1) & & \\ \ddots & \ddots & \ddots & & \\ & p_d(J-1) & 0 & p_u(J-1) & \\ & & p_d(J) & p_u(J) & \end{pmatrix} \tag{4.14}$$

The stationary transmission power distribution is shown in Fig. 4.3(b) for a 12.2 kbps user located at a distance of 1 km from the BS of a medium loaded cell ($\tilde{\rho} = 0.5$). Due to the Gaussian loop driving function, the transmission power also resembles roughly a Gaussian distribution.

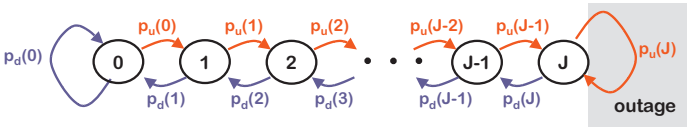


Figure 4.4: *State space of simple Markov model*

### 4.1.2 Outage Events

For the evaluation of the performance we are especially interested in the probability of *outage*. This event occurs whenever the SIR (or $E_b/N_0$) drops below a threshold for a period of time causing that the call is dropped, cf. Mandayam et al. (1996). The evaluation of outage probabilities is among the most important issues in planning the coverage areas of newly rolled-out wireless networks, see Schröder et al. (2001).

Veeravalli and Sendonaris (1999) state two possible causes for outage:

1. the power control equations, see Eqn. (4.5), do not have a feasible solution regardless how high the received powers are, and

2. the power control equations have a feasible solution, but the maximum transmit power of the MS is exceeded.

In line with Veeravalli and Sendonaris (1999) we will refer to the first case as $A_{\text{out}}$ and the second as $B_{\text{out}}$.

It is further shown that the power control equations have a feasible solution, if the following condition is satisfied:

$$\sum_{i=1}^{K} \frac{R_i \hat{\varepsilon}_i^* \nu_i}{W + R_i \hat{\varepsilon}_i^* \nu_i} < 1.$$

The variable $\hat{\varepsilon}_i^*$ denotes the $E_b/N_0$-target level of user $i$. As we are concentrating on the situation where a user is already admitted to the system, we will focus on outage event $B_{\text{out}}$. Clearly, this will happen when the dynamic range is exceeded which we define as *range exceeding* (RE) event. The probability of range exceeding $p_{\text{RE}}$ is identical with the probability of a $B_{\text{out}}$ outage event.

In Fig. 4.4 this will happen when the MS is transmitting with maximum level $J$ and a power-up command is received. At this point the MS can not further increase its power and remains in state $J$. In order to have an outage, we need to have successive range exceeding events, which we will denote by the random variable $Y$. In this simple case, $Y$ is geometrically distributed and we can easily specify the probabilities

$$p_{\text{RE}} = p_u(J), \tag{4.15}$$

$$\Pr[Y = i] = p_u(J)^i \, p_d(J), \qquad i \geq 1. \tag{4.16}$$

Curves for the range exceeding probability are shown in Fig. 4.5(a). With increasing distance the MS is not capable to fulfill its target $E_b/N_0$-requirement within the dynamic range of its transmission power. Additionally, the use of higher data rates increases this effect, leading to a higher probability of outage. In Fig. 4.5(b) the probability of successive

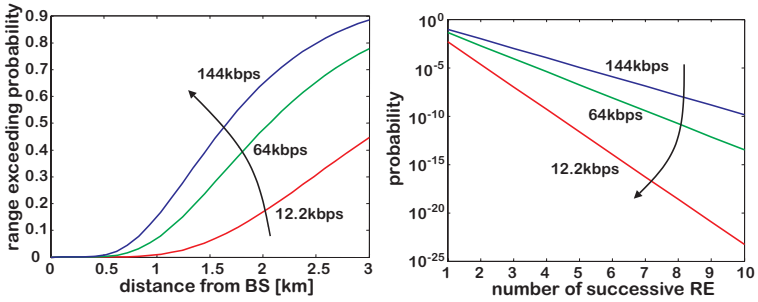


(a) Sensitivity of distance

(b) Probability of successive outages

Figure 4.5: *Range exceeding probability*

range exceeding events is illustrated. An increase in data rate results also here in a higher probability due to the smaller processing gain.

In the next section our focus lies on how we can extend this simple model to include also the processing delays for computing the new power control command.

## 4.2 Modeling of Power Control Delays

So far we have assumed that there is no power control processing delay $\delta$ and that the power update commands are issued directly in the next time slot after the signal is received. However, in a real cdmaOne system the time dependent behavior of the inner loop is greatly influenced by the delay which causes that the power control command will take effect $\delta = 3$ time increments after the power control command was issued, see Leibnitz, Tran-Gia, and Miller (1998). In this specific case, the 3-step delay

results from a delay of $k\,T_D = 2$ at the base station (Fig. 4.1) and a processing delay of 1 time slot at the mobile station, although the model can be extended to any arbitrary delay.

Transitions from one discrete power level to the next take place each cycle and are only performed between adjacent levels. The dependency structure of the power levels for reaching a given level $j$ is illustrated in Fig. 4.6(a).

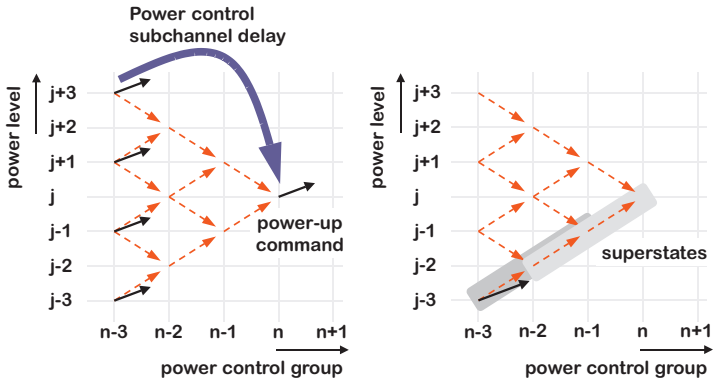


(a) Dependencies of power levels

(b) Super-state transitions

Figure 4.6: *State transitions in power control model*

Fig. 4.6(a) illustrates that the power-up command for level $j$ at time $n$ depends on the probabilities for power-up of the 4 possible states, i.e. power levels, that could have been assumed 3 cycles before, i.e. levels $j+3$, $j+1$, $j-1$, and $j-3$ at time $n-3$. Note that for state $j$ it is not possible to have been in the same state 3 cycles before.

Since the probability for each state at time $n-3$ is computed by an equivalent sub-tree structure, we are also dependent on the probability of

reaching these originating states at time $n-3$. We therefore cannot simply assume that the probabilities $p_u^{(n)}(j)$ are the transition probabilities in our case because we must also include the paths for reaching these states. In order to incorporate these paths as well, we define new super-states $\bar{z}^{(n)}(j_1, j_2, j_3)$ containing 3 successive ordinary states which indicate the sequence that was taken.

$$\bar{z}^{(n)}(j_1, j_2, j_3) = \Pr\left[P^{(n)} = j_3 \mid P^{(n-1)} = j_2, P^{(n-2)} = j_1\right] \tag{4.17}$$

Since we only have transitions between neighboring states to $j_2 = j_1 \pm 1$ and $j_3 = j_2 \pm 1$, we can further limit the state space. In this case we have $4(J+1)$ possible preceding super-states $\bar{z}^{(n-1)}(j_1, j_2, j_3)$ and a transition to super-state $\bar{z}^{(n)}(j_2, j_3, j_4)$ takes place with $p_u^{(n-3)}(j_1)$ or $p_d^{(n-3)}(j_1)$ depending on whether $j_4 = j_3 + 1$ or $j_4 = j_3 - 1$. The transitions between super-states will then look like in Fig. 4.6(b).

Based on these super-state transitions, it is possible to give a state space diagram at time $n$ with the transition probabilities given by $p_u^{(n)}(j)$ and $p_d^{(n)}(j)$, see Fig. 4.7. The transition probabilities at time $n$ can again be arranged in a matrix $\mathbf{Q}^{(n)}$.

### 4.2.1 Stationary Analysis

At first we perform a stationary analysis of the power control loop. Stationary in this sense means that the probability distribution of the random variables $P^{(n)}$ is independent of $n$ and we can drop the index $n$ denoting the power control cycle.

Solution of this Markov process is straightforward, see for example Kleinrock (1975). Since the transition probabilities of these states are given, we can compute the solution of the state probabilities by the following homogeneous linear Eqn. (4.18).

$$(\bar{z}(0,0,0), \ldots, \bar{z}(J,J,J)) \cdot (\mathbf{Q} - \mathbf{I}) = 0 \tag{4.18}$$

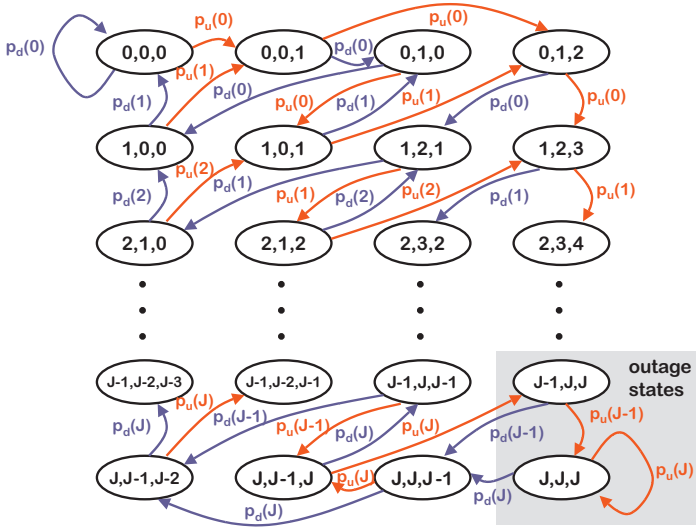


Figure 4.7: *Super-state space of Markov chain*

## Range Exceeding Probability

We can also formulate the range exceeding probability when considering processing delays. Again, this is defined as the probability that channel and / or interference conditions will require the mobile's transmitter to exceed the maximum permissible power. This occurs in the super-states $\bar{z}(J-1, J, J)$ and $\bar{z}(J, J, J)$ as illustrated in Figure 4.7.

The probability to be in an RE state can then be given as

$$p_{\mathrm{RE}} = \bar{z}(J-1, J, J) + \bar{z}(J, J, J).$$

We can easily obtain the distribution of successive range exceedings $Y$

under the condition that we have an RE as

$$\Pr[Y = i \mid \text{RE}] = \begin{cases} p_d(J-1) & i = 1 \\ p_u(J-1)\, p_u(J)^{i-1}\, p_d(J) & i > 1 \end{cases} \tag{4.19}$$

In order to get an unconditioned probability for the number of successive range exceeding cases, we need to uncondition Eqn. (4.19) of $p_{\text{RE}}$.

$$\Pr[Y = i] = \Pr[Y = i \mid \text{RE}]\ p_{\text{RE}} \tag{4.20}$$

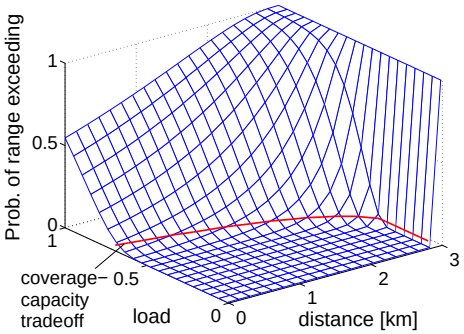


Figure 4.8: *Outage probability sensitivity to distance and load*

The sensitivity of the range exceeding probability to the cell load and the distance of the MS is depicted in Fig. 4.8. It can be seen that even when one of these parameters is zero, outage can occur due to the other parameter. Furthermore, Fig. 4.8 contains a curve indicated “coverage-capacity tradeoff”. This refers to the pair of corresponding load and distance values that reach a maximum tolerable outage probability, in this case 5%. We will deal with greater detail with this sort of tradeoff curves in Chapter 5.

### 4.2.2 Non-stationary Analysis

We now consider a non-stationary case, where we start with an initial mobile transmit power distribution $P^{(0)}$ at time $n = 0$ and iteratively compute the successive power distribution $P^{(n)}$ of the considered user in cycle $n$.

Computation of the power $P^{(n+1)}$ is done in accordance to the scheme described in the previous sections with consideration of the possible transition paths. The new state probabilities $P^{(n+1)}$ can be computed from $P^{(n)}$ by first determining the corresponding super-state vector $\bar{Z}^{(n)}$ and multiplying it recursively with the corresponding transition probability matrix $\mathbf{Q}^{(n)}$[1]

$$\bar{Z}^{(n+1)} = \bar{Z}^{(n)} \cdot \mathbf{Q}^{(n)}.$$

The transformation from $\bar{z}^{(n+1)}(j_1, j_2, j_3)$ to $z^{(n+1)}(j)$ yields the new state probabilities. This can be easily achieved by adding all super-states which have a common last state

$$z^{(n+1)}(j) = \sum_{j_1, j_2} \bar{z}^{(n+1)}(j_1, j_2, j) \qquad j = 0, \ldots, J.$$

Since we are interested in the dynamic behavior of the system, we examine the reaction time until the system converges from one stable condition to another. Our focus lies on the impact of the load currently served within this cell on the convergence of power control.

The choice of the initial vector at time $n = 0$ has a great impact on the speed of convergence in the system. To make sure that the system originates from a steady state and is no longer transient, we need to perform a stationary analysis, in which we derive a power distribution that is independent of the time $n$. This is an estimation for a steady state distribution that we also use in our experiments as initial power for the non-stationary experiments.

[1] This approach is also known as the power method.

Figure 4.9(a) illustrates the non-stationary analysis method. Here, we initially consider a system with load $\tilde{\rho} = 0.25$. At time slot 1 we suddenly increase the load from 0.25 to 0.5 and compare the mean MS transmit power from the stationary analysis (marked as "theoretical") with the one from the non-stationary analysis (marked as "iterative"). Such an event occurs when at the same time many users with low data rate or few users with high bit rate enter the system. It can be seen that the non-stationary mean overshoots the target value and converges after oscillating around the theoretical mean. If the distance between both distribution vectors is less than $10^{-5}$ for a window of 10 PCGs, we will consider the system to have stabilized. The time for the system to recover after a sudden change in the load also depends on the level of increase, as can be seen from Fig. 4.9(b). In this figure, a longer time is required for the system to regain stability when the load increase is larger.

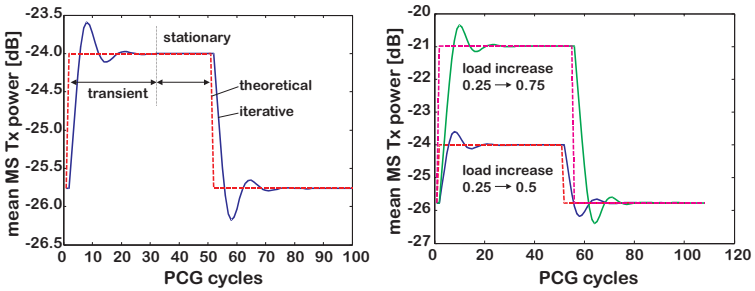


(a) Mean MS power

(b) Increase of load from 0.25

Figure 4.9: *Mean MS power from the non-stationary analysis*

Similar to the study from Leibnitz, Tran-Gia, and Miller (1998) where the influence of batch arrivals of users in a cdmaOne system was inves-

tigated, we consider the case when the load is suddenly increased or decreased. As stated before, due to the different data rates of the users in a 3G system, it is more useful to consider the load here than simply the number of users.

We will assume an already "perfectly" power controlled cell obtained by the stationary analysis with different initial load ($\tilde{\rho} = 0.25$, $0.5$, and $0.75$). Then, we increase or decrease the load for each of these cells to a certain target load as shown in the abscissa of Figures 4.10(a) and 4.10(b). In both cases the observed user is located at a distance of 1 km from the BS and transmits with a bit rate of 12.2 kbps. The staircase shape in both figures stems from the fact that we have a discrete number for necessary power control cycles.

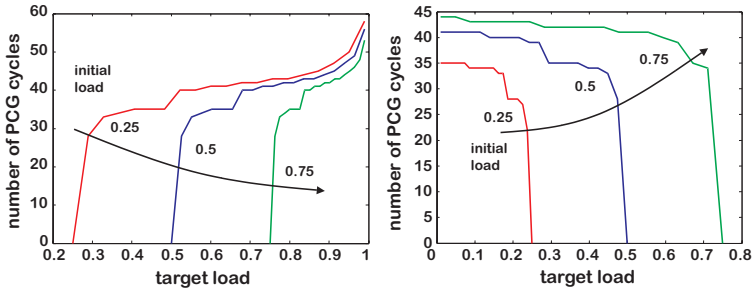


(a) Increase of load

(b) Decrease of load

Figure 4.10: *Convergence time for variation of load*

In Fig. 4.10(a) we increase the load of a system with an initial load of 0.25, 0.5, and 0.75, respectively. It is obvious that the higher the increase is, the more time to converge to a stable state is required. It should be noted

that when we near a fully loaded cell ($\tilde{\rho} > 0.9$), there is a steep increase in the number of cycles. The reason for this effect lies in the increased occurrences of outage which need to be compensated by the loops. Fig. 4.10(b) shows the analogous case when we remove a fraction of the load from the system. It can be seen that the system requires also nearly a constant number of steps when we remove a fraction of the load. Of course the stability problems that we encountered when reaching the full load do not arise.

### 4.2.3 Investigation of Arbitrary Processing Delays

We are now interested in the influence of the processing delay on the convergence speed of the power control algorithm. For including this into our model, we redefine the super-states from Section 4.2 to be no longer limited to a delay of 3 PCGs, but use an abstract index $\delta$. Super-states therefore define now the sequence that was taken over the last $\delta$ states.

$$\bar{z}^{(n)}\left(j_1, j_2, \ldots, j_\delta\right) = \Pr\left[P^{(n)} = j_\delta \mid P^{(n-1)} = j_{\delta-1}, \ldots, P^{(n-\delta)} = j_1\right] \tag{4.21}$$

The only difference in the implementation of the model based on Eqn. (4.21) compared to Eqn. (4.17) with the fixed delay of 3 lies in a suitable mapping of the states using a binary encoding. The remaining steps stay basically the same as described in Section 4.2.

The results depicted in Fig. 4.11(a) show that the mean MS transmit power is not affected by the processing delay. However, the duration of the transient phase is significantly extended when the delay is increased from 3 PCG to 5 PCG. This is caused by the more delayed reaction of the system to the power control commands which in turn causes the mean value of the distribution to oscillate more around the theoretical mean. The contrary effect can be seen in Fig. 4.11(b) when the processing delay is reduced from 3 PCG to 2 PCG. There are less oscillations and the duration

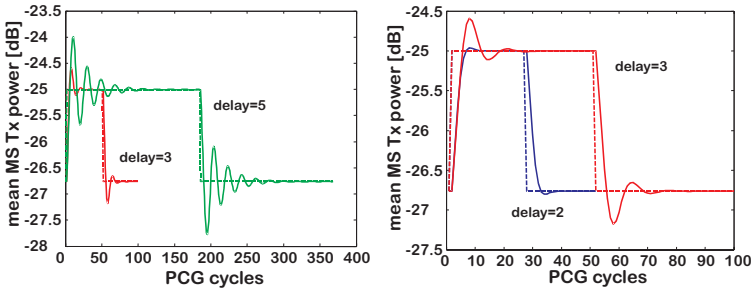


(a) Comparison of $\delta = 3$ and $\delta = 5$

(b) Comparison of $\delta = 2$ and $\delta = 3$

Figure 4.11: *Influence of the processing delay on the mean MS transmit power*

of the transient phase is reduced to approximately the half than when using a delay of 3.

Fig. 4.12 illustrates the convergence time as a function of the processing delay, when increasing the load from 0.1 to 0.25, 0.5, and 0.75. An almost exponential increase with the processing delay can be recognized in all curves. It can further be seen that the target load matters much only when it is low and that target loads above 0.5 behave quite similar.

## 4.3 Inner and Outer Loop Model

So far only the dynamic behavior of the inner loop of power control was investigated. In this section we will also consider an outer loop which updates the threshold $\theta$, see (Leibnitz 1999). This is done as a function of the Radio Resource Management layer which monitors the frame error

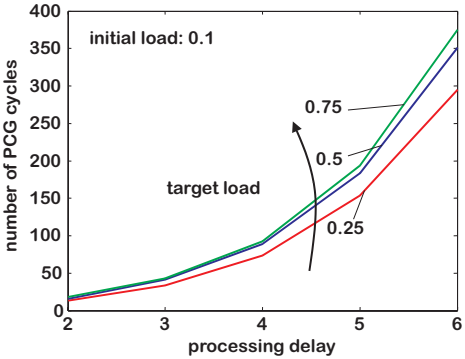


Figure 4.12: *Convergence time dependent on delay*

rate as performance criterion. Therefore, updates are done on the basis of frames, i.e. every 15 or 16 PCG for UMTS or cdmaOne, respectively.

In the following, we will use an algorithm similar to the one presented by Sampath et al. (1997). Let $\theta^{(m)}$ be the threshold level at frame $m$. If the frame is in error, the threshold is too low and it is increased by $\Psi\Delta$, otherwise decreased by $\Delta$. The algorithm for adjusting the target $E_b/N_0$ in the outer loop is summarized as follows:

1. Use CRC to check if frame $m$ is in error.

2. If frame $m$ is in error: $\theta^{(m+1)} = \theta^{(m)} + \Psi\Delta$
   otherwise $\theta^{(m+1)} = \theta^{(m)} - \Delta$,

where $\Delta$ is the step size, typically 0.3-0.5 dB, and $\Psi$ is an integer indicating the target FER. The frame is considered to be in error if at least one bit in the frame is erroneous.

We will approximate the probability of bit error in a QPSK modulated

channel by the equation well known from textbooks, e.g. (Yang 1998),

$$p_b = \frac{1}{2} Q\left(\sqrt{\hat{\varepsilon}}\right) \tag{4.22}$$

Let $B$ be the number of bits per frame. A frame error occurs when at least one bit is in error. Therefore, we can obtain the probability $q_u(i)$ for increasing and the probability $q_d(i)$ for decreasing the $E_b/N_0$ threshold from level $i$ from the Binomial distribution function as

$$q_u(i) = 1 - (1 - p_b(i))^B \tag{4.23}$$

$$q_d(i) = 1 - q_u(i). \tag{4.24}$$

These equations rely on the assumption that interleaving makes the occurrence of bit errors within a frame independent. For the sake of simplicity, we will furthermore assume that the $E_b/N_0$ threshold will be limited by a maximum value $M$.

In order to derive a model which includes also the outer loop, we will use a Markov chain with two-dimensional states $z(i,j)$, with $1 \leq i \leq M$ and $1 \leq j \leq J$. The first index $i$ describes the $E_b/N_0$ threshold value and $j$ is the transmitter power level. The state transitions to and from a single state $z(i,j)$ are illustrated in Fig. 4.13.

Analogous to the Eqn. (4.10), the power level will be increased and decreased with $p_u(i,j)$ and $p_d(i,j)$, respectively.

$$\begin{aligned} p_u(i,j) &= P\left[G \leq \theta - P \mid P = j,\ \theta = i\right] \\ &= \frac{1}{2} + \frac{1}{2} \operatorname{erf}\left(\frac{i - j - \mu_G}{\sqrt{2}\sigma_G}\right), \end{aligned} \tag{4.25}$$

$$p_d(i,j) = 1 - p_u(i,j). \tag{4.26}$$

Since the inner loop is performed more frequently than the outer loop, where a threshold update is performed in cdmaOne every 16th cycle and in UMTS every 15th cycle, the transitions with the same SIR threshold

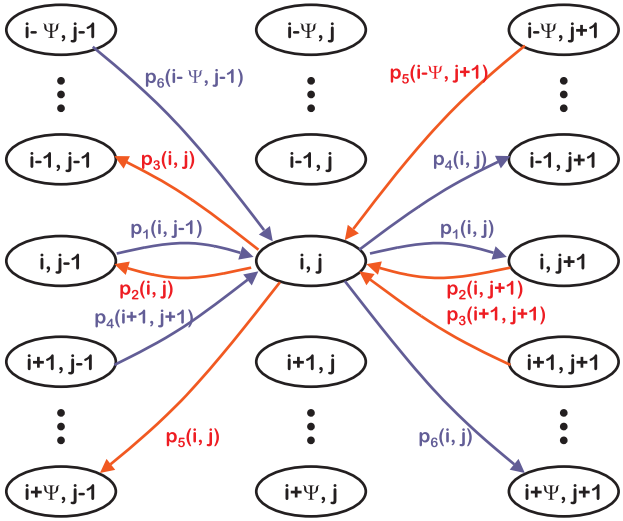


Figure 4.13: *Markov chain state transitions*

must be weighted with a factor $\omega$.

$$\omega = \begin{cases} \frac{15}{16} & \text{for cdmaOne} \\ \frac{14}{15} & \text{for UMTS} \end{cases}$$

The transitions from $z(i,j)$ to states with other thresholds must consider the probability for threshold updates $q_u(i)$ and $q_d(i)$. Therefore, the following transition probabilities are used.

$$p_1(i,j) = \omega\, p_u(i,j) \qquad p_2(i,j) = \omega\, p_d(i,j)$$
$$p_3(i,j) = (1-\omega)\, p_d(i,j)\, q_d(i) \qquad p_4(i,j) = (1-\omega)\, p_u(i,j)\, q_d(i)$$
$$p_5(i,j) = (1-\omega)\, p_d(i,j)\, q_u(i) \qquad p_6(i,j) = (1-\omega)\, p_u(i,j)\, q_u(i)$$

Note that special care has to be taken at the range boundaries for $i \in \{0, M\}$ and $j \in \{0, J\}$. We can now order all probabilities in a transition probability matrix $\mathbf{Q}$.

$$\mathbf{Q} = \begin{pmatrix} \mathbf{A}_0 + \mathbf{B}_0 & \overbrace{0 \quad \dots \quad 0}^{\Psi-1} & \mathbf{C}_0 & & \\ \mathbf{B}_1 & \mathbf{A}_1 & & \mathbf{C}_1 & \\ \ddots & \ddots & & \ddots & \\ & \mathbf{B}_{M-\Psi} \quad \mathbf{A}_{M-\Psi} & & & \mathbf{C}_{M-\Psi} \\ & \ddots \quad \ddots & & & \vdots \\ & \mathbf{B}_{M-2} & \mathbf{A}_{M-2} & 0 & \mathbf{C}_{M-2} \\ & & \mathbf{B}_{M-1} & \mathbf{A}_{M-1} & \mathbf{C}_{M-1} \\ & & & \mathbf{B}_M & \mathbf{A}_M + \mathbf{C}_M \end{pmatrix}$$

The matrices $\mathbf{A}_i$, $\mathbf{B}_i$, and $\mathbf{C}_i$ can be given in the following way. If we define a matrix $\tilde{\mathbf{Q}}_i$, $i = 1, \dots, M$, by

$$\tilde{\mathbf{Q}}_i = \begin{pmatrix} p_d(i,0) & p_u(i,0) & & \\ p_d(i,1) & & p_u(i,1) & \\ \ddots & & \ddots & \\ & p_d(i,J-1) & & p_u(i,J-1) \\ & & p_d(i,J) & p_u(i,J) \end{pmatrix}$$

then we can define

$$\mathbf{A}_i = \omega\, \tilde{\mathbf{Q}}_i \qquad \mathbf{B}_i = (1-\omega)\, q_d(i)\, \tilde{\mathbf{Q}}_i \qquad \mathbf{C}_i = (1-\omega)\, q_u(i)\, \tilde{\mathbf{Q}}_i .$$

With knowledge of matrix $\mathbf{Q}$ it is now possible to compute the equilibrium state distribution $z(i,j)$. The stationary MS power distribution can be derived by the sum of all states with common second index and the

distribution of the outer loop threshold by summation of the states with common first index, see Eqn. (4.27).

$$\Pr[P = j] = \sum_{i=0}^{M} z(i, j) \tag{4.27}$$

$$\Pr[\theta = i] = \sum_{j=0}^{J} z(i, j) \tag{4.28}$$

The following figures depict the stationary distributions of the MS uplink transmit power and the outer loop target threshold as described in Eqns. (4.27) and (4.28). Again the nearly Gaussian shaped induced by the loop driving function can be recognized.

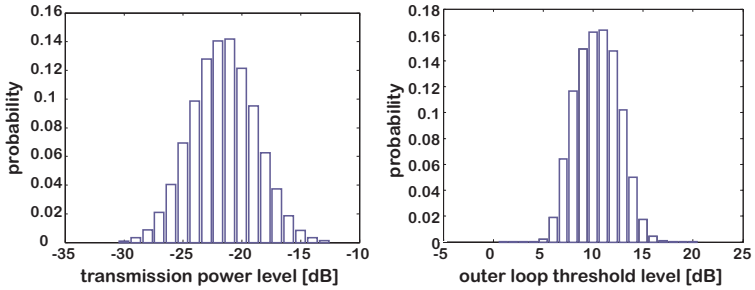


(a) MS transmit power $P$ (b) Outer loop target $\theta$

Figure 4.14: *Stationary distributions from inner and outer loop model*

We are now interested in a comparison of the three models so far presented in order to observe the influences of the outer loop and the processing delay. Summarizing, we consider the following cases:

- inner loop model with fixed outer loop threshold and without any processing delay
- inner loop with fixed outer loop threshold including a processing delay of 3 PCG
- inner and outer loop model without processing delay

The CDFs of all three models are shown in Fig. 4.15. The user bitrate is again chosen to be 12.2 kbps and the user is located at 1 km distance from the BS of a moderately loaded cell ($\tilde{\rho} = 0.5$).

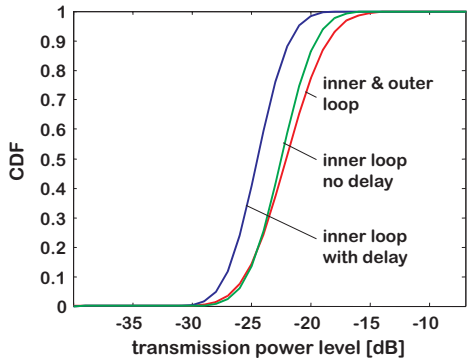


Figure 4.15: *Comparison of power distribution from different power control models*

It can be seen that the outer loop and the inner loop model are quite similar as both models do not include any processing delay. The similarity is expected since the mean value of the outer loop target distribution corresponds roughly to the fixed threshold in the inner loop model. Furthermore, it can be seen that the model with processing delays causes a

lower uplink transmission power. This is caused by the delayed reaction of the loops which leads to a less erratic behavior.

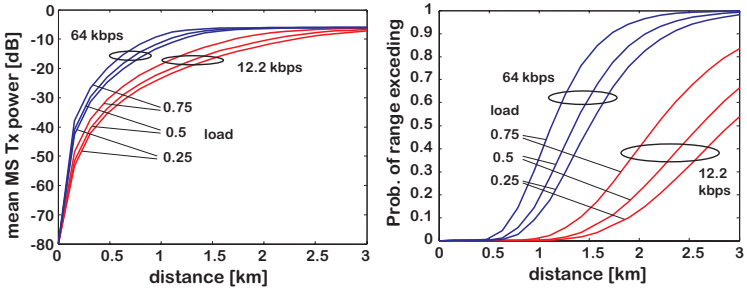


(a) Mean uplink transmit power

(b) Range exceeding probability

Figure 4.16: *Inner and outer loop power control model*

Considering only the model with both loops, the mean MS uplink transmit power as a function of the distance from the BS is given in Fig. 4.16(a). Power control operating with inner and outer loop are capable of covering ranges up to about 1.5 km for 64 kbps and even more for 12.2 kbps services. The mean MS transmit power increases only by little (2-3 dB) when increasing the load by 0.25. From Fig. 4.16(a) we can also recognize that in order to operate efficiently with data rates of greater than 64 kbps, the MS needs to be located at a distance of at most 1 km. This fact can also be recognized in Fig. 4.16(b). The range exceeding probability reaches 0.1 at 1 km for a user with 64 kbps and a load of 0.25. For greater loads this value is reached even earlier. As expected the higher processing gain for 12.2 kbps users results in a lower range exceeding probability and thus larger coverage areas.

In this chapter we derived an analytical model for the power control loops of a WCDMA system. The model itself is based on a discrete time, discrete state Markov chain and allows the computation of the MS uplink transmission power and the probability for exceeding the dynamic range. We have seen that the distribution is greatly influenced by the loop driving function and the parameters distance from the BS and load in the cell. Another item of interest for us is the dynamic behavior of the power control loops and the influence of the processing delay on the convergence speed. To include all aforementioned factors in one analytically tractable model was the main goal of the studies described in this chapter. In the next chapter we will investigate the WCDMA performance on system level by utilizing some of the obtained results.

# 5 Analysis of WCDMA Capacity with Spatial Traffic

In the previous chapters we have investigated the behavior of power control for a single user and modeled the other users implicitly by the load they create in the cells. It could be seen that the locations of all subscribers play an important role on the performance of CDMA power control. Therefore, in this chapter we extend our model and include also the spatial distribution of the users in the system. In order to characterize the spatial traffic in a mathematical way, we use basic definitions and relations of spatial point processes. With this traffic model we are able to evaluate some key performance metrics on the coverage and the capacity of WCDMA cells. This is at first examined for a single cell with no neighboring cells and is later extended to a multi-cell case with soft handover.

## 5.1 Spatial Traffic Modeling

In this section we introduce some approaches to spatial traffic modeling. We provide a definition of stochastic spatial processes and continue with

the *demand node concept*, another method for generating spatial traffic patterns by discrete points which was introduced by Tutschku and Tran-Gia (1998).

### 5.1.1 Spatial Point Processes

In general, a spatial point process is the extension of a one-dimensional point process to a two-dimensional plane where the points are represented by their two-dimensional coordinates. We use the following definition of a spatial point process from Stoyan and Stoyan (1994).

**Definition 5.1**
*A **spatial (or planar) point process** is a random variable $N$, which takes random choices of mappings $B \rightarrow N(B)$, where $B$ is a Borel set and $N(B)$ is a counting measure. An instance of $N$ is called a point pattern.*

Similar to its one-dimensional counterpart, we can characterize a spatial point process by its first moment, which is called its *intensity measure*:

$$\Lambda(B) = E\left[N(B)\right].$$

A special case is given if the process is invariant under translation of its points. We then speak of a *homogeneous* process and can describe the intensity $\Lambda(B)$ as:

$$\Lambda(B) = \lambda\ A(B),$$

where $\lambda$ is a constant intensity and $A(B)$ is the surface area of the Borel set $B$. In a similar manner we speak of an *isotropic* process when the rotated point process has the same distribution for any rotation angle around the origin.

The simplest example of a spatial process is given by a homogeneous spatial Poisson process, see Kingman (1993). The number of points $K$ in

any Borel set $B$ on the plane follows a Poisson distribution, depending on the area $A(B)$ of the set and the intensity of the process $\lambda$.

$$P[K = k] = \frac{(\lambda\, A(B))^k}{k!}\, \exp(-\lambda\, A(B)) \qquad k = 0, 1, \ldots \tag{5.1}$$

Another important feature of the homogeneous Poisson process is that for an arbitrary integer number $\ell$ and non-overlapping (disjoint) Borel sets $B_1, \ldots, B_\ell$, the random variables $N(B_1), \ldots, N(B_\ell)$ are independent. Due to these two properties, the spatial Poisson process is both homogeneous and isotropic. An instance of the homogeneous spatial Poisson process is depicted in Fig. 5.1(a).

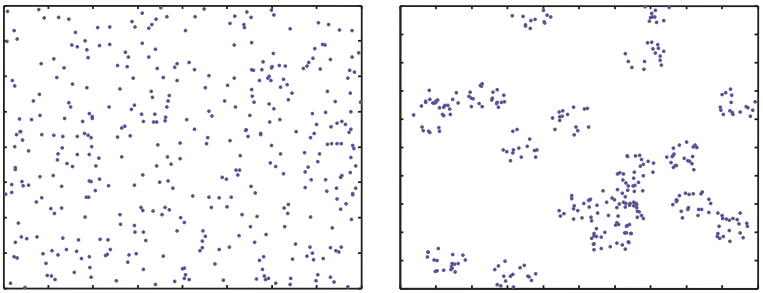

(a) Homogeneous Poisson process (b) Matern cluster process

Figure 5.1: *Samples of different spatial processes*

Non-homogeneous Poisson processes are stochastic models for point patterns with regular differences in the density of points. Here, the two-dimensional intensity function $\lambda(x, y)$ is used instead of the intensity parameter $\lambda$.

Several other variants of spatial processes exist that can have a non-uniform density of points. The class of Neyman–Scott point patterns is often used in spatial statistics to model clustered point patterns. For their construction, a homogeneous Poisson pattern is at first used to generate a set of parent points. Around each parent point a cluster of children points is distributed. An example of a Neyman-Scott process is the *Matern cluster process*. Here, the number of points per cluster is also Poisson distributed and the points are distributed uniformly in a circle with a fixed radius around each cluster center, see Fig. 5.1(b). Other spatial processes that are based on MAP (Markovian Arrival Process) are for example the Isotropic Phase Type Planar Point Process ($IPhP^3$), see Remiche (1998), or the Markovian Spatial Arrival Process by Baum (1998). The application of these processes in the context of performance of wireless systems has also been investigated to some extent.

Some research work can be found in the literature, where spatial point processes are applied to the performance analysis of CDMA networks. Fleming et al. (1997) derive an analytical expression of the loading factor (see Section 2.4) when considering that all MSs and BSs are distributed according to a spatial Poisson process. The authors showed that the loading factor increases for a more irregular layout of the BSs. Baccelli and Blaszczyszyn (2000) define and analyze a class of random coverage processes and study the properties of the process, which permit the computation of the outage probability and the handover regions. Another work by Baccelli et al. (2001) provides a generic stochastic model to estimate the spatial averages of geometrical characteristics, e.g. shape of the cells or soft handover regions, while taking the irregular nature of the point patterns into account. Chan and Hanly (2001) use a spatial Poisson process to calculate approximations and bounds on the outage probability in a cell.

### 5.1.2 The Demand Node Concept

The demand node concept was first introduced in Tutschku, Gerlich, and Tran-Gia (1996). The basic traffic characterization is the representation of the spatial distribution of the demand for teletraffic by discrete points, called *demand nodes*. Demand nodes are widely used in economics for solving facility location problems.

**Definition 5.2**
*A **demand node** represents the center of an area that contains a quantum of demand from teletraffic viewpoint, accounted in a fixed number of call requests per time unit.*

The notion of demand nodes introduces a discretization of the demand in both space and demand. In consequence, the demand nodes are dense in areas of high traffic intensity and sparse in areas of low traffic intensity. Together with the time-independent geographic traffic model, the demand node concept constitutes a static population model for the description of the mobile subscriber distribution. The advantage of this discrete characterization is that the use of discrete network planning algorithms is facilitated, see Tutschku (1998).

Figure 5.2 shows the spatial traffic distribution of demand nodes generated with the partitional clustering method presented in Tutschku and Tran-Gia (1998) and Tran-Gia, Leibnitz, and Tutschku (2000). It shows a 160 km $\times$ 160 km area around the Dallas-Fort Worth metroplex in Texas. The input for this point distribution was generated by a traffic matrix obtained from measurements. As can be clearly seen, the pattern is of a very clustered nature. The areas around downtown Dallas and downtown Fort Worth show a much higher traffic intensity, indicated by the much higher density of points, than the areas of the surrounding smaller cities or suburbs.

In the following sections we deal with the evaluation of CDMA performance when the user locations are modeled by spatial point patterns.

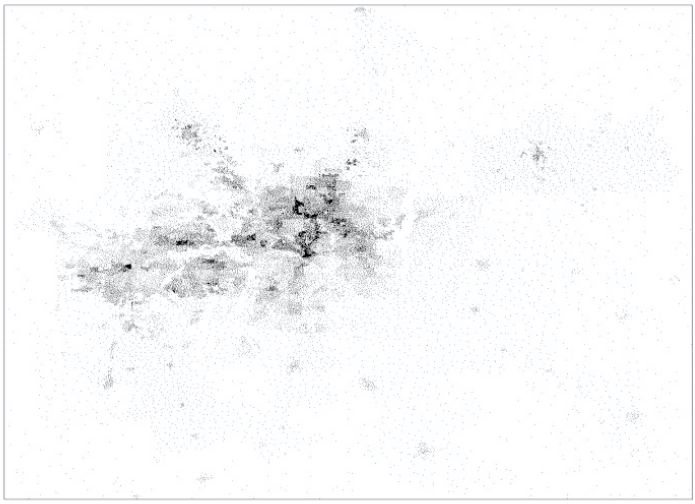

Figure 5.2: *Two-dimensional demand node distribution of the Dallas-Fort Worth metroplex*

Our focus lies on a spatial homogeneous Poisson process for modeling the location of the users in the cells. An extension to non-homogeneous processes is possible as well. However, an examination of non-homogeneous scenarios makes it more difficult to illustrate the general influence of the system parameters.

## 5.2 Single Cell Outage Analysis

This section is intended to provide the infrastructure for the analysis of a CDMA cell. We define an outage condition metric that can be used in the network design process. When analyzing a CDMA cell, its complexity is determined by the stochastic property of the customer population and the probabilistic nature of the radio transmission. Due to these issues, the cell capacity and the cell radius become probabilistic quantities. It is therefore also necessary to define the coverage and the capacity in a probabilistic fashion.

Let us consider in the following a single CDMA cell in a network with a BS supporting a certain number of calls. At the instant of the observation there are $k$ calls that are supported in the coverage area and power-controlled by this BS, see Fig. 5.3.

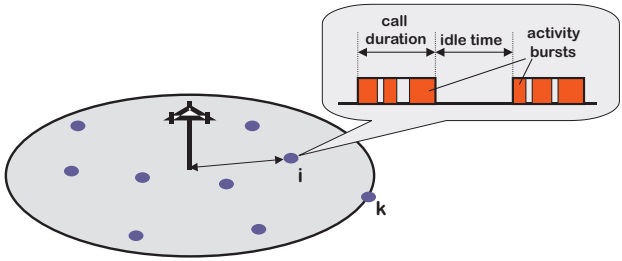


Figure 5.3: *Single CDMA cell with $k$ supported calls*

We observe in particular a user $i$ in an activity phase. This is the period of time, when a customer transmits an activity burst during his call. These bursts are separated by idle phases, like illustrated in Fig. 5.3. This general behavior of on–off activity can be applied to both, voice calls and data transmissions, e.g. World Wide Web browsing, see. Tran-Gia, Staehle, and Leibnitz (2001).

Considering at this stage only voice connections, we can see in Fig. 5.3 that a call is active for a certain period. After this time, the user is idle for a period until starting a new connection. However, during an active call, the user does not transmit all the time. As the connection is bidirectional, the user is active ("talking") for a time followed by inactive phases during which he listens to his counterpart. For the AMR (Adaptive Multi-Rate) vocoder used in UMTS voice transmission, different frame types are used in active and idle phases.

The ratio between active and total call duration is denoted as the activity factor (see also Section 2.4). While voice traffic is rather symmetrical when observing the activity of the user (activity factor of about 0.45), data traffic is highly asymmetrical. In Section 5.3 we deal with this type of traffic in greater detail.

For the further model of the cell, we consider the number of the (active) connections in the cell to be a random variable denoted by $K$, which is governed by a spatial process. At any observation instant, $K$ takes an instantaneous value denoted by $k$.

### 5.2.1 Outage Model for a Fixed Number of Users

If we look at the customer $i$ at a point in the cell, let the distance of this customer from the transmitter be $x$. The transmit power (in dBW) of the customer is given in terms of his received power $S_i$ at the BS by

$$P_i = S_i + G(x) + Z, \tag{5.2}$$

where $G(x)$ is the link gain at distance $x$ from the BS (including antenna and receiver gains) and $Z$ is a random variable representing shadow fading. Path loss is usually well modeled using Hata's model, see Eqn. (4.4). The shadow fading variable $Z$ is well modeled as a zero-mean Gaussian random variable with variance $\sigma_Z^2$, see Rappaport (1996).

The measure that indicates the quality of a CDMA link is given by the $E_b/N_0$ level. Due to fluctuations from channel fading, imperfections in power control, and influences from other users, the $E_b/N_0$ value becomes a random term. If we recall the results from Chapter 4, the $E_b/N_0$ can be well modeled by a log-normal random variable. Outage occurs for user $i$ when the $E_b/N_0$ requirement can not be fulfilled. This happens when the interference in the system is so high that user $i$ would require to transmit at a power level greater than the maximum level $P^{\max}$, i.e.

$$p_{\text{out}} = \Pr\left[S_i + G(x) + Z > P^{\max}\right]. \tag{5.3}$$

After giving the definition of the outage event, its probability can be computed. All variables and notation are used in analogy to Veeravalli, Sendonaris, and Jain (1997) and its extension by Tran-Gia, Jain, and Leibnitz (1998), especially the notation that for any power or signal–to–interference ratio $\chi$ in dB, its transformation to linear space is denoted by $\hat{\chi}$.

The $E_b/N_0$ $\hat{\varepsilon}_i$ for the $i$-th customer at the BS may be expressed in terms of the received powers $\hat{S}_i$ of the various customers as:

$$\hat{\varepsilon}_i = \frac{\frac{\hat{S}_i}{R_i}}{\sum\limits_{j \neq i} \frac{\nu_j \hat{S}_j}{W} + N_0 + I} \tag{5.4}$$

Here, $\nu_j$ is the voice activity factor of the $j$-th user, as described above, cf. Fig. 5.3. The variables $\{\nu_j\}$ are modeled as independent Bernoulli random variables

$$\Pr[\nu_j = 1] = \rho$$
$$\Pr[\nu_j = 0] = 1 - \rho$$

$R_i$ denotes the information bit rate of user $i$ in bits per seconds and $W$ is the frequency bandwidth in Hz. The total interference in the denominator is added by the background noise power spectral density $N_0$ and the other-cell interference density $I$.

The random variables $\hat{S}_1$, $\hat{S}_2, \ldots, \hat{S}_{k-1}$ are modeled as i.i.d. log-normal distributed random variables. Since the required $E_b/N_0$ $\hat{\varepsilon}$ is also log-normal, $\varepsilon = 10 \log \hat{\varepsilon}$ is Gaussian with typical values for the mean and standard deviation of $m_\varepsilon = 7$ dB and $\sigma_\varepsilon = 2.5$ dB, cf. Viterbi and Viterbi (1993). The mean $m_{\hat{\varepsilon}}$ and second moment $\delta_{\hat{\varepsilon}}$ of the random variable $\hat{\varepsilon}$ are:

$$m_{\hat{\varepsilon}} = \exp\left(\frac{(\beta\sigma_\varepsilon)^2}{2}\right) \exp\left(\beta m_\varepsilon\right) \tag{5.5}$$

$$\delta_{\hat{\varepsilon}} = \exp\left(2(\beta\sigma_\varepsilon)^2\right) \exp\left(2\beta m_\varepsilon\right) \tag{5.6}$$

where $\beta = (\ln 10)/10$.

The mean and the second moment of $\hat{S}$ are then derived as:

$$m_{\hat{S}}(k) = \frac{(N_0 + I)W m_{\hat{\varepsilon}}}{\frac{W}{R} - \rho(k-1)m_{\hat{\varepsilon}}} \tag{5.7}$$

$$\delta_{\hat{S}}(k) = \frac{\left(((N_0 + I)W + \rho(k-1)m_{\hat{S}}\right)^2 - (k-1)\rho^2 m_{\hat{S}}^2\big)\,\delta_{\hat{\varepsilon}}}{\left(\frac{W}{R}\right)^2 - \rho\,(k-1)\,\delta_{\hat{\varepsilon}}}. \tag{5.8}$$

Examination of Eqn. (5.7) shows that $k$ cannot exceed the value for which the denominator is zero. This value is the pole capacity, see Section 2.4.

$$k_{\text{pole}} = \frac{W}{R\, m_{\hat{\varepsilon}}\, \rho} + 1 \tag{5.9}$$

and can be interpreted as the limit on the number of customers a cell can support when the coverage shrinks to zero.

Since $\hat{S}$ is log-normal, $S$ is Gaussian. The mean and variance of $S$ can easily be calculated in terms of $m_{\hat{S}}$ and $\delta_{\hat{S}}$ as given below:

$$m_S(k) = 20 \log_{10} m_{\hat{S}}(k) - 5 \log_{10} \delta_{\hat{S}}(k) \tag{5.10}$$

and

$$\sigma_S^2(k) = \frac{1}{\beta}\left(10 \log_{10} \delta_{\hat{S}}(k) - 20 \log_{10} m_{q\hat{S}}(k)\right) \tag{5.11}$$

Assuming that $S$ and $Z$ are uncorrelated, we can hence rewrite Eqn. (5.3) as:

$$p_{\text{out}}(x,k) = Q\left(\frac{P^{\max} - G(x) - m_S(k)}{\sqrt{\sigma_S^2(k) + \sigma_Z^2}}\right) \tag{5.12}$$

where $Q(x)$ is the tail of the Gaussian PDF as defined in Eqn. (4.12).

Eqn. (5.12) yields the probability of an outage as function of the distance of the customer from the BS and the number of customers that are supplied in this cell. However, it is desired to have a term that is unconditional of the second parameter, i.e. making $p_{\text{out}}$ a function of only $x$ or $k$. Considering the outage perceived by the customer at distance $x$ from the BS, we can formulate $p_{\text{out}}(x)$ as:

$$p_{\text{out}}(x) = \sum_k p_{\text{out}}(x,k) \cdot P\left[\text{“}k \text{ calls in cell with radius } x\text{”}\right]. \tag{5.13}$$

The derivation of the probability to have $k$ customers in a cell based on a certain traffic behavior is done with a spatial Poisson process and is described in Section 5.2.2. In a similar fashion we can later describe the outage probability as a function of the number of users.

$$p_{\text{out}}(k) = \int_0^\infty p_{\text{out}}(x,k) \cdot P\left[\text{“radius of cell with } k \text{ users is } x\text{”}\right] dx \tag{5.14}$$

### 5.2.2 CDMA Coverage in a Clustered Environment

So far, the randomness was only taken into account for the modeling of the transmission channel. The equation for the probability of outage requires as parameters the number of customers in the cell and the distance of the observed customer. Our aim is to uncondition the outage probability of one of the parameters. By modeling the location of the customers with a spatial process, we can obtain a mathematical description of the

customer distribution within the cell. We can then use the point process to characterize the relationship between number and location of the customers.

Based on this Poisson process assumption we consider now a cell modeled by a circle with radius $R_c$. One active call is assumed to be on the circle and $k-1$ connections are inside the circle, see also Fig. 5.3. The corresponding coverage area is $A = \pi R_c^2$, where both $A$ and $R_c$ are random variables. To give a mathematical description, we can define the random variable $A$ as the surface of the smallest circle containing $k$ points. Due to the property of the spatial Poisson process, the size of the surface $A$ is distributed according to an Erlang-distribution of order $k$:

$$A(y) = P\left[A \leq y\right] = 1 - \sum_{i=0}^{k-1} \frac{\left(\lambda\, y\right)^i}{i!} \exp\left(-\lambda\, y\right),$$

with the probability density function:

$$a(y) = \frac{d}{dy} A(y) = \frac{\lambda(\lambda y)^{k-1}}{(k-1)!} \exp\left(-\lambda y\right).$$

It is more useful, however, to consider the radius of the cell rather than its surface, as this translates directly to the distance between customer and BS. The distribution of the radius $R_c$ can be derived as

$$R_c(x) = 1 - \sum_{i=0}^{k-1} \frac{\left(\lambda \pi x^2\right)^i}{i!} \exp\left(-\lambda \pi x^2\right),$$

with the probability density function

$$r_c(x) = \frac{\left(\lambda 2\pi x\right)\left(\lambda\, \pi x^2\right)^{k-1}}{(k-1)!} \exp\left(-\lambda \pi x^2\right) \tag{5.15}$$

With Eqn. (5.15) we can now calculate the probability that we have a cell radius of $x$ for a cell currently supporting $k$ calls assuming an intensity of $\lambda$ users per unit area size.

The following figures illustrate the shape of the curve of $r_c(x)$. Fig. 5.4(a) depicts the sensitivity of $r_c(x)$ to variations of $k$. It shows that to support fewer calls, the mean cell radius is in general smaller than for larger values of $k$, for a fixed traffic intensity of $\lambda = 10$. The shape and variance of the curves stay the same. In Fig. 5.4(b) the curve for $r_c(x)$ is plotted with a fixed value of $k = 50$ and varying traffic intensities $\lambda$. It indicates that for areas with high values of $\lambda$, e.g. urban or dense urban regions, the cell radius is more clearly defined than for areas with lower intensity, like the curve for $\lambda = 10$. The range of the radius is here much larger than the one of the curves with higher $\lambda$.

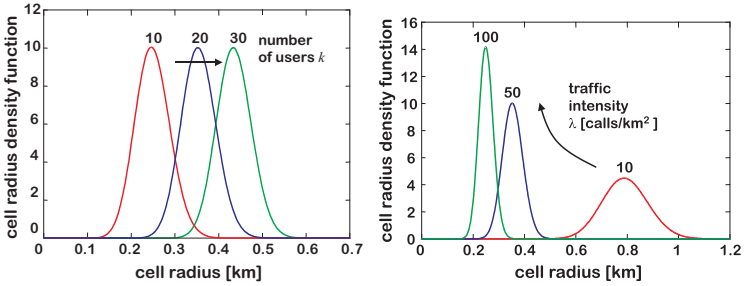


(a) Cell radius vs. number of calls

(b) Cell radius vs. spatial traffic intensity

Figure 5.4: *Sensitivity of the cell radius density function*

## Dynamics of CDMA Cell Coverage

Considering the two-dimensional customer traffic process as discussed above, the coverage area of a cell in a CDMA network is estimated, where

the outage probability given in Eqn. (5.12) is taken as the criterion to define the boundary of a cell.

We can now get back to Eqn. (5.13) and Eqn. (5.14). With the Poisson process we now have a mechanism to describe the probability to have $k$ calls in the cell with radius $x$ and the probability that the radius of the cell with $k$ calls is $x$. Thus, the r.v. for the number of users distributed in a cell with area $A = \pi\, x^2$ is Poisson distributed with density $\lambda$, which translates to an expected number of users in the cell $\xi = \lambda A = \lambda\, \pi\, x^2$.

First we look at a cell with radius $R_c = x$. The probability to have $k$ connections in the cell with radius $x$ is simply Poisson distributed, as shown in Eqn. (5.1). The overall unconditioned outage probability for this cell can then be derived as:[1]

$$p_{\text{out}}(x) = \sum_{k=1}^{\infty} p_{\text{out}}(x,k)\, \frac{\xi^k}{k!} \exp\left(-\xi\right) \tag{5.16}$$

The resulting outage probability in Eqn. (5.16) is now no longer dependent on the number of calls in the cell like Eqn. (5.12), but only on the distance from the base station and the intensity of the cluster process. This translates to an assumed traffic value for the area of the cell. Therefore, it is enough to know the environment of the cell, such as urban or suburban, and map this value to a certain value of $\lambda$.

Given a value of $p_{\text{out}}(x,k)$ and a number of calls currently being supported by the cell, the radius of the cell is fixed. Similarly, given a value of $p_{\text{out}}(x,k)$ and the radius of a cell, the number of calls supported by the cell is fixed. These ideas are summarized in Fig. 5.5(a), where we plot $p_{\text{out}}(x,k)$ from Eqn. (5.12) versus calls and Fig. 5.5(b) with $p_{\text{out}}(x,k)$ versus distance.

Some interesting observations about the behavior of these relationships can be made. Both curves have a slowly increasing part and a very fast increasing part. In general, we would like to operate in the slowly

[1] For the summation over $k$, values for $P_{out}(x,k) = 1$ are assumed, where $k$ exceeded $k_{\text{pole}}$.

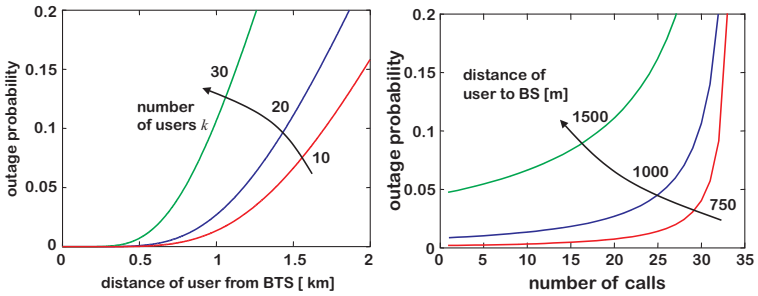


(a) Influence of distance between user and BS

(b) Influence of number of users

Figure 5.5: *Impact of distance and number of users on outage probability*

changing part of the curve as far as possible to ensure stability of the QoS for the customers.

### Interaction of Capacity and Customer Dynamics

We now focus on the question, how large the coverage area of a CDMA cell is if we want to cover a given number of $k$ active calls. From network design viewpoint the coverage corresponds to a chosen outage probability, which can be derived by combining Eqn. (5.12) and Eqn. (5.15).

$$p_{\text{out}}(k) = \int_0^\infty p_{\text{out}}(x,k)\; r_c(x)\; dx \tag{5.17}$$

Eqn. (5.17) gives us a relationship between probability of outage and number of calls. Here, it is no longer necessary to know the distances of

the individual customers as these are being implicitly represented by the Poisson process.

The results analyzed here suggest that the CDMA cell has to be provisioned like a processor in a queuing system. This implies that like queueing systems we can construct load service curves and use stability arguments to determine how heavily they should be loaded. These curves are presented in this section. Like average delay, the QoS for a CDMA cell would be the outage probability $p_{\text{out}}$.

The choice of $p_{\text{out}}$ depends on the area over which the coverage of a CDMA cell is desired. In this analysis, $p_{\text{out}}$ is maintained along the edge of the cell, the area over which the outage is maintained extends from the BS to the edge of the cell. In general, the target of about 90-95% edge coverage is desired. In other words we would like $p_{\text{out}}$ to be between 5-10 %. In the following section we discuss this issue in more details with some numerical examples.

The interaction between customer dynamics and the capacity dynamics leads to the new definitions of the coverage and the capacity of the cell as given by Eqn. (5.16) and Eqn. (5.17). In particular, consider Fig. 5.6(a) and 5.6(b).

It is clear that in Fig. 5.6(b) the rate of change of $p_{\text{out}}(x)$ as a function of distance is small until it reaches a certain point where it grows exponentially (much like the delay curves of the queuing system). Similarly, if we look at the curve in Fig. 5.6(a), the rate of change of $p_{\text{out}}(k)$ is initially small but extends exponentially as the number of calls increase. This is due to the fact that the probability to find more users in a certain area is higher for high user densities. For a small traffic intensity, the cells will be larger when supporting a certain number of users, leading to higher outage probabilities due to propagation loss. Both curves approach a step function for a limit of $\lambda \to \infty$.

We are now interested in the tradeoff between cell radius and capacity in terms of the average number of users $\xi$ in the cell. For this we assume a

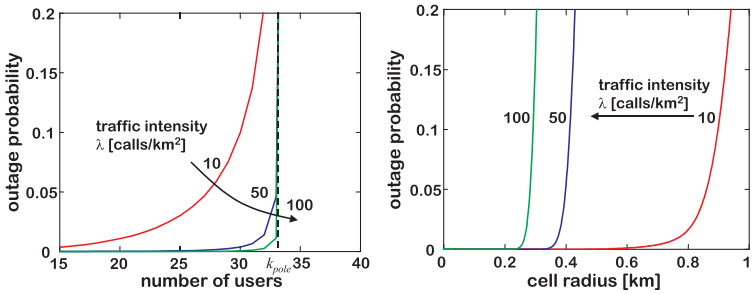


(a) Influence of capacity

(b) Influence of radius

Figure 5.6: *Relationship between capacity, coverage, and outage probability*

fixed maximum outage probability $p^*_{\text{out}}$ defining our quality of service and which we do not wish to exceed. In solving Eqn. (5.16) for $x$ we can derive the maximum cell radius for which $p^*_{\text{out}}$ is still maintained. The curves for the coverage-capacity tradeoff are given in Fig. 5.7. Note that the stricter we get with our outage requirements, i.e. $p^*_{\text{out}}$ becoming smaller, we also reduce the maximum cell radius for the same mean number of users.

Thus, for a CDMA cell the capacity and coverage are both provisionable quantities and are dominated by stability issues rather than by actual resource constraints. In general, given a spatial traffic intensity $\lambda$ and $p_{\text{out}}$, the capacity and the coverage of the cell can both be determined by stability arguments.

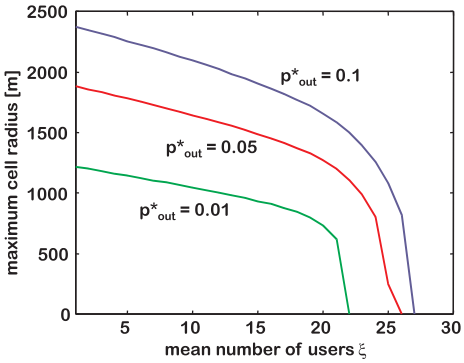


Figure 5.7: *Coverage and capacity tradeoff*

## 5.3 Influence of Activity on Outage Probability

In this section we investigate the impact of both voice and data services in a cell. Both types of users are assumed to be distributed according to a spatial Poisson process, which makes it possible to obtain a stochastic description of the QoS in the cell, which is again measured by the probability of outage. The results in this section were presented in Tran-Gia and Leibnitz (1999).

### 5.3.1 TCP/IP Data Transmission over CDMA

Data applications are expected to play an increasingly important role in the next generation mobile communication services. The demand for wireless access to the Internet, e.g. applications such as the World Wide Web (WWW) or Electronic Mail (E-mail), is expected to rapidly increase

over the next decade. It has become a necessity that a user can have access to such applications from anywhere he wants just like using a wireless phone.

Internet applications operate with a TCP / IP protocol stack. The main components here are the *Internet Protocol* (IP) on the network layer and the window based flow control mechanism TCP (*Transmission Control Protocol*) on the transport layer. While in principle TCP should work anywhere regardless of the underlying network architecture, it was primarily designed for operating in wired networks with low BER of approximately $10^{-8}$. For each transmitted TCP segment a timer is set and when a timeout occurs, network congestion is assumed. In order to allow the network to recover from this congestion, TCP reduces its window size and thus the transmission rate. Problems occur when part of the transmission goes over a wireless link. Here, the BER is much higher and can be between $10^{-2}$ and $10^{-4}$, which leads to lost packets being the major cause for timeouts instead of network congestion. However, TCP misinterprets these packet corruptions as congestion and reduces the window size. Additionally, due to the slow start algorithm the rate at which the window is increased is restricted. All of this leads to a decrease in end-to-end throughput and latency since the window sizes is never optimal.

One approach to increase TCP performance for a heterogeneous wired and wireless environment is to introduce a link layer protocol employing either *Forward Error Correction* (FEC) or more commonly *Automatic Repeat Request* (ARQ) or a combination of both. The advantage here is to operate in a layered structure of network protocols independently of the transport layer protocol without any further modification to TCP. The protocol stack for a CDMA cellular system is depicted in Fig. 5.8, cf. TIA / EIA / IS-707 (1997). The *Radio Link Protocol* (RLP) given here operates with a NAK-based ARQ mechanism with Selective Repeat (SR) and operates seamlessly in the layer above the cellular IS-95 physical layer.

In the following, we analyze the performance of the SR-ARQ in the

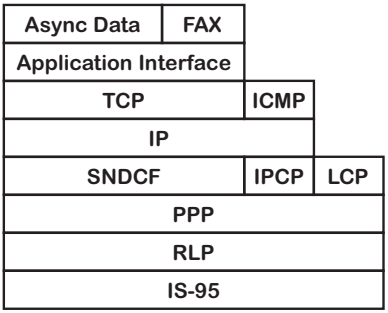


Figure 5.8: *Wireless CDMA protocol stack*

RLP. This permits us to dimension the buffers on the uplink and downlink in order to maintain a desired QoS. We also see how the system parameters influence the activity time of data bursts (which we refer to as packet calls) and show the impacts that data users have on an integrated voice / data cell.

### 5.3.2 Analysis of the IS-707 Radio Link Protocol (RLP)

In the North American IS-707 standard on data transmission the RLP is defined as a NAK-based SR-ARQ scheme. Its purpose is to achieve an acceptable frame error performance for the IP packets that are transferred to higher layers. In a similar fashion, the *Radio Link Control* (RLC) Protocol is implemented also for UMTS, see Holma and Toskala (2000). Here, three modes of operation are defined: transparent mode, unacknowledged mode, and acknowledged mode. Only the acknowledged mode guarantees the correct delivery of the data and is therefore used for applications like E-mail or WWW.

RLP in cdmaOne uses the 20 ms frame structure. Since IS-95 was originally designed for voice transmission, it includes a variable bit rate vocoder, which produces frames with variable lengths. For data transmission this can be utilized by filling the space of voice packets which are not transmitted at full rate. Therefore, a CDMA frame can be used for voice, data and mixed voice / data operation. This permits a subdivision in primary traffic which is usually voice and secondary traffic (usually data). It should be noted that at full rate the payload of a frame is 171 bit which requires that an IP packet, which usually consists of several hundred bytes, is split up into many frames. Furthermore, it can be assumed that outer loop power control maintains a nearly constant FER of approximately 1%.

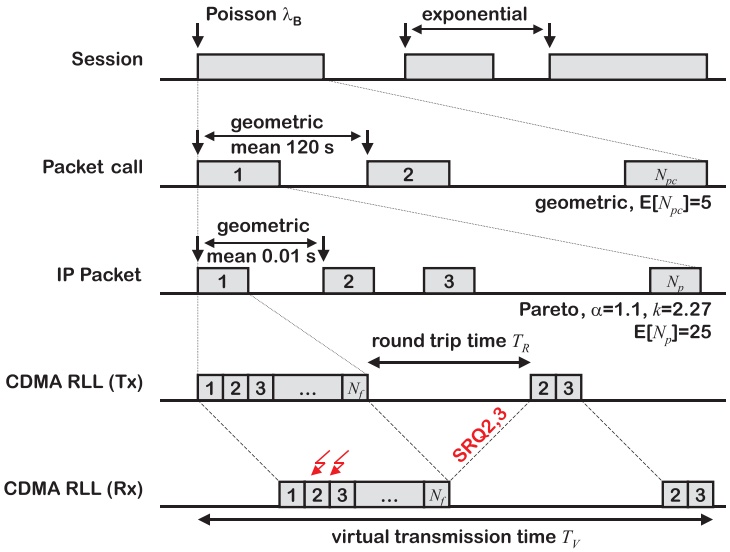


Figure 5.9: *CDMA user connection process*

For our analysis we assume a user source model which corresponds to the one given in the proposal for the next generation CDMA system ITU (1998). A more detailed source traffic model for wireless applications can be found in the paper by Tran-Gia, Staehle, and Leibnitz (2001). Two major classes of users exist: class A describes users with short messages, e.g. Telnet or E-Mail, and class B describes users performing WWW sessions. We can assume that the mobile unit is always a client and that the server is located within the wired network. Since WWW accesses are asymmetric, the traffic in the client-server direction is less than the traffic being transmitted from the server to the client. Therefore, we use class B for the description of the downlink traffic and introduce another user category (class C) for describing the uplink.

Users in classes B and C behave in the following way, cf. Fig. 5.9. The user activates a WWW session with a Poisson arrival rate $\lambda_B$. Each session contains $N_{pc}$ packet calls which is a geometric random variable with mean $E[N_{pc}] = 5$. The interarrival time is also geometric with a mean of 120 s. Within each packet call $N_p$ packets are generated. The number of packets is Pareto-distributed with the parameters $\alpha = 1.1$, $k = 2.27$ and a mean of $E[N_p] = 25$, see Eqn. (5.18).

$$\Pr[N_p = x] = \begin{cases} 1 - \left(\frac{k}{x}\right)^{\alpha} & x \geq k > 0 \\ 0 & x < k \end{cases} \tag{5.18}$$

The IP packets have a fixed size of 480 bytes on the downlink and 90 bytes on the uplink. The interarrival time between two packets is geometric with a mean of 0.01 s. Thus, at the RLL each IP packet is split into $N_f$ RLL frames, each with 171 bits payload.

### Analysis of the Radio Link Protocol

Let the size of an IP packet be given as $N_I^{DL} = 480$ bytes and $N_I^{UL} = 90$ bytes for the downlink and the uplink, respectively. Assuming only pri-

mary channels, we can transport in each 20 ms RLL frame $X = 171$ bits. Therefore, an IP packet must be split into $N_f = N_I/X$ frames for transmission over the radio link. In our case, we have $N_f^{DL} = 23$ and $N_f^{UL} = 5$ on the downlink and uplink, respectively. We now compute the transmission time for one IP packet over the wireless link. All IP packets are transmitted in sequence, however, if an error during the transmission occurs, the IP packets become interleaved. This again increases the duration of the transmission of a packet.

If we consider the virtual transmission time $T_V$ of an IP packet, we need to take into account the number of round trips $N_R$ and the number of frame transmissions $N_T$, then

$$T_V = N_R\, T_R + N_T\, T_T.$$

We assume that the time needed for the transmission of one frame is $T_T = 20$ ms and due to the frame structure the round trip time can be estimated as $T_R = 2\, T_T$.

Each of the frames is transmitted $Y$ times until it is successfully received depending on the frame error probability $p_f$ in the wireless channel. We can assume that frame errors occur independently and that $Y$ is geometrically distributed with distribution $y(i)$ and cumulative distribution function (CDF) $Y(i)$ according to

$$\begin{aligned} y(i) &= \Pr[Y = i] = p_f^{i-1}(1 - p_f) && i = 1, 2, \ldots \\ Y(i) &= \Pr[Y \leq i] = 1 - p_f^{i} && i = 1, 2, \ldots \end{aligned}$$

The random variable for the number of round trips $N_R$ can then be expressed depending on $Y$ as

$$N_R = \max\{\underbrace{Y, Y, \ldots, Y}_{N_f \text{ times}}\}.$$

The cumulative distribution function of $N_R$ can be computed from the CDF of $Y$ which leads to the distribution given by

$$N_R(i) = \Pr[N_R = i] = (1 - p_f^i)^{N_f} \qquad i = 1, 2, \ldots$$

$$n_R(i) = \Pr[N_R \leq i] = \begin{cases} 0 & i = 1 \\ N_R(i) - N_R(i-1) & i = 2, 3, \ldots \end{cases}$$

The number of frame transmissions $N_T$ can be computed as the $N_f$-fold sum of the random variable $Y$, which corresponds to the $N_f$-fold convolution of the distribution $y(i)$ with itself.

$$N_T = \underbrace{Y + Y + \cdots + Y}_{N_f \text{ times}}$$

$$n_T(i) = \Pr[N_T = i] = y(i) \circledast y(i) \circledast \cdots \circledast y(i) \qquad i = 1, 2, \ldots$$

Figure 5.10(a) depicts the complementary distribution function of the virtual transmission time $T_V$ of a single IP packet. The time scale is in milliseconds. We assumed that the frame error rate in this case is $p_f = 0.01$, $0.05$, and $0.1$ and that the number of frames required for one IP packet is $N_f^{UL} = 5$ and $N_f^{DL} = 23$, which corresponds to the size of an IP packet on the up- and downlink, respectively.

### Dimensioning Packet Buffer Sizes

With the knowledge of the transmission time of a single IP packet, we can dimension the buffer size needed to compensate for the high retransmission rate due to the bad link quality at an acceptable rate of blocking. For this we can assume our system to be an $M/G/n - 0$ system, i.e. we have Poisson arrivals of IP packets, the service time is given by the distribution of $T_V$ and $n$ is the number of buffer slots. On the downlink the mean number of packets transmitted during a 120 s packet call is 25. If the

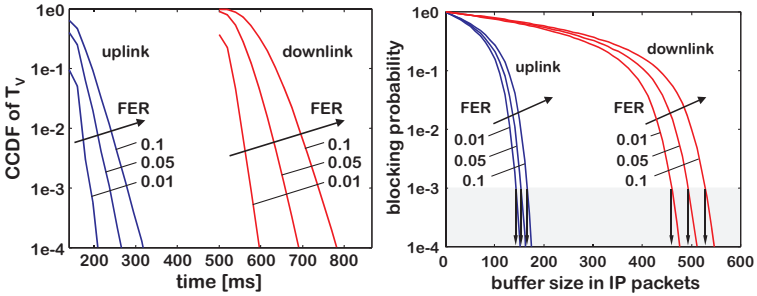


(a) Virtual transmission time for up- and downlink

(b) Uplink and downlink buffer dimensioning

Figure 5.10: *Analysis of IP packet transmission time*

packet size on the downlink is on average 480 bytes, we have an arrival rate of:

$$\lambda^{DL} = \frac{25 \cdot 480 \cdot 8 \text{ bits}}{120 \text{ s}} = 800 \text{ bps}$$

The link utilization in this case is

$$\rho^{DL} = \frac{800 \text{ bps}}{9600 \text{ bps}} = 8.33\%.$$

On the uplink, we can compute the same values and obtain $\lambda^{UL} = 150$ bps and $\rho^{UL} = 1.56\%$.

We can now compute the required buffer size for both links by using the Erlang-B formula for an $M/G/n-0$ system with $a = \lambda E[T_V]$ and finding the minimum number of servers $n$ that satisfies our QoS requirements of a blocking probability $p_b < 10^{-3}$. The resulting curves are depicted in Fig. 5.10(b).

### 5.3.3 Outage Probability in an Integrated Voice/Data System

Analogously to Section 5.2.1 we can now compute the outage probability for a cell currently supporting a number of $k$ voice and data connections at an observed time instant. Let the percentage of data users be $\omega$. However, voice and data connections differ significantly when considering the burstiness of the user activity. Measurements of human conversations have yielded that the time when one party is active is only about 45% of the whole conversation time. As shown in Section 5.2.1 we can model the voice activity of user $j$ by a Bernoulli random variable $\nu_j$ that is active with probability $\rho_v = 0.45$ and inactive with probability $1 - \rho_v$.

The activity in data connections, however, is very asymmetric and depends on the direction of the examined link. As a client the MS needs only little bandwidth on the uplink for applications such as E-mail or WWW. Most traffic that is generated is from requests for data which is transmitted on the downlink. For modeling purposes, we assume that the data user $i$ is active with probability $P(\psi_i = 1) = \rho_d$ using the Bernoulli random variables $\psi_i$. In the previous section we could see that the utilization of both links is below 10%. We therefore use $\rho_d = 0.1$ as the uplink activity.

Let the cell be loaded with $(1 - \omega)\ k$ voice and $\omega\ k$ data users. The $E_b/N_0$ of user $i$ can be expressed in terms of the received powers of the other users in the cell $\hat{S}_j$.

$$\hat{\varepsilon}_i = \frac{\frac{\hat{S}_i}{R}}{\sum\limits_{j \neq i}^{(1-\omega)\ k} \frac{\nu_j \hat{S}_j}{W} + \sum\limits_{j \neq i}^{\omega\ k} \frac{\psi_j \hat{S}_j}{W} + N_0 + I}$$

We can assume that the power control mechanism is the same for both voice and data users. Therefore, the random variables $\hat{S}$ are again modeled as i.i.d. random variables. The first and second moment of the log-

normal variable $\hat{\varepsilon}$ can then be computed analogously to Eqns. (5.7) and (5.8) by

$$m_{\hat{S}}(k,\omega) = \frac{W\, m_{\hat{\varepsilon}}\, (N_0 + I)}{\frac{W}{R} - m_{\hat{\varepsilon}}\, \kappa} \tag{5.19}$$

$$\delta_{\hat{S}}(k,\omega) = \frac{\delta_{\hat{\varepsilon}}\, \left((W\, (N_0 + I) + m_{\hat{S}}\, \kappa)^2 - m_{\hat{S}}^2\, \kappa\right)}{\left(\frac{W}{R}\right)^2 - \delta_{\hat{\varepsilon}}\, ((1-\omega)\, k\, \rho_v + \omega\, k\, \rho_d)}, \tag{5.20}$$

where $\kappa = (1-\omega)\, k\, \rho_v + \omega\, k\, \rho_d$. Then, the pole capacity of the system with mean SIR of $m_{\hat{\varepsilon}}$ and a fraction of $\omega$ data users is

$$k_{\text{pole}} = \frac{W}{R\ (\omega\, \rho_d + (1-\omega)\, \rho_v)\ m_{\hat{\varepsilon}}}.$$

With the same argumentation as in Section 5.2.1 we can give the mean and variance of the Gaussian random variables $S$ as

$$m_S(k,\omega) = 20 \log m_{\hat{S}}(k,\omega) - 5 \log \delta_{\hat{S}}(k,\omega)$$

$$\sigma_S^2(k,\omega) = \frac{1}{\beta}(10 \log \delta_{\hat{S}}(k,\omega) - 20 \log m_{\hat{S}}(k,\omega))$$

where again $\beta = \ln(10)/10$.

This leads to an outage probability at a distance $x$ with $k$ users and a percentage of $\omega$ data users of

$$p_{\text{out}}(x,k,\omega) = Q\left(\frac{P^{\max} - G(x) - m_S(k,\omega)}{\sqrt{\sigma_S^2(k,\omega) + \sigma_Z^2}}\right)$$

Like in Section 5.2.2 it is now possible to give an outage probability term unconditioned of the number of users $k$ by using a spatial Poisson process to characterize the relationship between the number and location of the users in the cell. The probability to have $k$ connections in a cell with radius $x$ is Poisson distributed and this leads to

$$p_{\text{out}}(x,\omega) = \sum_{k=1}^{\infty} p_{\text{out}}(x,k,\omega)\ \frac{\xi^k}{k!}\ \exp(-\xi) \tag{5.21}$$

Fig. 5.11(a) shows the impact of the percentage $\omega$ on the outage probability as function of the cell load. The distance of the observed user is fixed at $x = 2$ km. It can be seen that the higher the percentage of data users is in the cell, the higher the cell capacity becomes for the same outage probability. This is due to the fact that the activity phase of data users on the uplink is much lower than that for voice users.

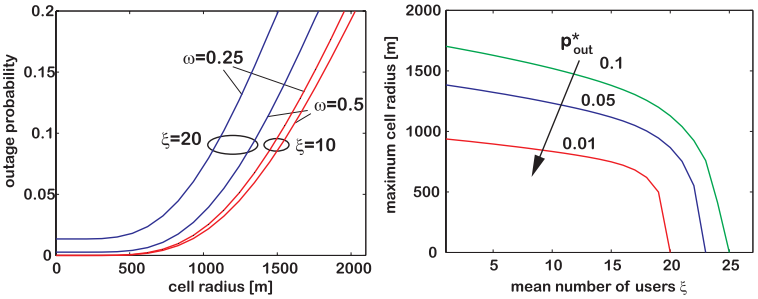


(a) Outage probability

(b) Coverage and capacity tradeoff

Figure 5.11: *Impact of number of data users*

The Eqn. (5.21) can be solved for $x$ in order to obtain the coverage and capacity tradeoff, cf. Fig. 5.11(b). In this case the maximum outage probability is given as $p_{\text{out}} = 0.01$, $0.05$, and $0.1$. The fraction of data users is kept constant at $\omega = 0.25$. It can be seen that the stricter the outage requirements the smaller the coverage areas get, which reach zero at $k_{\text{pole}}$.

## 5.4 Outage Computation under Soft Handover

In this section, we extend the above characterization of coverage and capacity from a single to a multi-cell environment. We assume a standard hexagonal layout of cells as shown in Fig. 5.12(a). In such an environment it is very important to account for soft handover because many studies, such as by Viterbi et al. (1994) and Sendonaris and Veeravalli (1997), have revealed that this feature of CDMA systems increases the performance in terms of both coverage and capacity. A mobile is in $N$-way soft handover if it is in simultaneous communication with $N$ BSs. If one of the $N$ links suffers deep fading, another one may still be acceptable. Thereby, outage probability is reduced because the mobile transmit power does not necessary have to be increased.

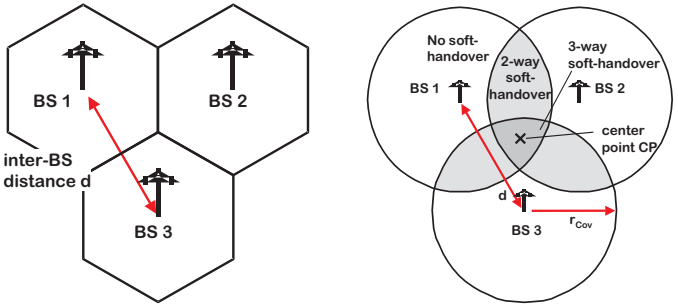


(a) Hexagonal BS layout

(b) Soft handover regions

Figure 5.12: *CDMA cell layout models*

### 5.4.1 Soft Handover Probabilities

Whether a mobile is in soft handover or not depends on the downlink path pilot signal-to-interference ratio received from the surrounding BSs. Since our primary interest is studying the long term system behavior, we do not consider mobility of the users and only need to focus on one of the soft handover thresholds, T_DROP. A mobile is in at least $N$-way soft handover if $N$ pilot-to-interference values are received above the drop threshold. Although higher degrees of soft handover are possible, they are extremely unlikely under our assumption of a hexagonal layout of BSs. We therefore only consider the case for $N = 2$ and $N = 3$.

Fig. 5.12(b) shows three BSs and the mean coverage areas of their pilot signals. As we can see, 3-way soft handover is confined to the region in the middle between all three BSs. No soft handover occurs in areas close to the cell sites and the 2-way soft handover regions cover the remaining area. Since the pilot signals are affected by shadow fading and their coverage is therefore varying, the soft handover regions are not as clearly defined as suggested by the figure. At any location there is a certain probability for 1-, 2-, and 3-way soft handover.

In the remainder of this section, we summarize and extend the characterization of the soft handover probabilities found by Patel, Goni, Miller, and Carter (1996). Let $x_1, \ldots, x_L$ be the distances from the investigated mobile location to the $L$ closest cell sites in ascending order, i.e. $x_1$ is the distance to the closest BS, $x_2$ the distance to the second closest BS, and so on. Further, $Ec_i$ denotes the pilot signal-to-interference-and-noise ratio from cell $i$, then $Ec_i$ is given as

$$Ec_i = \frac{\beta_i E_i \, G(x_i) \, \hat{Z}_i}{\sum_{\ell=1}^{L} E_\ell \, G(x_\ell) \, \hat{Z}_\ell + N_0 W}, \tag{5.22}$$

where $Z_\ell$ is the random variable for shadow fading with $Z_\ell = a\,\zeta + \sqrt{1-a^2}\,\zeta_\ell$. The variables $\zeta$ and $\zeta_\ell$ are i.i.d. distributed zero mean Gaus-

sian random variables with standard deviation $\sigma_\zeta$. The parameter $a$ determines the degree of fading correlation. The fraction of cell power allocated to the pilot signal is $\beta_i$ and $E_i$ is the total effectively radiated power (ERP) of cell $i$. $G(x_i)$ denotes the path loss from cell site $i$ to a mobile at distance $x_i$.

Neglecting the term for background noise $N_0 W$, Eqn. (5.22) can be rewritten as

$$Ec_i = \frac{\beta_i}{1 + 10^{\frac{Y_i}{10}}} \tag{5.23}$$

with $Y_i$ being the normal distributed ratio of interference received from cell sites $k \neq i$ to the signal power received from BS $i$. The mean and standard deviation $m_{Y_i}$ and $\sigma_{Y_i}$ of $Y_i$ are functions dependent on $x_l$, $\sigma_Z$, and $a$. Assuming independence of $Y_i$ and $Y_j$ ($i \neq j$), the desired soft handover probabilities are given as

$$p_{3\text{-sh}}(\{x_L\}) = \prod_{i=1}^{3} \left(1 - Q\left(\frac{10 \log_{10}\left(\left(\frac{\beta_i}{T_{drop}}\right) - 1\right) - m_{Y_i}}{\sigma_{Y_i}}\right)\right) \tag{5.24}$$

$$p_{2\text{-sh}}(\{x_L\}) = \prod_{i=1}^{2} \left(1 - Q\left(\frac{10 \log_{10}\left(\left(\frac{\beta_i}{T_{drop}}\right) - 1\right) - m_{Y_i}}{\sigma_{Y_i}}\right)\right) - p_{3\text{-sh}}(\{x_K\}). \tag{5.25}$$

A user is accordingly not in soft handover with probability $p_{1\text{-sh}} = 1 - p_{2\text{-sh}} - p_{3\text{-sh}}$.

Fig. 5.13(b) shows the 2- and 3-way soft handover probabilities encountered by a user moving from BS 1 along a line in the direction to point $CP$ in Fig. 5.13(a). The 3-way soft handover probability is greatest at the center point $CP$ at a distance of about 1000 m, whereas the 2-way soft handover probability is greatest for distances above 1300 m. This corresponds to the region of soft handover between BS 2 and BS 3.

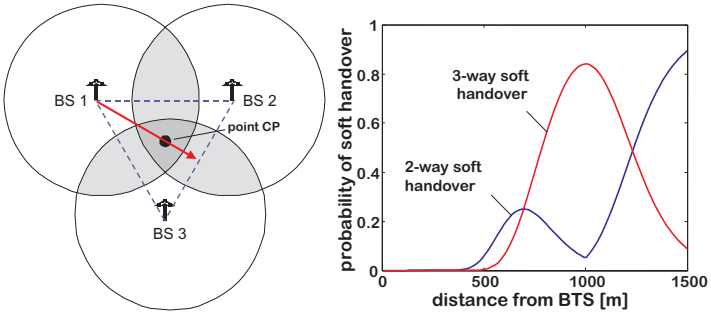


(a) Position of soft handover plot (b) Soft handover probability

Figure 5.13: *Probability for 2- and 3-way soft handover*

### 5.4.2 Outage Probability under Soft Handover

If a mobile is in $N$-way soft handover, it has links to the $N$ closest BSs. Therefore, outage only occurs if the transmit power required for all these links exceeds the maximum transmit power $P^{\max}$. Thus, under soft handover Eqn. (5.3) becomes

$$p_{\text{out}} = \Pr\left[\bigcap_{n=1}^{N} \{S_n + G(x_n) + Z_n > P^{\max}\}\right]$$

where $S_n$ is the received power from our observed user at BS $n$. As mentioned in the previous section, $Z_n$ is a random variable representing shadow fading for the link to BS $n$.

Sendonaris and Veeravalli (1997) show that the probability of outage for a customer at distance $x_n$ to the $n$-th closest BS that is serving $k_n$ active

users is

$$p_{\text{out}}(N, \{k_n\}, \{x_L\}) = \int_{-\infty}^{\infty} \left[ \prod_{n=1}^{N} Q\left( \frac{P^{\max} - G(x_n) - m_S(k_n) - a\sigma_Z x}{\sqrt{(1-a^2)\sigma_Z^2 + \sigma_S^2(k_n)}} \right) \right] \times \frac{1}{\sqrt{2\pi}} \exp\left(-\frac{x^2}{2}\right) dx$$

where $m_S(k_n)$ and $\sigma_S^2(k_n)$ are the mean and the variance of the required received power for a cell site with $k_n$ mobiles.

Since from the previous section we know the probabilities for being in soft handover, Eqns. (5.24) and (5.25), we can give an expression for the outage probability not any more depending on the degree of soft handover $N$:

$$p_{\text{uncond}}(\{k_n\}, \{x_L\}) = \sum_{n=1}^{3} p_{\text{out}}(n, \{k_n\}, \{x_n\}) p_{n\text{-sh}}(\{x_L\}). \tag{5.26}$$

As in Section 5.2.2, we assume that the customers are distributed according to a spatial Poisson process. Therefore, the number of customers per cell is Poisson distributed with mean $\xi = \frac{3\sqrt{3}}{2} r^2 \lambda$. Here, $r$ is the cell radius as introduced in Fig. 5.12(a) and $\lambda$ the traffic intensity of the Poisson process. Using the customer distribution, Eqn. (5.26) becomes

$$p_{\text{pois}}(\{x_L\}) = \sum_{k_1=1}^{\infty} \sum_{k_2=1}^{\infty} \sum_{k_3=1}^{\infty} \left( \prod_{n=1}^{3} \frac{\xi^{k_n} \exp(-\xi)}{k_n!} \right) p_{\text{uncond}}(\{k_n\}, \{x_L\}). \tag{5.27}$$

Fig. 5.14 shows the contour plot of $p_{\text{pois}}$. Base stations are located in the lower left and lower right corner and in the top center. It can be clearly seen that outage probability increases with the distances to the BS. However, due to soft handover the area between the cells sees smaller outage probabilities than in the case without soft handover.

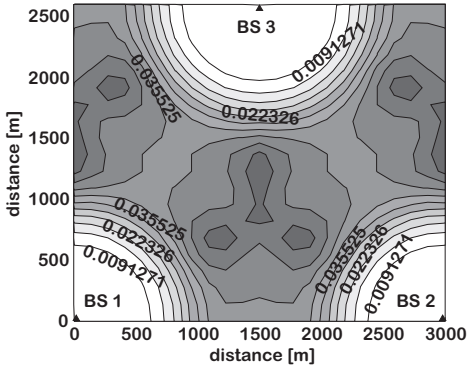


Figure 5.14: *Unconditioned outage probability with* $\xi = 20$ *users*

### 5.4.3 Determining the Coverage-Capacity Tradeoff

Like in Section 5.2.2 the greatest outage probability value within a cell $p_{\text{worst}}$ is only a function of $r$ and $\lambda$. The multi-cell counterpart to Fig. 5.6(a) is Fig. 5.15(a). It shows the same behavior: the greater the cell radius and the mean number of users, the worse $p_{\text{worst}}$ becomes. The curves lie below the ones in Fig. 5.6(a), indicating the gain from soft handover.

From this we can derive the multi-cell coverage-capacity tradeoff that is relating the mean number of users per cell with the maximum cell radius. This tradeoff is derived exactly like in Section 5.2.2. For a varying mean number of users per cell $\xi$, we determine the maximum cell radius, for which $p_{\text{worst}}$ equals the maximum allowed outage probability $p^*_{\text{out}}$. Fig. 5.15(b) depicts the resulting tradeoff together with the single cell tradeoff both for $p^*_{\text{out}} = 0.05$. We see that soft handover leads to a gain in coverage as well as capacity. For a fixed $\xi$, the maximum cell radius

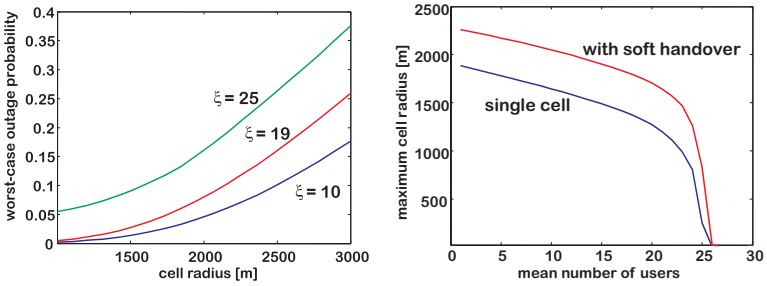


(a) $p_{\text{worst}}$ as function of cell radius

(b) Coverage-capacity tradeoff

Figure 5.15: *Outage probability and coverage-capacity tradeoff in a multi-cell environment*

is greater for the soft handover curve and vice versa a certain cell radius corresponds to a greater $\xi$. The tradeoff curves will be used to determine the coverage areas in the algorithmic approach to network planning described in Chapter 6.

# 6 Issues in CDMA Network Planning

The previous sections have shown the relationship between coverage, capacity and quality of service in a cell. In this section we consider some issues on planning CDMA networks based on the results from Chapter 5. It is not intended to be a comprehensive description of how to perform network planning in CDMA but rather to show the application of our findings in this context.

In this chapter, we focus on two issues dealing with spatial user distributions. Part one discusses an algorithmic approach on how to plan the locations of base stations when the traffic distribution is given. We will not limit to the homogeneous spatial distribution used for our analysis in the previous chapter, but consider more clustered traffic patterns as well. In the second part we describe how to compute the thresholds for soft handover in an optimal way in order to balance the traffic load in the cells and achieve a target soft handover area size.

## 6.1 An Algorithmic Approach to CDMA Network Planning

In second generation wireless FDMA systems, the planning task consists mainly of finding the optimal locations of base stations and assigning the available frequencies in an optimal way. While in the conventional approach the planning process is driven by area coverage considerations, a demand oriented planning approach to wireless networks is presented by Tutschku (1999). The aim here is not to cover as much area as possible but to supply as many users and their traffic demand as possible. Additionally, existing interactions between planning constraints are taken into account when resolving conflicting planning objectives. By doing so, the approach automatically obtains planning solutions which are optimized under multiple aspects. The key concept to achieve this is the introduction of demand nodes as spatial description of the teletraffic, see Section 5.1.2.

In CDMA based systems the spatial traffic distribution becomes a crucial issue. Due to the universal frequency reuse in all cells, it is no longer necessary to consider the frequency assignment in the manner of FDMA systems. However, as seen in the previous chapters, power control is used to overcome the near-far problem and thus the spatial user distribution has a great impact on the interference and thus the capacity of the system. Recently, most existing planning tools, e.g. T-Mobile's *Pegasos*® (Fig. 6.1), are being enhanced to consider WCDMA networks as well, see Schröder et al. (2001).

In the literature some work can be found that deals with the planning of CDMA networks. Wallace and Walton (1994) present a model which provides uplink / downlink coverage and availability maps. This is done by determining interference margins for link budget calculations considering effects due to loading, voice activity, power control, and soft / softer

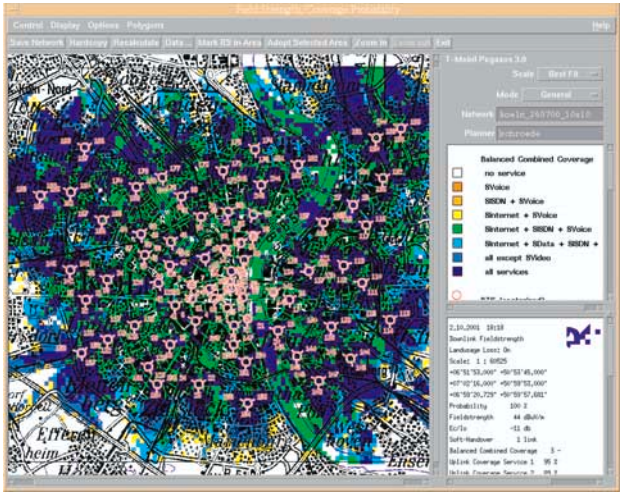


Figure 6.1: *Coverage plot in T-Mobile's Planning Tool Pegasos*

handover. It is shown that the selection of the parameters for soft handover and thus the percentage of soft handover play a critical role in network planning. The paper by Takeo and Sato (1998) presents an algorithm for setting the downlink pilot power and the uplink desired power level. The authors investigate the $E_b/N_0$ of all BSs in a non-uniform environment and show that its mean can be kept nearly at the same value, but the variance is reduced by half. A similar study is presented by the same authors in another paper. Here, Takeo et al. (2000) illustrate the necessity of observing both link directions, uplink and downlink, as they differ significantly due to the orthogonality factor. They show that when using an adaptive BS selection, this selective transmission diversity results in optimum cell boundaries. In the work by Akl et al. (1999) the capacity of the system is maximized by varying the downlink pilot powers and the

BS locations. Especially, non-uniform traffic requires relocating BSs to accommodate hot spot regions. The calculation is performed by iterations, which is applied to capture the interdependence among the interference to and from other cells, see also Staehle et al. (2002).

### 6.1.1 Specification of the Algorithm

In this section, we consider arbitrary cluster processes as user distributions and show how the results from the previous chapters can be used to perform network planning. The instance of a cluster process can be viewed as a snapshot of the user distribution in the planning region at a certain point in time. Alternatively, the spatial distribution of demand for mobile services can be represented by demand nodes as described in Section 5.1. Those demand nodes also form a cluster point pattern.

We present an algorithm that takes as input the coverage-capacity tradeoff, an arbitrary user distribution and planning parameters, such as

- the dimensions of the planning region,
- the desired fraction of overlap of cells, i.e. soft handover regions,
- the minimum percentage of users to be covered by the cells,

and which yields as result the positions of the required BSs and their coverage areas. The steps of the algorithm are outlined in the following.

#### Step 1: Generate the Candidate Set of BSs

The first step aims at discretizing the planning problem. Instead of considering an infinite number of possible locations, we place a limited number of candidate BSs on a grid with uniform distances between two BSs. Thereby, the planning task is simplified considerably and is reduced to a

set covering problem, i.e. the problem of selecting as few base stations as possible that suffice to supply the required percentage of users.

First, the locations of the initial BS locations are determined by computing the distance between neighboring BSs according to the target number of cells to be distributed. Then each BS is placed on a grid with this distance. The coverage area size of each cell is determined by the coverage–capacity tradeoff and the cell radius is first set to this initial estimate. In case that this radius is too large, there are too many users within this cell, and the radius is reduced, otherwise it is increased. This adaptation is repeated with decreasing step size until the step size falls below a certain threshold.

### Step 2: Select an Optimal BS Subset

The goal of the second step is to select from the initial set as few cells as possible that suffice to supply the required percentage of users. We also want to approximately reach the desired degree of cell overlap, i.e. soft handover areas, as specified by the corresponding planning parameter.

The task can be stated as set covering problem (SCP) which is given here adapted from Chvatal (1979).

$$\text{Minimize} \qquad |\mathcal{A}^*| \left(1 + w \left(\frac{\sum_{j \in \mathcal{A}^*} |\mathcal{N}_j|}{|\mathcal{B}|} - 1 - ovl\right)^2\right) \tag{6.1}$$

$$\text{subject to} \qquad |\mathcal{B}| \geq cov|\mathcal{M}| \tag{6.2}$$

where the variables are given as follows:

$\mathcal{M} = \{1, \ldots, K\}$ set of mobile stations

$\mathcal{A} = \{1, \ldots, L\}$ starting set of candidate cells

$\mathcal{A}^* \subseteq \mathcal{A}$ set of the selected base stations being the solution to the planning problem

| | |
|---|---|
| $\mathcal{B} = \bigcup_{j \in \mathcal{A}^*} \mathcal{N}_j$ | set of all mobiles covered by the base stations in $\mathcal{A}^*$ |
| $\mathcal{N}_j \subseteq \mathcal{M}, j \in \mathcal{A}$ | set of mobiles supplied by BTS j, i.e. those mobiles inside the circle representing the BTS |
| $cov \in [0.5, 1.0]$ | planning parameter denoting the minimum fraction of users to be covered |
| $ovl \in [0.2, 0.7]$ | planning parameter for the desired degree of cell overlap |
| $w$ | weight factor for the influence of the cell overlap criterion |

The constraint in Eqn. (6.2) enforces that at least the desired percentage of users is covered by the selected base stations. The objective in Eqn. (6.1) states that as few cell sites as possible are to be used. The factor multiplied with $|\mathcal{A}^*|$ measures how well the desired degree of cell overlap is reached. The term

$$\frac{\sum_{j \in \mathcal{A}^*} |\mathcal{N}_j|}{|\mathcal{B}|} - 1$$

is the cell overlap given by the planning solution $\mathcal{A}^*$. The closer this term is to the planning parameter $ovl$, the lower the factor and the better the solution. The weight factor $w$ is used to determine the importance of the cell overlap criterion. A reasonable value is such that the solution is indifferent between a 20% cell overlap mismatch and an additional BS in $\mathcal{A}^*$, i.e. $w = \frac{25}{|\mathcal{A}^*|}$. This $w$ value is used for the planning tool.

Unfortunately, from complexity theory point of view, the SCP is NP-complete, cf. Garey and Johnson (1979). Therefore, we employ a greedy heuristic for solving it in polynomial time. It is assumed that the desirability of using a BS increases with the number of users it supplies in addition to those already covered by other cells. The objective to reach the desired degree of cell overlap is accounted for in a way similar to Eqn. (6.1).

1. Set $\mathcal{A}^* = \emptyset$
2. Set $\mathcal{B} = \bigcup_{j \in \mathcal{A}^*} \mathcal{N}_j$.
3. If $|\mathcal{B}| \geq cov|\mathcal{M}|$ return solution $\mathcal{A}^*$.

   Otherwise find an index $j \in \mathcal{A} \backslash \mathcal{A}^*$ maximizing $(|\mathcal{N}_j| - |\mathcal{B} \cap \mathcal{N}_j|) \left(1 - w \left(\frac{\sum_{\ell \in \mathcal{A}^* \cup \{j\}} |\mathcal{N}_\ell|}{|\mathcal{B} \cup \mathcal{N}_j|} - \ell - ovl\right)^2\right)$ and let $k$ denote that index.
4. Add $k$ to $\mathcal{A}^*$ and return to 2.

The set $\mathcal{A}^*$ contains the selected base stations. $\mathcal{B}$ is the set of all mobiles already covered by the base stations in $\mathcal{A}^*$. If the constraint in Eqn. (6.2) is fulfilled, the selected base stations are returned as the solution. Otherwise the BS being optimal under the greedy heuristic is identified and added to $T$. The greedy objective is to maximize the number of additionally covered users $|\mathcal{N}_j| - |\mathcal{B} \cap \mathcal{N}_j|$. The factor multiplied with this term accounts for the mismatch between desired and actual cell overlap incurred by the potential new BS. This time, the weight factor $w$ is chosen such that a cell overlap mismatch of 30 % reduces the desirability for selecting the BS to 0.

After determining the optimal set of base stations, the drop threshold for each cell is updated. Cells with few users have a large radius and those with many users have a small radius according to the coverage–capacity tradeoff. The pilot signal should cover the whole cell area but should not go far beyond it and the drop thresholds determine the coverage of the pilot signal. Consequently, the threshold for larger cells has to be decreased and the one for smaller cells has to be increased. Otherwise, the later computed soft handover and outage probabilities would be incorrect because the soft handover probabilities depend on the drop threshold.

Finally, the radius of each cell has to be updated. This is necessary because each cell has a different overlap with its neighbors. Only half of the 2-way soft handover users and one third of the 3-way soft handover users are accounted to each cell. Thus, for a cell with large 2- and 3-way soft handover regions the cell radius can be increased because the number of users in the cell is lower than originally expected. On the other hand, the cell radius has to be decreased for cells with lower than expected overlap. The radius update takes place based on the coverage–capacity tradeoff. Additionally, the worst outage probabilities can be computed and taken into account. If the tradeoff criterion is met, but the outage probabilities in the cell are too high, the cell radius is decreased. Each cell radius change necessitates the update of the cell's drop threshold for the reasons mentioned above.

### Step 3: Employ a Location Optimization

Location optimization is performed to improve the solution of the greedy heuristic because this solution is usually not optimal. The goal is to increase the total coverage of users and to reduce the overlap of the cells. This step consists of two phases.

In the first phase, for each BS the desirability of moving the BS is computed and the ones with the highest value are selected. The desirability increases with the number of surrounding uncovered MSs and with the number of multiply covered users. This way, a cell that could cover some more nearby users and additionally has a high overlap with surrounding cells is very likely to be selected.

In the second phase, the selected cells are moved towards uncovered MSs and away from multiply covered users. Thereby, our goal of increasing the total coverage is reached because more users are covered without letting any MS become uncovered, as they also are also covered by at least another cell. The cell radius has to be recalculated after each movement

step because of the possible change in the number of users per cell. These cell radius adaptations takes place in the same way like for newly generated cells as described in Step 2.

### 6.1.2 Results of the Optimization

We now use the planning tool to analyze the influence of user clustering on teletraffic engineering of CDMA networks. Planning was performed for a region of $10 \times 5$ km containing 100 users with a requirement of covering 90% of the users and a 30% desired cell overlap. Fig. 6.2(a) shows the result for an unclustered and Fig. 6.2(b) for a heavily clustered user distribution. As we can see, on average a cell contains more users and has a smaller radius in Fig 6.2(b) than in the unclustered case. This leads to a lower required number of base stations.

To provide more evidence for this result, 1000 planning experiments for each user distribution are performed. Additionally, the deterministic user distribution is considered, where mobiles are placed on a regular grid with constant and equal distance from each other. Tables 6.1–6.1 show the results for the average number of users per cell, the average cell radius, and the number of required base stations. The corresponding 95% Student-t confidence intervals are also given in the table. Like in the above example, the mean number of base stations is the lower the less uniform the user distribution is because a lower average cell radius is required and, thus, more users can be accommodated in a cell. The variance is 0 for the deterministic case since there is no source of randomness. We also see that the more clustered the user distribution, the greater the variance and, consequently, the wider the confidence intervals are.

The explanation for the result that less BSs are needed for more clustered traffic is easy. Due to the greedy heuristic, areas with high user density are selected first as BS locations. In the presence of clusters, we therefore have more users per BS compared to a more uniform user dis-

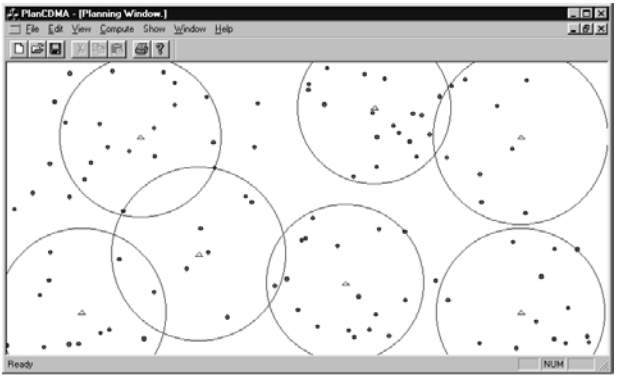


(a) Homogeneous spatial Poisson distribution

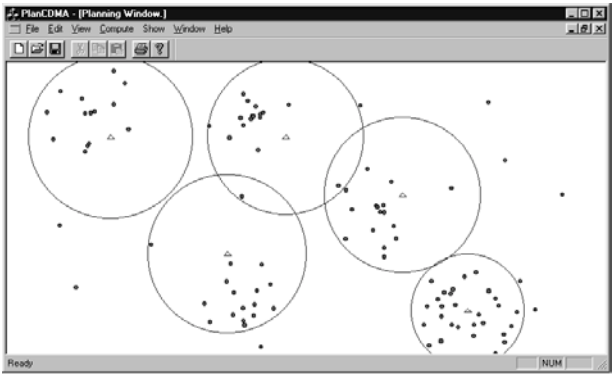


(b) Matern cluster distribution

Figure 6.2: *Planning results for different spatial traffic*

| user distribution | mean | variance | 95% confidence interval |
|---|---|---|---|
| Deterministic | 11.4 | 0 | $[11.4; 11.4]$ |
| Poisson | 12.381 | 0.687 | $[12.03; 12.73]$ |
| Clustered | 13.608 | 1.493 | $[13.09; 14.12]$ |

Table 6.1: *Average number of users per cell*

| user distribution | mean | variance | 95% confidence interval |
|---|---|---|---|
| Deterministic | 1770 | 0 | $[1770; 1770]$ |
| Poisson | 1679 | 4911 | $[1649; 1709]$ |
| Clustered | 1499 | 23780 | $[1433; 1563]$ |

Table 6.2: *Average cell radius in m*

tribution. Thus, if it is only the goal to cover mobiles and not also area, less BSs are needed to supply a certain number of users.

Since in the real world the demand for mobile services is very high in some areas like cities or highways and very low in other areas such as forests and farmland, demand oriented network planning can lead to a substantial decrease of the required number of BSs. Thereby, setup and operating costs can be significantly reduced because cell sites are among the most important cost factors in cellular communication systems.

| user distribution | mean | variance | 95% confidence interval |
|---|---|---|---|
| Deterministic | 8 | 0 | $[8; 8]$ |
| Poisson | 7.414 | 0.405 | $[7.14; 7.68]$ |
| Clustered | 6.614 | 4.411 | $[5.73; 7.49]$ |

Table 6.3: *Required number of base stations*

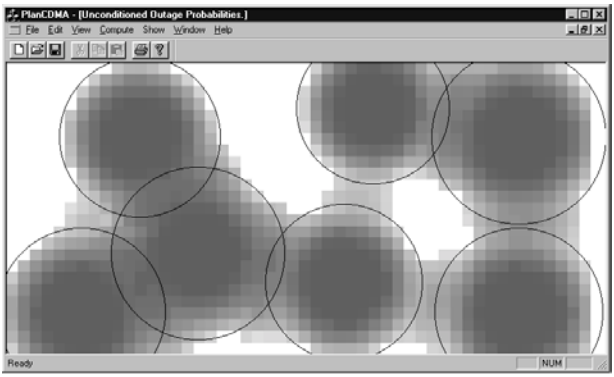


(a) Unconditioned outage probabilities

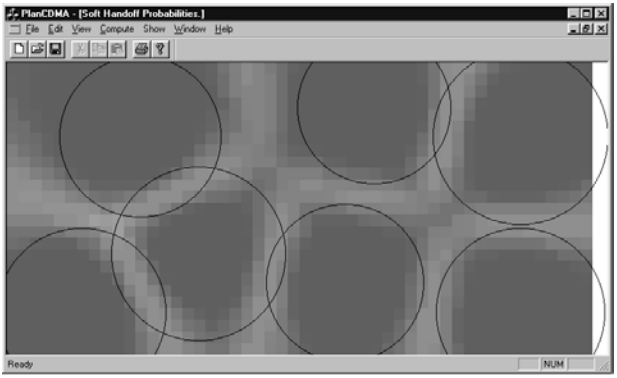


(b) Soft handover probabilities

Figure 6.3: *Visualisation of outage and soft handover probabilities*

In addition to performing the planning steps as described above, the planning tool can visualize soft handover and outage probabilities. Like for determining the coverage-capacity tradeoff, these probabilities can be computed using Eqns. (5.24), (5.25) and (5.26). This time the distances $x_L$ to the closest BS are not given by the hexagonal layout of BS but by the actual BS locations after planning. These are depicted in Fig. 6.3(a) and Fig. 6.3(b) for the planning result of Fig. 6.2(a).

The areas in Fig. 6.3(a) which are colored light gray are areas with low outage probabilities. In Fig. 6.3(b), the dark gray areas represent low probabilities of soft handover, whereas lighter shading indicates a high degree of soft handover.

## 6.2 Soft Handover Area Size with Spatial Traffic

So far we have seen that the soft handover area size plays an important role in network planning. The percentage of soft handover is a required input parameter for the planning algorithm presented in the previous section. We now examine the interactions of the soft handover thresholds on the traffic load of a CDMA cell, see Remiche and Leibnitz (1999). Again, we assume a spatial user distribution and determine the joint probability distribution of the cell radius of two cells involved in soft handover. With these values, we can obtain optimal threshold values obeying the fluctuations of the cell radius for an expected target traffic load.

### 6.2.1 Spatial User Distribution Model

Suppose now that customers are randomly located within the plane according to a homogeneous Poisson process of rate $\lambda$ (see Section 5.1.1). In such a process, the number $N(B)$ of active users in some cell $B$ depends

only on the area of the cell in the following manner:

$$\Pr[N(B) = k] = \frac{(\lambda A(B))^k}{k!} \exp(-\lambda A(B)), \tag{6.3}$$

where $k \in \mathbb{N}$ and $A(B)$ denotes the area of the set $B$. Another important feature is that non-overlapping cells do not interact on each other's capacity, i.e. if the cells $B_1$ and $B_2$ are disjoint, then

$$\Pr[N(B_1) = k, N(B_2) = \ell] = \Pr[N(B_1) = k] \ \Pr[N(B_2) = \ell], \tag{6.4}$$

where both $k, \ell \in \mathbb{N}$. Due to these two properties, the Poisson process is first completely stationary, i.e. the process keeps the same characteristics under any translation or rotation of the plane. Secondly, users are observed as homogeneously spread over any studied area $B$.

The independence assumption between sets of users is only met when those sets do not overlap. In case $B_1$ and $B_2$ do overlap, the joint distribution of $N(B_1)$ and $N(B_2)$ depends on the actual number of points lying in the overlapping area $B_1 \cap B_2$, denoted in the following by $V$. The distribution is then simply obtained by conditioning on $N(V)$. So we have

$$\begin{aligned}
&\Pr[N(B_1) = k, N(B_2) = \ell] \\
&\quad = \sum_{j=0}^{\min(k,\ell)} \Pr[N(B_1) = k, N(B_2) = \ell \mid N(V) = j] \ \Pr[N(V) = j] \\
&\quad = \sum_{j=0}^{\min(k,\ell)} \Pr[N(V) = j] \ \Pr[N(B_1 \setminus V) = k - j] \\
&\qquad \times \Pr[N(B_2 \setminus V) = \ell - j]
\end{aligned} \tag{6.5}$$

using Eqn. (6.4).

Given the observed number of users both in $B_1$ and $B_2$, the conditional distribution of $N(V)$ can then be obtained using

$$\Pr\left[N(V) = k \mid N(B_1) = \ell, N(B_2) = m\right] = \frac{\Pr\left[N(V) = k\right]}{\Pr\left[N(B_1) = \ell, N(B_2) = m\right]} \Pr\left[N(B_1) = \ell, N(B_2) = m \mid N(V) = k\right]. \tag{6.6}$$

### 6.2.2 Radius of Cells According to the Expected Traffic Load

Let $\mathcal{C}(a_1, r_1)$ and $\mathcal{C}(a_2, r_2)$ be two cells of circular shape where $a_i$ is the center and $r_i$ the radius of cell $i$, for $i = 1, 2$. The distance between the two base stations located at the center of each cell is fixed to be equal to $d$.

Let $p_{k_1 k_2}(r_1, r_2)$ be defined as

$$p_{k_1 k_2}(r_1, r_2) = \Pr\left[N(\mathcal{C}(a_1, r_1)) \geq k_1, N(\mathcal{C}(a_2, r_2)) \geq k_2\right]. \tag{6.7}$$

Eqn. (6.7) states that $\mathcal{C}(a_1, r_1)$ and $\mathcal{C}(a_2, r_2)$ must contain at least $k_1$ and $k_2$ users, respectively. This implies that for example $r_1$ can be viewed as the minimum radius of the cell $\mathcal{C}(a_1, r_1)$ when exactly $k_1$ users are expected to be located in that cell. We can then heuristically interpret $p_{k_1 k_2}(r_1, r_2)$ in the following manner

$$p_{k_1 k_2}(r_1, r_2) = \Pr\left[\text{radius of cell 1} < r_1, \text{radius of cell 2} < r_2 \mid \text{cell 1 contains } k_1 \text{ users, cell 2 contains } k_2 \text{ users}\right]. \tag{6.8}$$

It follows that according to fixed $k_1$ and $k_2$, we can derive the minimum corresponding radius of each cell.

We then have

$$p_{k_1 k_2}(r_1, r_2) = \sum_{j_1=k_1}^{\infty} \sum_{j_2=k_2}^{\infty} \Pr[N(\mathcal{C}(a_1, r_1)) = j_1, N(\mathcal{C}(a_2, r_2)) = j_2] \,. \tag{6.9}$$

Two cases now have to be distinguished according to the values of $r_1$ and $r_2$.

First, if $r_1 + r_2 \leq d$, then the two cells have no intersection, and the two random variables corresponding to the number of points in $\mathcal{C}(a_1, r_1)$ and $\mathcal{C}(a_2, r_2)$ are independent, as stated before. We can then simply use Eqn. (6.4).

Secondly, if $r_1 + r_2 > d$, the random variables are dependent and we should use Eqn. (6.5). In this computation, the area of the overlapping area $V$ is needed as a function of the radius $r_1$ and $r_2$, denoted as $V(r_1, r_2)$. Without loss of generality, we assume $a_1 = (0, 0)$ and $a_2 = (d, 0)$. The area $V(r_1, r_2)$ is equal to the sum of $V_1$ and $V_2$, where

$$V_1 = \alpha \; r_1^2 - \tilde{X} \; \tilde{Y}$$
$$V_2 = \beta \; r_2^2 - (d - \tilde{X}) \; \tilde{Y}.$$

The following quantities have to be defined as

$$\tilde{X} = \frac{d^2 + r_1^2 - r_2^2}{2d} \qquad \alpha = \arccos \frac{\tilde{X}}{r_1}$$
$$\tilde{Y} = \sqrt{r_1^2 - \tilde{X}^2} \qquad \beta = \arccos \frac{d - \tilde{X}}{r_2}.$$

### 6.2.3 Minimum Soft Handover Area Size

We now compute the values of $p_{k_1 k_2}(r_1, r_2)$ for some fixed $k_1$ and $k_2$ and propose here to look at a simple case where $d$ is fixed to 2.2 km. Additionally, it is assumed that in the average case, 3 users/km$^2$ are observed;

it implies that $\lambda$ is equal to 3.0. Due to the geographical and teletraffic properties of the region, we would like the first base station to be able to manage at least 10 customers and the second one 7.

Figure 6.4(a) represents the numerical results obtained for the joint distribution of $r_1$ and $r_2$. It is obvious that the greater the radius, the greater the probability to observe at least the desired number of customers. The curve shown here is not symmetrical, this is explained by the introduction of different target parameters $k_1$ and $k_2$.

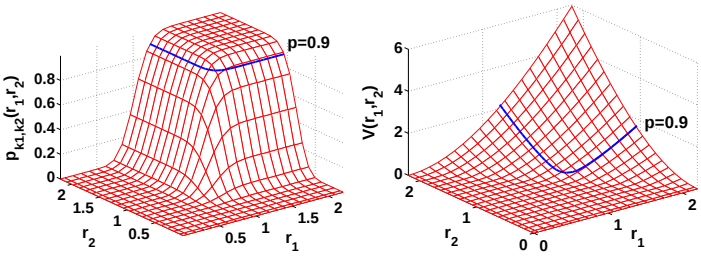


(a) Joint radius probability distribution

(b) Size of overlapping area

Figure 6.4: *Radius distribution and overlapping area*

The corresponding area size $V(r_1, r_2)$ is presented in Figure 6.4(b). Also shown on that picture is a curve identifying all values of $r_1, r_2$ for which the probability is at 90% to observe at least 10 customers in cell $\mathcal{C}(a_1, r_1)$ while at least 7 customers lie inside the second cell. The quantity of interest here is the minimum overlapping area size, since it represents the worst case where soft handover occurs. In this case, where $d = 2.2$ km, the minimum soft handover region would be about 0.14 km$^2$. One

should then expect to encounter on average 0.42 users in such a region.

Figure 6.5 illustrates different values of the soft handover area size according to the distance $d$, separating the two studied BSs, given that the other parameters keep the same value. One can observe that the greater $d$, the smaller the value of the minimum overlapping area of the two cells. Indeed the Poisson process keeps the same properties for whatever $d$. We can also immediately observe in Figure 6.5 that the soft handover area decreases as $\lambda$ increases. That is intuitive since in the same area, one can observe more users when the density is high.

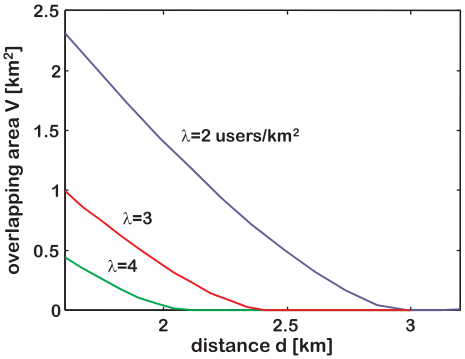


Figure 6.5: *Minimum soft handover region for different traffic intensities*

### 6.2.4 Thresholds while Maintaining Traffic Load

Let us suppose we have another user entering the system at the margin of the cells, see point "D" in Fig. 6.6. The user here has a probability $p_D$ to leave the cell 1 at this point, i.e. $p_D = \Pr[E_c/I_0 < \text{T\_DROP}]$. In the same way, at point "A" we can consider the probability $p_A$ of not adding cell 2

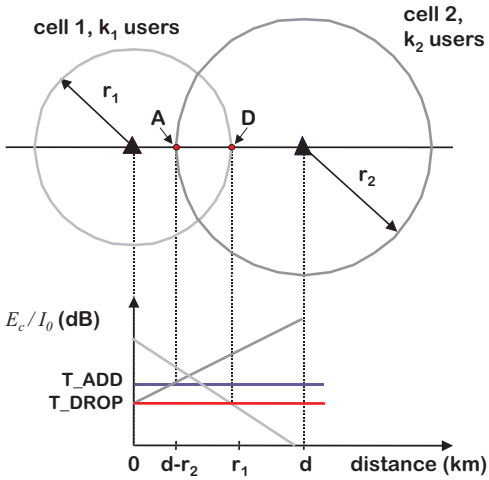


Figure 6.6: *Variations of soft handover thresholds due to fluctuations of traffic*

to the active set to be $p_A = \Pr[E_c/I_0 < \text{T\_ADD}]$. The probabilities $p_D$ and $p_A$ should be proportional to the cell loading of cell 1 and 2, respectively:

$$p_D = \frac{k_1}{k_{\text{pole}}} \qquad \text{and} \qquad p_A = \frac{k_2}{k_{\text{pole}}} \tag{6.10}$$

where $k_i$ is the number of users in cell $i$ and $k_{\text{pole}}$ is the pole capacity, i.e. the theoretical maximum number of users in each cell. If the loading of cell 1 is high, the user should leave the cell with a higher probability than if it is low. Equivalently, if the load of cell 2 is high, we want the probability of cell 2 participating in soft handover to be low.

The probability of leaving the cell 1 at point "D" is given in Eqn. (6.11)

using Eqn. (5.23).

$$\begin{aligned}\Pr[Ec_1 < \text{T\_DROP}] &= \Pr\left[\frac{\beta_1}{1+10^{\frac{Y_1}{10}}} < \text{T\_DROP}\right] \\ &= Q\left(\frac{10\log\left(\frac{\beta_1}{\text{T\_DROP}}-1\right)-m_{Y_1}}{\sigma_{Y_1}}\right) \\ &= p_D\,.\end{aligned} \tag{6.11}$$

Thus, if we give a predefined $p_D$ from Eqn. (6.10), we can solve Eqn. (6.11) in order to obtain T_DROP as

$$\text{T\_DROP} = \frac{\beta_1}{1+10^{\left(\sigma_{Y_1}Q^{-1}(p_D)+m_{Y_1}\right)/10}}. \tag{6.12}$$

We can perform the same kind of computation for T_ADD at point "A" and obtain Eqn. (6.13):

$$\text{T\_ADD} = \frac{\beta_2}{1+10^{\left(\sigma_{Y_2}Q^{-1}(p_A)+m_{Y_2}\right)/10}}. \tag{6.13}$$

We now have an expression for T_DROP that depends on the random variable $Z_1$, which in turn contains the distance $r_1$ to cell 1. In T_ADD we have the distance $r_2$ to BS 2. In the next section we describe how we can use the size of the overlapping area from Section 6.2.3 to obtain the values of $r_1$ and $r_2$. This permits us to set T_DROP and T_ADD in an optimal way.

### 6.2.5 Threshold Values as a Function of Capacity Loss

In Section 6.2.3, we obtained the minimum soft handover area when the desired traffic load in each cell was observed with a probability equal to

90%. Fig. 6.5 shows the minimum soft handover area according to the inter-BS distance $d$.

To each minimum soft handover area corresponds some given values of the radius $r_1$ and $r_2$. With this pair of $r_1$ and $r_2$, we can compute the variations of the T_DROP and T_ADD thresholds as a function of the inter-BS distance $d$ using Eqns. (6.12) and (6.13).

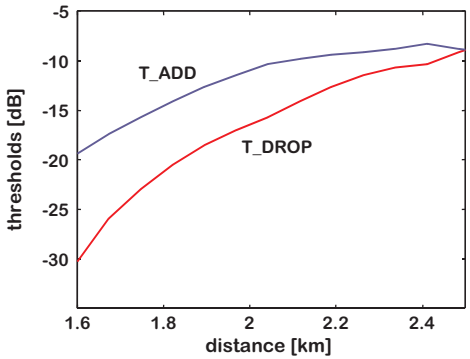


Figure 6.7: *Soft handover thresholds depending on the inter-BS distance ($\lambda = 3$)*

Figure 6.7 shows the thresholds obtained in the same conditions as described in Section 6.2.3, i.e. $k_1 = 10$, $k_2 = 7$ and the intensity $\lambda$ of the Poisson process is set to 3 users/km$^2$. Results corresponding to an inter-BS distance greater than 2.5 km are not shown here. Indeed there is no overlapping area in such conditions as depicted in Figure 6.5. It is then not necessary to study the probability that a user participates in soft handover as soon as he is out of the range of the other BSs. An expected effect, see Chopra, Rohani, and Reed (1995), is that T_ADD should be greater than T_DROP whatever the inter-BS distance $d$. Moreover the greater $d$ becomes, the smaller the difference gets between the two con-

sidered thresholds.

We can now propose a way to set the thresholds according to an accepted loss of capacity due to soft handover. As assumed in Section 6.2.3, the minimum traffic load handled by cell 1 and cell 2 is $k_1$ and $k_2$, respectively. Moreover users in the overlapping region $V$ use two traffic channels, one in each cell. It implies a loss of as many channels as the number of users in $V$ (say $k$), in the whole system. So the percentage of channel loss is

$$\mathrm{L} = \frac{k}{k_1 + k_2}. \tag{6.14}$$

Let us fix the loss percentage at 7%, let $k_1$ and $k_2$ be respectively equal to 10 and 7. From Eqn. (6.14) the number of users in soft handover is 1.2. Because users are randomly located within the plane according to a Poisson process of rate $\lambda = 3$, a soft handover region containing 1.2 users is expected to have an area equal to 0.4 km$^2$. According to Figure 6.5, this corresponds to a distance $d = 2.0$ km. Using the results we have presented above (see Figure 6.7), we can propose the network designer to separate the BSs by a distance of 2.0 km and fix the thresholds T_ADD to -10.38 dB and T_DROP to -15.71 dB.

It is clear that the traffic density varies over the time of the day. Thus, we now investigate when the thresholds change with the traffic conditions. In Figures 6.7, 6.8(a), and 6.8(b), corresponding thresholds versus inter-BS distance are shown for different values of $\lambda$. One major comment is that the greater the traffic density $\lambda$ is, the smaller the value of corresponding thresholds are. Let us take the case we have discussed above, where the inter-BS distance has been fixed to 2.0 km. We can see from Table 6.4 that for an increasing traffic load with higher $\lambda$, both thresholds decrease. That is intuitive since in the same area, one can observe more users when the density is high. From this small example we can see that it is necessary to be able to adapt the soft handover thresholds for varying traffic conditions in order to maintain a target traffic values in the cells.

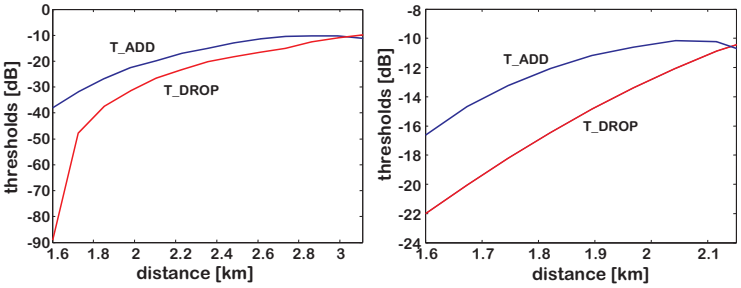


(a) Lower traffic density ($\lambda = 2$) (b) Higher traffic density ($\lambda = 4$)

Figure 6.8: *Soft handover thresholds depending on inter-BS distances*

| | $\lambda = 2$ | $\lambda = 3$ | $\lambda = 4$ |
|---|---|---|---|
| T_DROP [dB] | -31.45 | -15.71 | -12.08 |
| T_ADD [dB] | -22.51 | -10.38 | -10.15 |

Table 6.4: *Threshold values for a fixed inter-BS distance of 2.0 km*

## 6.3 Concluding Remarks

In this chapter we discussed some issues on CDMA network planning. The presented methods are not intended as a concise guide on how to perform network planning but rather to show the applicability of the theory of spatial point processes in this area. We, therefore, only considered some specific aspects. We could see that the degree of clustering of the users greatly influences the number and locations of the BSs, if we consider a demand-oriented network planning. Secondly, the percentage of

soft handover is an important planning parameter, which can be used for fine tuning in order to maintain a target traffic load in the cells. It should also be noted at this point that for a detailed network planning the demographic and morphological features of the considered area always makes each planning case unique. The findings in this chapter merely serve as orientation and illustrate the influence of some generic planning parameters.

# 7 Conclusions

This monograph was concerned with the analytical modeling of the transmission power control mechanism in a CDMA wireless system and the investigation of the system performance in the presence of a spatial user distribution.

After a review of the basic properties of the CDMA transmission technology and a brief overview of power control techniques found in the literature, we derived an analytical Markov chain model of the inner and outer power control loop. The aim was mainly to derive an analytic description of the transmission power of an arbitrarily observed mobile station. The states in the first model consisted of the transmission level within the dynamic power range. As metric for the performance evaluation of the system we used the outage probability which was computed by the probability of exceeding the dynamic range of the transmitter.

The first extension of the model included the processing delay and the dependencies of the power transitions. This was done by aggregating the paths between individual states that were taken when updating the power level. Experiments on the sensitivity of the dynamic behavior of the uplink power control were performed and yielded the system reaction on sudden variations of the traffic load. It could be seen that an increase in the processing delay also resulted in a longer time that was required until convergence was reached. Especially for a sudden increase to a nearly

fully loaded cell could be seen that due to the occurrence of outage events a much higher convergence time was necessary.

A further extension of the model not only took the inner loop but also the stochastic behavior of the outer loop into account. This facilitated not only the computation of the distribution of the mobile station's transmission power but also the distribution of the outer loop target. It could be seen that higher data rates could only be served sufficiently at close distances to the base station.

After studying the stochastic behavior of the uplink transmission power, the next step was to consider a whole cell with users distributed by a spatial homogeneous Poisson process. Extending the model by Veeravalli, Sendonaris, and Jain (1997) we could see that the size and the capacity of the cell are completely determined by the spatial traffic density and stability arguments. The notion of coverage–capacity tradeoff proved to be a useful parameter for network planning and its derivation was performed for a cell with only voice users and later in a mixed voice and data environment. Furthermore, it could be seen that when considering individual cells a pessimistic view of the performance was made due to the omission of soft handover. When also including soft handover into the analysis, we could see that this resulted in a gain in coverage as well as in capacity.

The obtained results were used in an algorithmic approach to the planning of CDMA wireless networks. Due to the description of the locations of the users as discrete points, the application of set covering algorithms was possible. The goal of this optimization was to use as input parameters the coverage–capacity tradeoff curves, the desired size of the soft handover regions, and the minimum percentage of covered users in order to determine the locations of the base stations and their coverage areas. This traffic oriented approach to network planning also illustrated the importance of considering the spatial traffic distribution. User distributions with a higher grade of clustering required in general less base

stations than more homogeneous traffic patterns.

In a further case study on network planning with spatial traffic, we discussed how to dynamically select the handover threshold values in order to maintain certain target traffic levels in the cells.

The models presented here, showed possible approaches to the analytical characterization of the power control loops and the transmission power of an arbitrary mobile station on the uplink in a CDMA system. The focus was on transmission aspects and the spatial distribution of the traffic. It should be noted, however, that only an examination of the uplink was performed. The downlink behavior differs significantly from the uplink as interference is caused here by the other base stations. Additionally, it can be observed that depending on the soft handover method implemented, i.e. equal power of all base stations with maximum ratio combining or site selection diversity transmit, the transmission power can vary considerably, see Staehle, Leibnitz, and Heck (2002). Furthermore, in the wake of the increased data traffic expected in 3G, the transported traffic is highly asymmetrical. The data flow is mostly in the direction from the base station to the mobile station and the performance of the scheduling of the data packets is a crucial issue. The capacity of the system is determined mainly on the downlink, whereas coverage is limited by the uplink. Another interesting issue that needs to be investigated is the interaction of 3G with other systems. With vertical handovers between UMTS and GSM / GPRS it is possible to utilize the good infrastructure of the 2G network and also perform a load balancing between the two systems. This seems an especially important planning issue, as in its initial roll-out UMTS will be most likely limited to hot-spot regions with high traffic density.

# List of Figures

# References


3GPP (1999a). Physical layer procedures (FDD). Technical Specification TR25.214, 3GPP, TSG RAN.

3GPP (1999b). Radio resource management strategies. Technical Specification TR25.942, 3GPP, TSG RAN.

3GPP (2000). RF system scenarios. Technical Specification TR25.942, 3GPP, TSG RAN WG4.

Aein, J. M. (1973). Power balancing in systems employing frequency reuse. *COMSAT Technical Review 3*(2), 277–299.

Akl, R. G., M. V. Hedge, M. Naraghi-Pour, and P. S. Min (1999). Cell placement in a CDMA network. In *Proc. of IEEE WCNC*, New Orleans, LA.

Ariyavisitakul, S. and L. F. Chang (1993). Signal and interference statistics of a CDMA system with feedback power control. *IEEE Transactions on Communications 41*(11), 1626–1634.

Baccelli, F. and B. Blaszczyszyn (2000). On a coverage process ranging from the boolean model to the poisson voronoi tessellation. Rapport de recherche 4019, INRIA, Rocquencourt, France.

Baccelli, F., B. Blaszczyszyn, and F. Tournois (2001). Spatial averages of coverage characteristics in large CDMA networks. Rapport de recherche 4196, INRIA, Rocquencourt, France.

Baum, D. (1998). On markovian spatial arrival processes for the performance analysis of mobile communication networks. Technical Report 98-07, University of Trier, Trier, Germany.

CDMA Developers Group (2001). CDMA worldwide subscribers. http://www.cdg.org/world/cdma_world_subscriber.asp.

Chan, C. C. and S. V. Hanly (2001). Calculating the outage probability in a CDMA network with spatial poisson traffic. *IEEE Transactions on Vehicular Technology 50*(1), 183–204.

Chopra, M., K. Rohani, and J. D. Reed (1995). Analysis of CDMA range extension due to soft handoff. In *Proc. of IEEE VTC'95*, Chicago, IL, pp. 917–921.

Chvatal, V. (1979). A greedy heuristic for the set-covering problem. *Mathematics of Operations Research 4*(3), 233–235.

ETSI (1998). Selection procedures for the choice of radio transmission technologies of the UMTS. Technical Report TR 101 112 V3.2.0, ETSI SMG-5, Sophia Antipolis, France.

Evans, J. and D. Everitt (1999). On the teletraffic capacity of CDMA cellular networks. *IEEE Transactions on Vehicular Technology 48*(1), 153–165.

Fleming, P. J., A. L. Stolyar, and B. Simon (1997). Closed-form expressions for other-cell interference in cellular CDMA. UCD / CCM 116, University of Colorado, Denver, CO.

Foschini, G. J. and Z. Miljanic (1993). A simple distributed autonomous power control algorithm and its convergence. *IEEE Transactions on Vehicular Technology 42*(4), 641–646.

Garey, M. R. and D. S. Johnson (1979). *Computers and Intractability: A Guide to the theory of NP-Completeness*. New York: W. H. Freemann and Company.

Garg, V. K. (2000). *IS-95 CDMA and cdma2000*. Upper Saddle River, NJ: Prentice Hall.

Gilhousen, K. S., I. M. Jacobs, R. Padovani, A. J. Viterbi, L. A. Weaver Jr., and C. E. Wheatley III (1991). On the capacity of a cellular CDMA system. *IEEE Transactions on Vehicular Technology 40*(2), 303–312.

Grandhi, S. A., R. Vijayan, and D. J. Goodman (1994). Distributed power control in cellular radio systems. *IEEE Transactions on Communications 42*(2 / 3 / 4), 226–228.

Haartsen, J. (2000). The Bluetooth radio system. *IEEE Personal Communications 7*(1), 28–36.

Hanly, S. V. (1993). *Information Capacity of Radio Networks*. Ph. D. thesis, University of Cambridge, UK.

Hanly, S. V. (1995). An algorithm for combined cell-site selection and power control to maximize cellular spread spectrum capacity. *IEEE Journal on Selected Areas in Communications 13*(7), 1332–1340.

Hashem, B. and N. Secord (1999). Combining of power commands received from different base stations during soft handoff in cellular CDMA systems. In *Proc. of International Symposium on Personal, Indoor and Mobile Radio Communications PIMRC*, Osaka, Japan.

Hata, M. (1980). Empirical formula for propagation loss in land mobile radio services. *IEEE Transactions on Vehicular Technology 29*(3), 317–325.

Holma, H. and A. Toskala (2000). *WCDMA for UMTS*. John Wiley & Sons, Ltd.

ITU (1998). The cdma2000 RTT candidate submssion. TR45.5.

Kingman, J. (1993). *Poisson Processes*, Volume 3 of *Oxford Studies in Probability*. New York: Oxford University Press.

Kleinrock, L. (1975). *Queueing Systems*, Volume 1. John Wiley & Sons.

Lee, T.-H., J.-C. Lin, and Y. Z. Su (1995). Downlink power control algorithms for cellular radio systems. *IEEE Transactions on Vehicular Technology 44*(1), 89–94.

Leibnitz, K. (1999). Impacts of power control on outage probabilities in CDMA wireless networks. In *Proc. of IFIP 5th International Conference on Broadband Communications*, Hong Kong.

Leibnitz, K., P. Tran-Gia, and J. E. Miller (1998). Analysis of the dynamics of cdma reverse link power control. In *Proc. of IEEE GLOBECOM*, Sydney, Australia.

Mandayam, N. B., P.-C. Chen, and J. M. Holtzman (1996). Minimum duration outage for cellular systems: A level crossing analysis. In *Proc. of IEEE VTC'96*, Atlanta, GA.

Mitra, D. (1994). An asynchronous distributed algorithm for power control in cellular radio systems. In *Proc. of 4th WINLAB Workshop on 3rd Generation Wireless Information Networks*, Kluwer.

Mouly, M. and M.-B. Pautet (1992). *The GSM System for Mobile Communications*. Palaiseau, France: published by the authors.

Nettleton, R. W. and H. Alavi (1983). Power control for a spread spectrum cellular mobile radio system. In *Proc. of IEEE VTC'83*, Toronto, Canada.

Ojanperä, T. and R. Prasad (2001). *WCDMA: Towards IP Mobility and Mobile Internet*. Artech House.

Patel, P. R., U. S. Goni, E. Miller, and P. P. Carter (1996). *A Simple Analysis of CDMA Soft Handoff Gain and its Effect on the Cell's Coverage Area*, Chapter Radio Resource Management, pp. 155–171. Boston: Kluwer Academic.

Pichna, R. and Q. Wang (1999). *Mobile Communications Handbook*, Chapter Power Control, pp. 25–1–25–13. CRC Press.

Pickholtz, R. L., D. L. Schilling, and L. B. Milstein (1982). Theory of spread-spectrum communications - a tutorial. *IEEE Transactions on Communications COM-30*(5), 855–884.

Rappaport, T. S. (1996). *Wireless Communications – Principles & Practice*. Upper Saddle River, NJ: Prentice Hall.

Remiche, M.-A. (1998). Variability of Event Count for Spatial Point Processes of phase-type. In *Proc. of the second International Conference on Matrix Analytic Methods*, Winnipeg.

Remiche, M.-A. and K. Leibnitz (1999). Adaptive soft-handoff thresholds for CDMA systems with spatial traffic. In *Proc. of the 16th International Teletraffic Congress*, Edinburgh, UK.

Rose, O. (1999). A memory markov chain for vbr traffic with strong positive correlations. In *Proc. of the 16th International Teletraffic Congress*, Edinburgh, UK.

Sampath, A., P. S. Kumar, and J. M. Holtzman (1995). Power control and resource management for a multimedia CDMA wireless system. In *Proc. of IEEE PIMRC*.

Sampath, A., P. S. Kumar, and J. M. Holtzman (1997). On setting reverse link target SIR in a CDMA system. In *Proc. of IEEE VTC'97*, Phoenix, AZ.

Schröder, B., B. Liesenfeld, A. Weller, K. Leibnitz, D. Staehle, and P. Tran-Gia (2001). An analytical approach for determining coverage probabilities in large UMTS networks. In *Proc. of IEEE VTC'01 Fall*, Atlantic City, NJ.

Sendonaris, A. and V. Veeravalli (1997). The capacity-coverage tradeoff in CDMA systems with soft handoff. In *Proc. Asilomar Conf. Sig. Sys. Comput.*, Pacific Grove, CA.

Staehle, D., K. Leibnitz, and K. Heck (2002). Effects of soft handover on the UMTS downlink performance. In *Proc. of IEEE VTC'02 Fall*, Vancouver, Canada.

Staehle, D., K. Leibnitz, K. Heck, B. Schröder, A. Weller, and P. Tran-Gia (2002). Approximating the othercell interference distribution in inhomogeneous UMTS networks. In *Proc. of IEEE VTC'02 Spring*, Birmingham, AL.

Stoyan, D. and H. Stoyan (1994). *Fractals, Random Shapes and Point Fields: Methods of Geometrical Statistics*. Wiley.

Sung, C. W. and W. S. Wong (1999). The convergence of an asynchronous cooperative algorithm for distributed power control in cellular systems. *IEEE Transactions on Vehicular Technology 48*(2), 563–570.

Takeo, K. and S. Sato (1998). Evaluation of a CDMA cell design algorithm considering non-uniformity of traffic and base station locations. *IEICE Trans. Fundamentals E81-A*(7), 1367–1377.

Takeo, K., S. Sato, and A. Ogawa (2000). Optimum cell boundary for uplink and downlink in CDMA systems. *IEICE Trans. Commun. E83-B*(4), 865–868.

TIA / EIA / IS-707 (1997). Data service options for wideband spread spectrum systems. Technical report, Telecommunications Industry Association.

TIA / EIA / IS-95 (1993). Mobile station – base station compatability standard for dual–mode wideband spread spectrum cellular systems. Technical report, Telecommunications Industry Association.

Tran-Gia, P., N. Jain, and K. Leibnitz (1998). Code division multiple access wireless network planning considering clustered spatial customer traffic. In *Proc. of the 8th International Telecommunication Network Planning Symposium*, Sorrento, Italy.

Tran-Gia, P. and K. Leibnitz (1999). Teletraffic models and planning in wireless IP networks. In *Proc. of IEEE Wireless Communications and Networking Conference (WCNC)*, New Orleans, LA.

Tran-Gia, P., K. Leibnitz, and K. Tutschku (2000). Teletraffic issues in mobile communication network planning. *Telecommunication Systems 15*(1-2), 3–20.

Tran-Gia, P., D. Staehle, and K. Leibnitz (2001). Source traffic modeling of wireless applications. *Int. J. Electron. Commun. (AEU) 55*(1), 1–10.

Tutschku, K. (1998). Demand-based radio network planning of cellular mobile communication systems. In *Proc. of IEEE Infocom*, San Francisco, CA.

Tutschku, K. (1999). *Models and Algorithms for Demand-oriented Planning of Telecommunication Systems*. Ph. D. thesis, University of Würzburg.

Tutschku, K., N. Gerlich, and P. Tran-Gia (1996). An integrated approach to cellular network planning. In *Proccedings 7th International Telecommunication Network Planning Symposium*, Sydney, Australia.

Tutschku, K. and P. Tran-Gia (1998). Spatial traffic estimation and characterization for mobile communication network design. *IEEE Journal on Selected Areas in Communications 16*(5), 804–811.

Veeravalli, V. V. and A. Sendonaris (1999). The coverage-capacity tradeoff in cellular CDMA systems. *IEEE Transactions on Vehicular Technology 48*(5), 1443–1450.

Veeravalli, V. V., A. Sendonaris, and N. Jain (1997). CDMA coverage, capacity and pole capacity. In *Proc. of IEEE VTC'97*, Phoenix, AZ, pp. 1450–1454.

Viterbi, A. J. (1995). *CDMA – Principles of spread spectrum communications*. Reading, MA: Addison–Wesley.

Viterbi, A. J., A. M. Viterbi, K. S. Gilhousen, and E. Zehavi (1994). Soft handoff extends CDMA cell coverage and increases reverse link capacity. *IEEE Journal on Selected Areas in Communications 12*(8), 1281–1288.

Viterbi, A. J., A. M. Viterbi, and E. Zehavi (1994). Other-cell interference in cellular power-controlled cdma. *IEEE Transactions on Communications 42*(2 / 3 / 4), 1501–1504.

Viterbi, A. M. and A. J. Viterbi (1993). Erlang capacity of a power controlled CDMA system. *IEEE Journal on Selected Areas in Communications 11*(6), 892–893.

Walke, B. (1998). *Mobile Radio Networks, Networking and Protocols*. Wiley.

Wallace, M. and R. Walton (1994). CDMA radio network planning. In *Proc. of IEEE ICUPC*, San Diego, CA, pp. 62–67.

Wong, W. S. and K. H. Lam (1994). Distributed power balancing with a sparse information link. In *Proc. of IEEE VTC'94*, Stockholm, Sweden, pp. 829–832.

Yang, S. C. (1998). *CDMA RF System Engineering*. Norwood, MA: Artech House.

Yanikömeroglu, H. (2000). The theory of transmit power control. Tutorial held at the IEEE WCNC'00.

Yates, R. D. (1996). *Uplink Power Control for CDMA Cellular Systems*, Chapter Radio Resource Management, pp. 189–200. Boston, MA: Kluwer Academic.

Yates, R. D. and C.-Y. Huang (1995). Integrated power control and base station assignment. *IEEE Transactions on Vehicular Technology 44*(3), 638–644.

Zander, J. (1992a). Distributed cochannel interference control in cellular radio systems. *IEEE Transaction on Vehicular Technology 41*(3), 305–311.

Zander, J. (1992b). Performance of optimum transmitter power control in cellular radio systems. *IEEE Transactions on Vehicular Technology 41*(1), 57–62.

Zander, J. and S.-L. Kim (2001). *Radio Resource Management for Wireless Networks*. Artech House.

ISSN 1432-8801